SECONDARY FLOW IN AXIAL COMPRESSORS

ROBERT CHARLES DEAN, JR.

S.B., S.M., Massachusetts Institute of Technology
(1949)

SUBMITTED IN PARTIAL FULFILLMENT
OF THE REQUIREMENTS FOR THE
DEGREE OF DOCTOR OF SCIENCE

at the

MASSACHUSETTS INSTITUTE OF TECHNOLOGY
June, 1954

Signature of Author..
                    Department of Mechanical Engineering, May 17, 1954

Certified by...   ....
                                         Thesis Supervisor

Accepted by..
            Chairman, Departmental Committee on Graduate Students
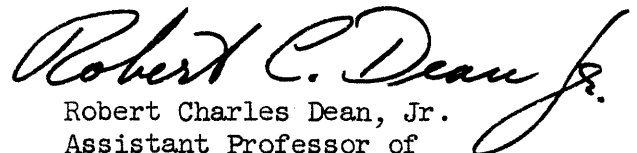
ME
Theis
1957

Gas Turbine Laboratory
Mass. Inst. of Tech.
Cambridge 39, Mass.
May 17, 1954

Professor J. P. Den Hartog
Chairman, Committee on Graduate Students
Mechanical Engineering Department
Massachusetts Institute of Technology
Cambridge, Massachusetts

Dear Professor Den Hartog:

A thesis entitled "Secondary Flow in Axial Compressors" is hereby submitted in partial fulfillment of the requirements for the degree of Doctor of Science at the Massachusetts Institute of Technology.

Very truly yours,

Robert Charles Dean, Jr.
Assistant Professor of
Mechanical Engineering

RCD:mep

Acknowledgments

The author is grateful to his thesis supervisor, Professor Edward S. Taylor, for his continuous guidance and inspiration during the course of this work.

The sponsorship of the General Electric Company, the Westinghouse Electric Corporation and the Office of Naval Research enabled the research program in three-dimensional flow from which has come the incentive and information necessary to this investigation.

The course of the analytical treatment was influenced beneficially by the teaching and advice of Professor Joseph Bicknell of the Aeronautical Engineering Department.

Without the extensive assistance of my wife, who supplied the patience and encouragement; of Miss Margaret Tefft, who carried out the computations; of Miss Maxine Phinney who created the final thesis form, and of Mr. George Mellor who checked the analytical work, this thesis would have been impossible.

To all these people and the others who contributed indirectly, the author is indebted.

ABSTRACT

SECONDARY FLOW IN AXIAL COMPRESSORS

ROBERT C. DEAN, JR.

(Submitted to the Department of Mechanical Engineering
on May 17, 1954, in partial fulfillment of the require-
ments for the degree of Doctor of Science in Mechanical
Engineering)

The subject of secondary flow in axial compressors is treated
by a review of previous experience and the analysis of simplified
models of the wall boundary-layer flow in turning passages.

From the experimental data re-evaluated and correlated, a
physical model is constructed of secondary flow, tip clearance,
relative wall motion and wall boundary-layer separation phenomena.
A tentative qualitative theory of the influence of tip clearance
on boundary-layer behavior is proposed. It is speculated that
controlled tip clearance might improve the performance of axial
compressors.

The problem of boundary-layer skewing in blade channels
is treated analytically. Approximate relations are derived relating
boundary-layer behavior to blade-row geometry and flow configuration.

The influence of streamwise pressure stresses upon boundary-
layer streamline patterns is demonstrated by an approximate theory.
The magnitude of the effects in the vicinity of the boundary indi-
cates the necessity of the inclusion of such stresses in any
analysis attempting to predict separation tendencies.

Integral momentum relations are derived for a quasi-two-di-
mensional laminar boundary-layer flow to demonstrate the importance
of shear stresses. The relations are applied to a flow model and
numerical results obtained which qualitatively agree with experi-
mental measurements.

Thesis Supervisor: Edward S. Taylor
Title: Professor of Aircraft Engines

I. Introduction

Today, most turbomachines are designed with the tacit assumption that the actual flow behaves in a manner predicted largely from two-dimensional analysis. Experience demonstrates that this model is not in great error and that, in this way, useful machines can be designed. However, there is a growing demand for optimum performance, particularly from axial compressors and turbines for aircraft propulsion and steam turbines for power generation. Perfection of such equipment requires a knowledge and control of the actual flow through the machine under all operating conditions.

While the three-dimensional flow patterns are complicated and analytically elusive, major progress is presently being achieved by several investigating groups.

In axial compressors the most obvious measured deviations of the actual three-dimensional flow from the ideal two-dimensional model are as follows:

1) There is rapid peaking or distortion along the flow path of an axial velocity profile initially nearly uniform with radius.

2) The overall pressure ratio and work input measure less than the values computed from two-dimensional analyses unless an "experience factor" is included. This situation is especially noticeable in multi-stage machines.

3) The peak pressure ratio a stage achieves before stalling is of smaller magnitude when the stage operates as part of a multi-stage machine than when it functions alone.
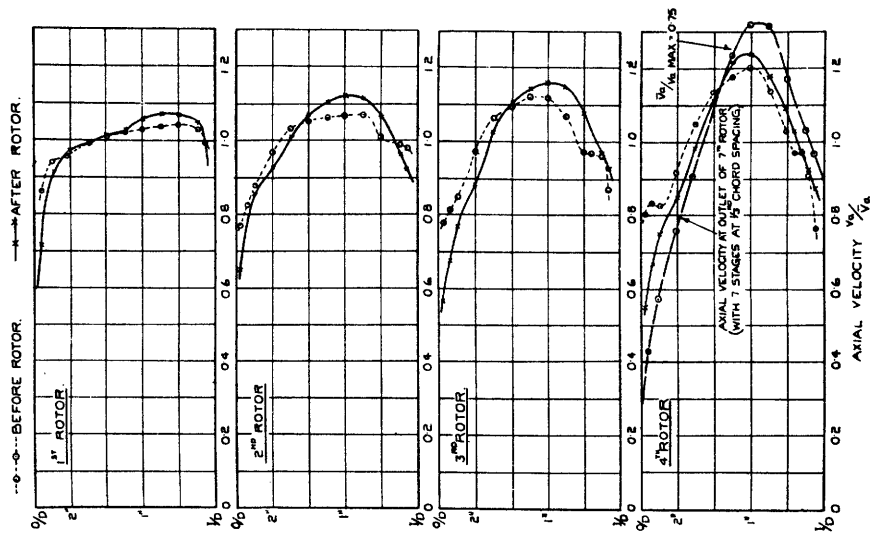
Fig. 1a. Development of axial velocity distribution in a half-vortex compressor reduced from A.R.C., R. and M. No. 2383. Reynolds number in first rotor 75,000; mass flow 7.25 lb./s. Stagnation pressure rise 1.026 per stage; efficiency 83 per cent.
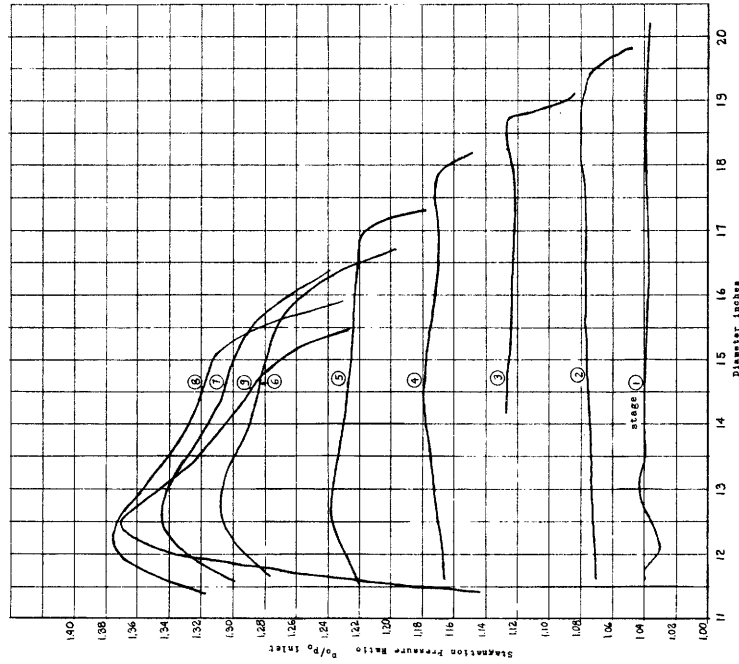
BEFORE ROTOR. ──── AFTER ROTOR.

1ˢᵀ ROTOR

2ᴺᴰ ROTOR

3ᴿᴰ ROTOR

4ᵀᴴ ROTOR

AXIAL VELOCITY $V_a/\bar{V}_a$

$V_a/\bar{V}_a$ MAX. 0.75

AXIAL VELOCITY AT OUTLET OF 7ᵀᴴ ROTOR
(WITH 7 STAGES AT ½ CHORD SPACING)

Fig. 1b. Stagnation-Pressure Contours from a Nine-Stage Axial Compressor

Stagnation Pressure Ratio p_0/p_0 inlet

Diameter inches

stage ①
②
③
④
⑤
⑥
⑦
⑧

The effects above are of sufficient magnitude to be of interest to the designer; they not only impair performance, but they reduce the accuracy of design prediction.

Velocity profile degeneration in compressors, a typical example of which is illustrated in Figure 1, is probably responsible for reduced performance in the high pressure stages, partially explaining item 2 above.

The rapidity with which the velocity profile degenerates suggests that wall friction alone cannot be responsible. Several other phenomena may produce similar effects. Among these phenomena may be:

1) Secondary flow.

2) Lack of radial equilibrium and resulting radial flows.

3) Boundary-layer instability in a centrifugal force field.

4) Overall boundary-layer thickening in a diffusion process.

5) Increased dissipation due to the shear flows arising near the blade extremities.

6) Reduction in stagnation pressure rise at the rotor extremities due to flow distortion.

7) Stall or boundary-layer separation near the blade extremities.

8) Local shocks arising from flow distortion.

Some of the phenomena listed above contribute direct and/or indirect influences. The occurrence of one or more events may be responsible for the initiation of others. The flow patterns are extremely complex; they must, therefore, be examined in great detail.

Mathematical description of an appropriate model of the flow phe-
nomenon is usually difficult while the solution of the complete
flow equations is presently impossible. This three-dimensional
flow represents the most general problem of fluid mechanics includ-
ing consideration of pressure, viscous and turbulent forces acting
on a three-dimensional, dissipative, compressible-flow pattern. In
the absence of analytical solution, experimental data and semi-
quantitative interpretation serve as our only guides.

Secondary Flow Phenomena in Axial Compressors

In the mechanism of secondary flow, we find one of the larger deviations of the actual flow from the idealized two-dimensional flow model. For this reason, the Gas Turbine Laboratory has concentrated particularly on this phenomenon over the last few years. Recently, some additional factors have come under investigation.

Definition of Secondary Flow

The meaning of the term "secondary flow" depends primarily on he who defines it. Taking advantage of this precedent, "secondary flow" will be defined, herein, as any measurable flow velocities and displacements which can be directly attributed to the presence of a stagnation pressure gradient in a stream which undergoes a change in direction. The mechanism which gives birth to the stagnation pressure gradient is not considered a part of the secondary flow phenomena, although there is evidence of mutual interaction between the two inside the turning passage.

The mechanism of secondary flow can be revealed in the following manner: Consider a two-dimensional stream approaching a bend in a channel. Take cylindrical coordinates, as shown in Figure 2.
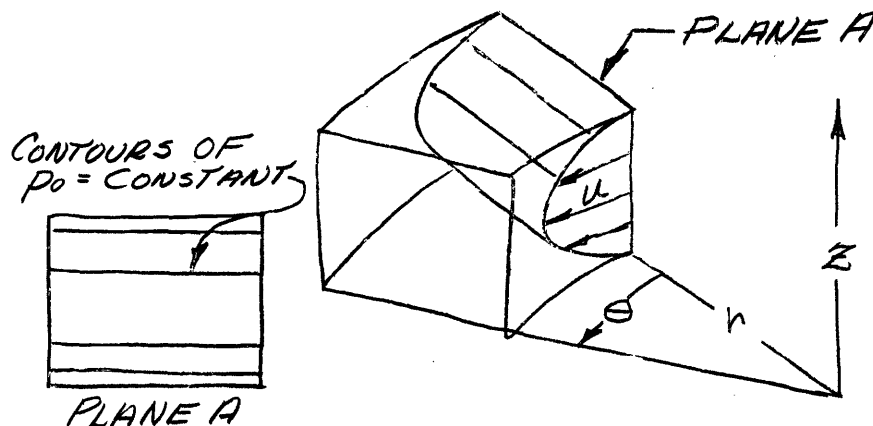

Figure 2

To simplify the treatment assume $\partial p_o/\partial r = 0$ at inlet to the bend

as shown. Under this assumption, the Bernoulli surfaces $(p_o = const.)$

will intersect with the plane of the inlet cross section as straight

lines perpendicular to the z direction. Now, if the fluid velocity

along the streamlines, u, varies in the z-direction, which is the

general result of a stagnation pressure variation, the radial cen-

trifugal pressure gradient in the bend must also vary in the z-direc-

tion. The pressure gradient normal to a streamline is expressed by:

$$\frac{\partial p}{\partial n} = \rho \frac{u^2}{R}$$

where R is the radius of curvature of the streamline. At the en-

trance to the bend, the streamlines turn primarily in the (r,θ)

plane of the bend. The simplifying assumption may then be employed

that $R \simeq r$ and $\frac{\partial p}{\partial n} \simeq \frac{\partial p}{\partial r}$.

The variable radial stream pressure gradient, $\frac{\partial p}{\partial r}$, will pro-

duce pressure gradients in the z-direction inside the bend (i.e., $\frac{\partial p}{\partial z}$),

as shown in Figure 3, driving the fluid into opposite rotation at
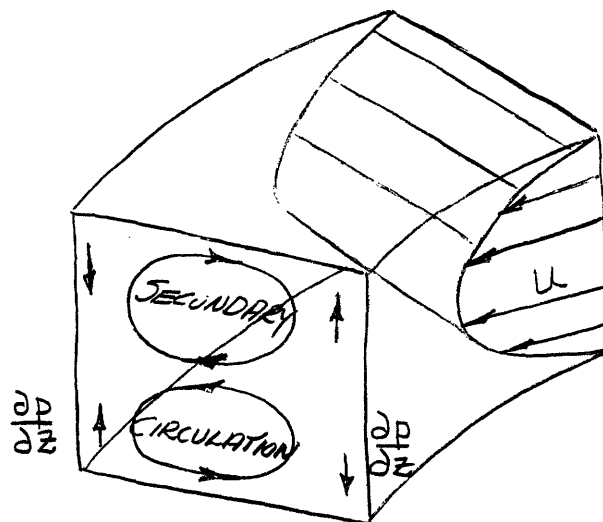
top and bottom walls.

Figure 3

The development of secondary flow may be described crudely, but more graphically, as follows. The main body of the flow establishes a pressure gradient in the r-direction $\frac{\partial p}{\partial r} = \rho \frac{\overline{V}^2}{R}$ where R is the radius of curvature of the streamlines and $\overline{V}$ the "main stream" velocity. The boundary layer fluid travels at lower velocity. If it did travel on streamlines of the same radius of curvature as those in the main flow, its radial acceleration could not match the radial pressure forces established by the bulk of the flow. Solve this problem the boundary fluid must, so it travels on streamlines of smaller curvature with a consequent increase in radial acceleration, in an attempt to match the imposed radial pressure force. Boundary layer fluid in this manner turns faster than the main stream and soon reaches the inner wall.

The resulting streamline displacements can be imagined if the secondary circulation is superimposed on the two-dimensional bend flow. (Figure 3).

The local rate of change along streamlines of the secondary vorticity is expressed by Hawthorne's equation (Ref. 1) for a steady flow of an incompressible, inviscid fluid without body forces.

$$V \cdot \nabla \left(\frac{\xi}{u} \right) = -2 \frac{\left| \nabla \left(\frac{P_0}{\rho} \right) \right|}{u} \frac{\sin \phi}{R} \tag{1a}$$

or integrating along a streamline:

$$\Delta \left(\frac{\xi}{u} \right) = -2 \int_1^2 \frac{1}{u^2} \left| \nabla \left(\frac{P_0}{\rho} \right) \right| \frac{\sin \phi}{R} \, ds \tag{1b}$$

where the terms are defined in Figure 4.
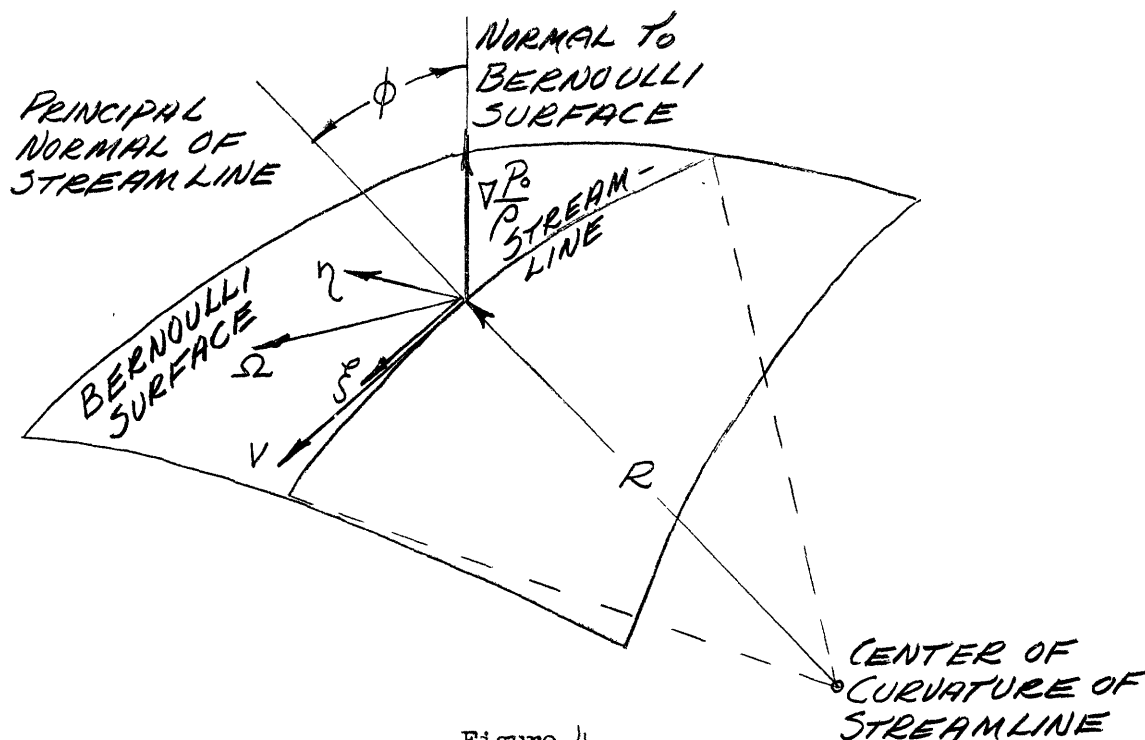
Figure 4

V = velocity vector, magnitude u

$\nabla (p_o/\rho)$ = gradient of p_o/ρ

p_o = stagnation pressure

ρ = stream density

Ω = vorticity vector

ξ = vorticity component tangent to streamline

η = vorticity component normal to streamline

R = streamline radius of curvature

ϕ = angle between principle normal to streamline and normal to Bernoulli surface

Examination of equations (1a, 1b) teaches that there will be a component of the vorticity gradient in the direction of the velocity vector if $0 < \phi < \pi$, $|\nabla (p_o/\rho)| \neq 0$, $R \neq \infty$. If the last two conditions are met, it follows that secondary flow will always develop in a curved channel unless the streamlines happen to be geodesics (i.e., $\phi = 0$) on the Bernoulli surfaces.

A stagnation pressure gradient most commonly arises from vis-cous shear near a solid flow boundary. Fluid friction, in this manner, is indirectly responsible for secondary flow; however, comparison of inviscid analysis with the experiments discussed below shows that the stagnation pressure gradient, not viscosity, largely controls the development of secondary flow in regions re-moved from the walls.

The secondary velocities and consequent fluid displacement cause the low energy boundary-layer fluid on the plane walls of the bend to flow toward the inside wall, accumulating there after a large angle of turn. The amount of fluid displacement, of course, increases with the turning angle of the bend. These displacements will be treated in greater detail below.

Most analytical attacks to date have solved equation (1), or equivalent expressions, by assuming that the Bernoulli surfaces do not rotate or rotate without warping. Such treatment is fairly successful in a circular pipe where the boundary conditions are favorable to the latter assumption. In rectangular passages, this assumption does not prevent reasonable accuracy in predicting secondary flow velocities after small turns, but is untenable for calculating the flow pattern in turns of large angle.

Before a discussion of the influence of secondary flow in turbomachinery, the data of Eichenberger (4), Van Le (5), and Toline and Watson (11) will be presented offering the reader a physical interpretation of the phenomenon based on experimental measurements.
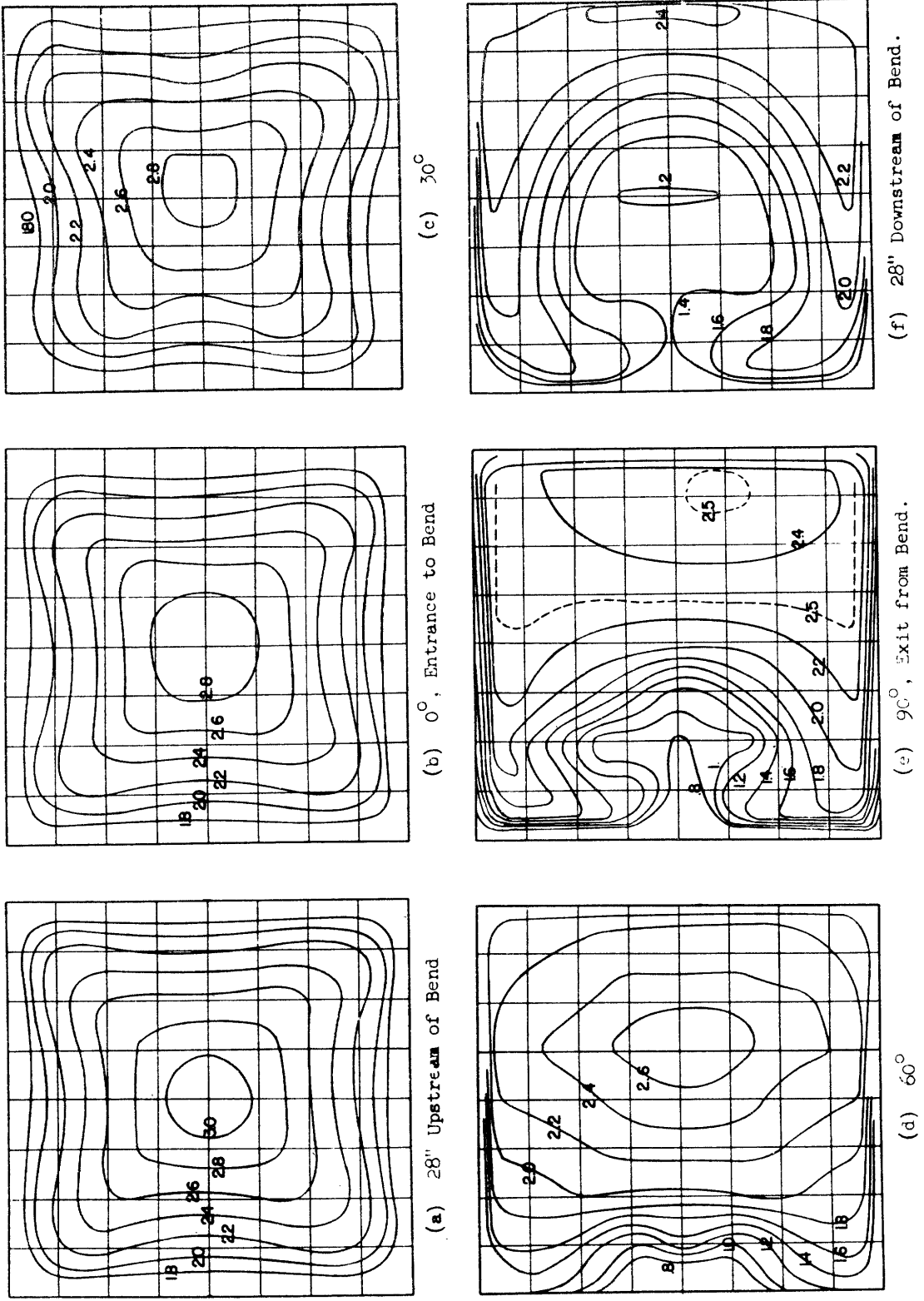
Secondary Flow in a Rectangular Bend

H. P. Eichenberger's investigation of secondary flow in a constant area bend was carried out under the sponsorship of the Office of Naval Research; his results are reported fully in Reference (1).

The purpose of this fundamental investigation was to reveal, by experiment and analysis, the nature of secondary flow in a simple channel which roughly approximated fluid machinery passages. Here, we are primarily concerned with his experimental data.

Two series of tests were performed, one set employing water with velocities from 0.1 to 1.3 ft/sec., the other set employing air flowing at velocities from 100 - 200 ft/sec. The Reynolds number variation was accordingly from 7×10^3 to about 7×10^5. The entry velocity profile to the bend was that of fully-developed turbulent flow. The bend was of square section 8" x 8" with an inside radius of 24". A well-rounded nozzle led from the room into a 20' long (i.e., about 30 hydraulic diameters) 8"x 8" pipe, preceding the 90° bend; a 40" straight section followed the bend preceding discharge to the fan.

Flow directions, stagnation- and stream-pressures were measured over six cross sections: 28" before the bend, 0°, 30°, 60°, 90° and 28" after the bend.

A comparison of the water flow data taken at Reynolds number of 7000 with that of air taken at Reynolds number of 720,000 demonstrated insignificant difference between the flow patterns at similar positions in the bend. This observation is not surprising since the flow was turbulent in all cases.

(a) 28" Upstream of Bend

(b) 0°, Entrance to Bend

(c) 30°

(d) 60°

(e) 90°, Exit from Bend

(f) 28" Downstream of Bend.

Contours of Constant Stagnation Pressure (in Inches of Water)

(Channel Cross Section 8" x 8"; 1" x 1" Grid on Figures; Left Side of Figure is the Inside of the Bend.)

Figure 6   DEVELOPMENT OF SECONDARY CIRCULATION IN A 90° CIRCULAR BEND
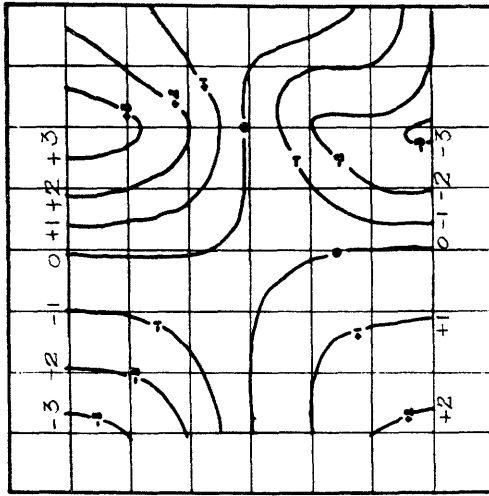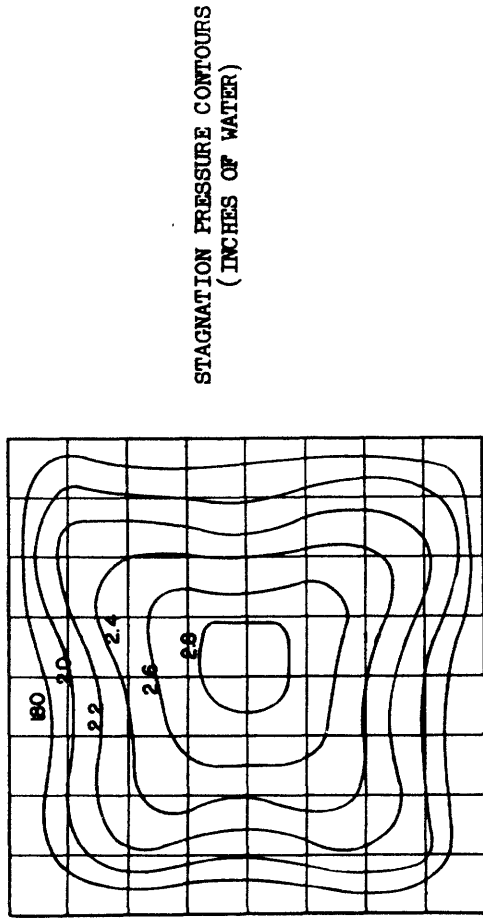
STAGNATION PRESSURE CONTOURS
(INCHES OF WATER)
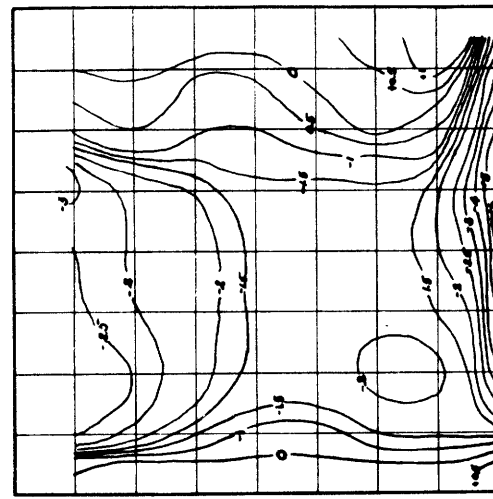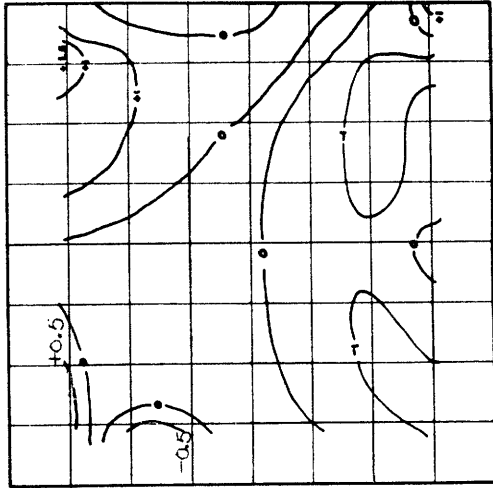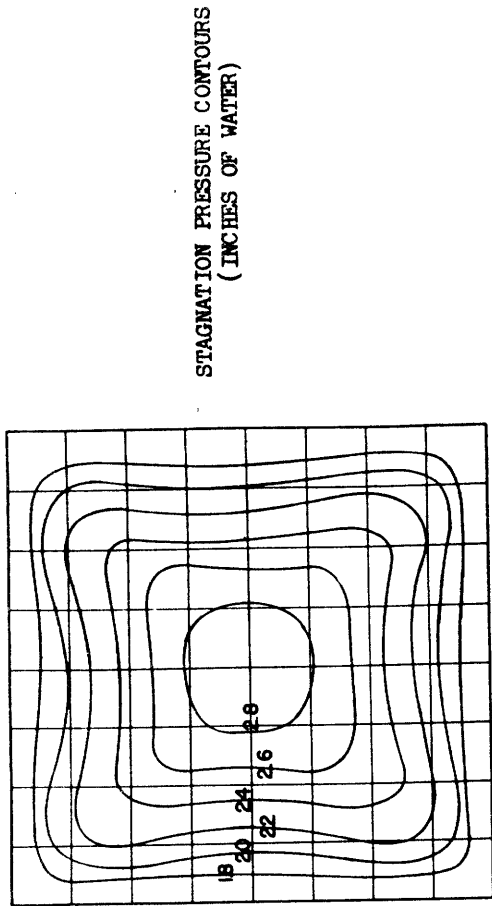
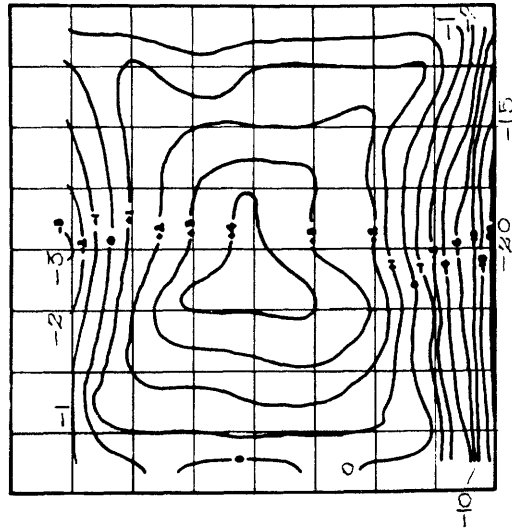TANGENT PLANE DEVIATION ANGLE

UNDERTURNING ANGLE

(CHANNEL CROSS SECTION 8 IN. X 8 IN. ; 1 IN. X 1 IN. GRID ON FIGURES ; LEFT SIDE OF FIGURE IS INSIDE OF BEND)

DEVELOPEMENT OF SECONDARY CIRCULATION IN A BEND

Figure 7a

SECTION AT INLET TO BEND (0°)

STAGNATION PRESSURE CONTOURS
(INCHES OF WATER)

TANGENT PLANE DEVIATION ANGLE

UNDERTURNING ANGLE

DEVELOPEMENT OF SECONDARY CIRCULATION IN A BEND

Figure 7b
SECTION AT 30°

(CHANNEL CROSS SECTION 8 IN. X 8 IN. ; 1 IN. X 1 IN. GRID ON FIGURES ; LEFT SIDE OF FIGURE IS THE INSIDE OF BEND)

STAGNATION PRESSURE CONTOURS
(INCHES OF WATER)

UNDERTURNING ANGLE

TANGENT PLANE DEVIATION ANGLE
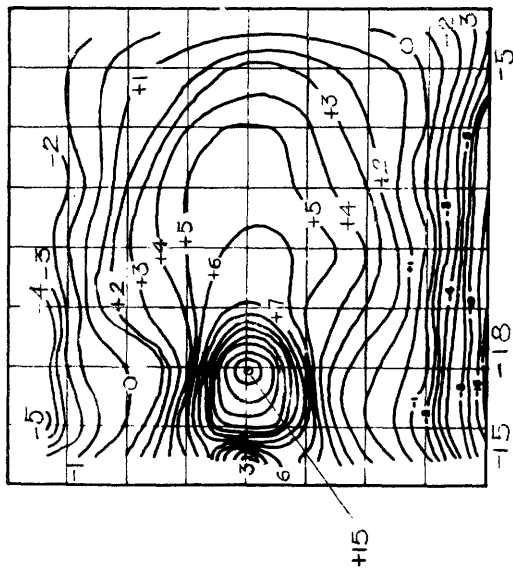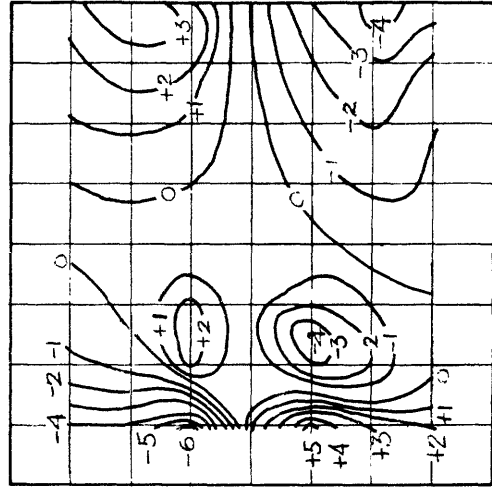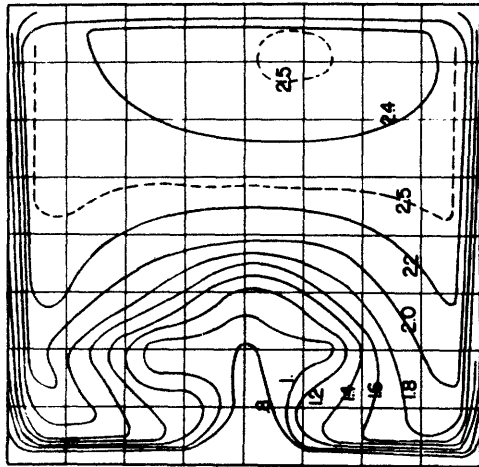
(CHANNEL CROSS SECTION 8 IN. X 8 IN. ; 1 IN. X 1 IN. GRID ON FIGURES ; LEFT SIDE OF FIGURE IS INSIDE OF BEND)

Figure 7c   DEVELOPEMENT OF SECONDARY CIRCULATION IN A BEND

SECTION AT OUTLET FROM BEND (90°)

Stagnation pressure contours and flow directions from the air tests are presented in Figures 6, 7a, 7b, and 7c.

The interpretation of these contour maps is not an obvious process. The fact that the stagnation pressure along a given circular arc (r,z) varies with the turning angle Θ can be the result of two distinct phenomena--fluid displacement and irreversible momentum exchange. Neglect of either mechanism will inevitably lead to misinterpretation. However, since fluid with a relative stagnation pressure defect $(\overline{p_0} - p_0)/ \rho/2\overline{V}^2$ (where $\overline{V}$ is the bulk mean velocity, $\overline{p_0}$ a mass weighted average stagnation pressure, and p_0 the local stagnation pressure) approaching a value of 100% enters the turn near the confining walls, large distortions of the Bernoulli surfaces (i.e., large changes in the stagnation pressure defect along a circular arc) are most likely to be due to fluid displacement. Momentum exchange by viscous shear forces and turbulent mixing can either raise or lower the stagnation pressure along a streamline, but the change is usually of the order of a few percent and cannot be responsible entirely for the large Bernoulli surface distortions evident in Figure 6. Thus, we are safest if we describe the Bernoulli surface distortion as a result of fluid displacement, remembering that the picture must be somewhat modified to account for dissipation. It is most certainly erroneous to describe the stagnation pressure controus, or differences between the contours at a given cross section plane from those in the inlet plane, as loss contours, although the terms energy defect or stagnation pressure defect are acceptable.

Accounting for regions of low stagnation pressure as losses and consequent neglect of three-dimensional displacement has led to considerable confusion in this field, has produced erroneous conclusions and has hindered a physical understanding of the phenomena.

Certainly, the determination of true loss contours (i.e., variation of stagnation pressure <u>along streamlines)</u> would be of essential value to secure an understanding of the importance of viscous or turbulent stresses, the sources of dissipation and methods by which it may be reduced.

Carter (18), by use of a streamline tracing technique, measured dissipation along streamlines; his values, however, seem high which may be due to an inherent uncertainty in his method of the order of magnitude of the measured dissipation. Some of his results show no increase in stagnation pressure along any streamline traversing a diffusing passage. It will be shown later that such increases are mandatory. The importance of an understanding of dissipation in a three-dimensional flow is concentrating serious effort on the problem

With the above comments in mind, let us return to Figure 6 and build a qualitative physical interpretation of that flow. Inspection of equation (1) shows that the magnitude of the component of the stagnation pressure gradient perpendicular to the principal normal of the streamline (i.e., $\left| \nabla \left(\frac{p_0}{\rho} \right) \right| \sin \emptyset$) controls the rate of development of secondary vorticity along the streamline.

At entrance to the bend, the principal normals of the streamlines are parallel to the r-direction. Then, only the z component

of the local stagnation pressure gradient will give rise to second-
ary vorticity. The boundary layer existing on the curved walls of
the bend will not develop secondary circulation as long as the
streamlines turn in the plane of the bend. The fluid on the plane
walls experiences a growth of secondary vorticity increasing in
rate as $\dfrac{\partial p_o}{\partial z}$ increases on approach to wall.
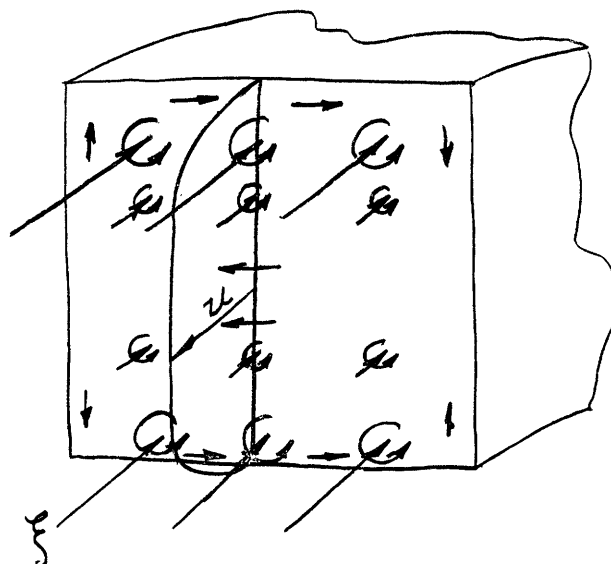
Figure 8

The resulting distribution of secondary vorticity initiates
secondary fluid motion toward the inside of the bend on the plane
walls. This flow may be observed in the underturning angle plots
of Figure 7.

The drift to, and accumulation at, the inner wall of low
velocity fluid forces the main stream, high-energy fluid to move
toward outer regions of the plane walls filling the regions evacuated
by the boundary layer. Viscous friction brought into action by the
high velocity gradients at these parts of the wall developes more
boundary layer fluid and the process continues. It is this removal

of the original boundary layer and growth of new, which is partially
responsible for the losses credited to secondary flow.

The production of the kinetic energy of secondary flow re-
quires little energy from the main stream. Eichenberger (4),
Van Le (5) and others have shown, by integration over the flow at
exit from a bend or cascade, that the kinetic energy of secondary
flow and the potential loss from complete dissipation of the second-
ary velocities amounts to only 0.2% and 1.0% of the total kinetic
energy of the entering stream for a 24° and 90° turn, respectively.
In contrast, the total dissipation credited to the bend amounts to
5% and 25% of the entering kinetic energy for respectively a 24°
and 90° turn.

The inward flow and production of new boundary layer con-
tinues as the angle of turn increases. At 60° bend angle a signi-
ficant accumulation of low energy fluid is apparent at the inside
of the bend. At 90° turning angle, the low energy accumulation
penetrates well into the stream. After the bend, the secondary
circulation persists until dissipated even though the driving pres-
sure forces are no longer acting; the distortion increases with
distance downstream. At a location 28" after the bend the flow had
turned virtually inside out.

Figure 9 plots mass averaged stream entropy at various
cross sections against distance along the bend. Inside the bend, a
large increase in the rate of change of stream entropy
is apparent compared to the initial rate in the straight pipe. The
rate of dissipation continues high even after the bend. Inversion

of the flow pattern and the resulting high shear gradients at the
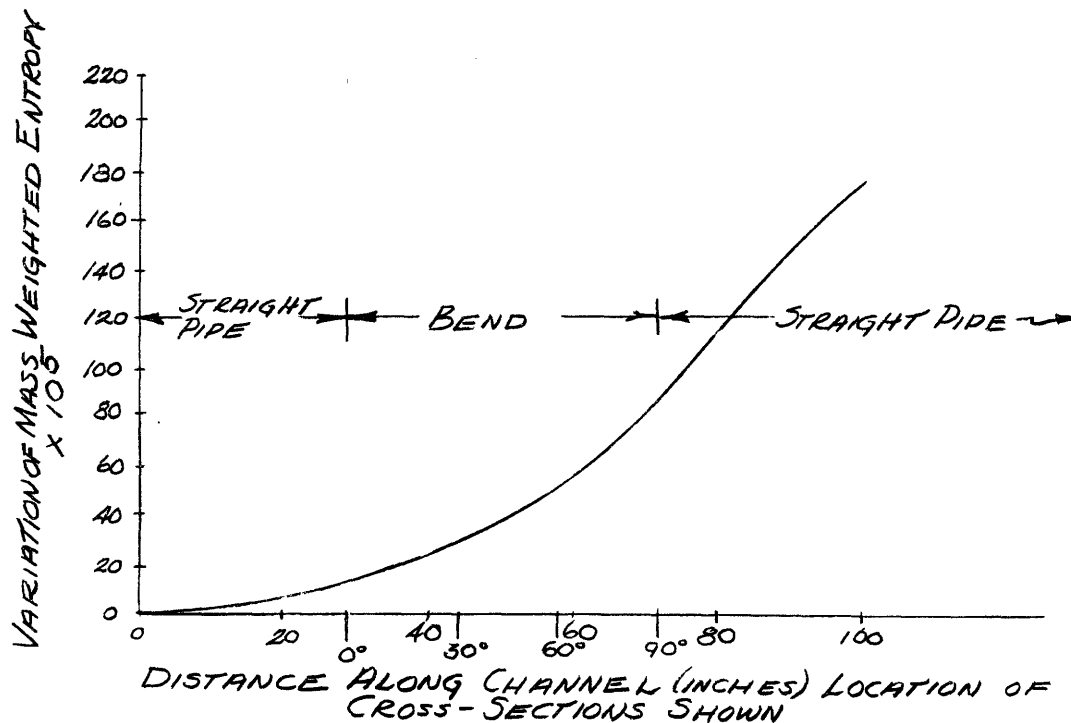
Figure 9

wall as well as mixing of the accumulated low-energy fluid with the

main flow are responsible for the high rate of dissipation continu-

ing after the bend.

A theory of secondary circulation in a constant area bend was

developed by Eichenberger which accurately predicts the distribution

of secondary velocities after a turn of about $30°$. With larger turns,

typical of turbines, the flow pattern can be seen to grow too con-

fused to allow mathematical treatment.

Secondary Flow in a Rectilinear Cascade

The next logical extension of the bend study, to approximate

more exactly the flow passages of a turbomachine, was investigation

of the development and influence of secondary flow in a rectilinear

cascade. Nguyen Van Le (5), employing the MIT Gas Turbine Labora-
tory low-speed cascade wind tunnel, investigated secondary flow in
a cascade of axial compressor blading under the sponsorship of the
General Electric Company and the Westinghouse Electric Corporation.

The wind tunnel has a cross section of 16" x 22". Fourteen
straight blades of 3-inch chord, 16" span and pitch-chord ratio of
0.77 were fitted with a 40° air inlet angle and 24° turning angle.
An infinite cascade was approximated by applying boundary layer
suction to the side walls. A splitter wall was fitted to the blades,
as shown in Figure 10, which allowed the wall to be adjusted rela-
tive to a stationary row of surface taps on the blade yielding the
variation of blade surface pressure distribution with distance from
the wall. Boundary layer shape and thickness were governed by the
length and roughness of the splitter wall.

The entering velocity was about 130 fps with a blade-chord
Reynolds number of 2×10^5. The cascade discharged directly into
the room, facilitating the use of traversing probes to determine
stagnation and stream pressure, underturning and spanwise deviation
angles. Special probes were developed which could resolve the flow
pattern with sufficient accuracy even in the high velocity gradients
of the blade wakes.

Stagnation pressure contours for a series of (y,z) planes
are presented in Figure 13. The location of the traversing planes
is illustrated in Figure 11.

Fluid displacement toward the suction surface is evident;
the phenomena resembles that of the constant area bend except that
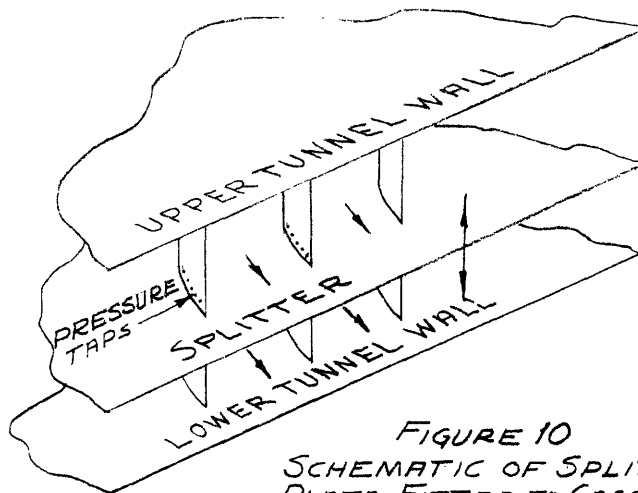
FIGURE 10
SCHEMATIC OF SPLITTER-
PLATE FITTED TO CASCADE
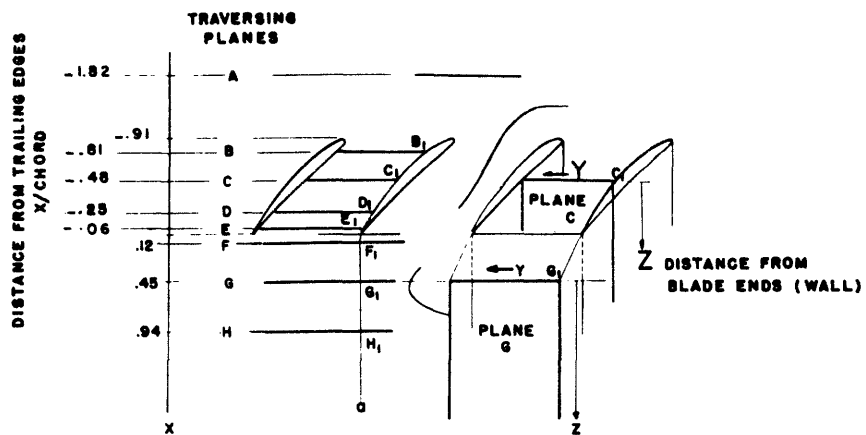
(Chord = 3.0", Pitch = 2.3", Dimensions in Inches)

Figure 11   LOCATION OF TRAVERSING PLANES

p = local stream pressure
p_1 = stream pressure ahead of cascade
V_1 = mid-span velocity upstream of cascade

$\dfrac{p-p_1}{\dfrac{\rho}{2g_0}V_1^2}$

$\dfrac{X}{C}$ = Distance Downstream of Cascade
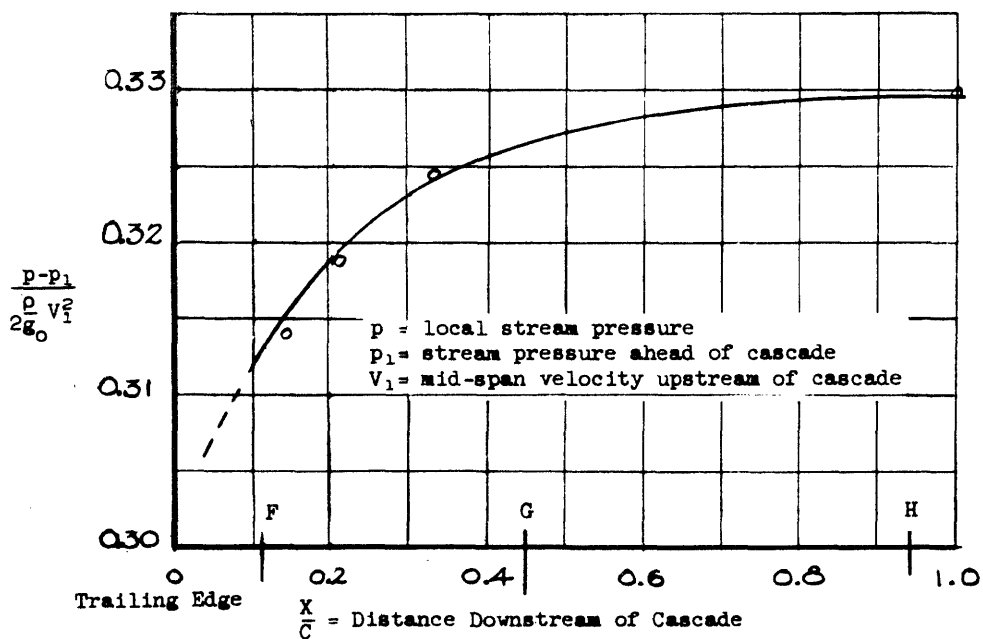
(Location of Traversing Planes. F, G, H is noted.
Data Taken Along Axis X, Normal to Plane of Cascade).

Figure 12   VARIATION IN STREAM PRESSURE DOWNSTREAM OF CASCADE AT BLADE MID-SPAN
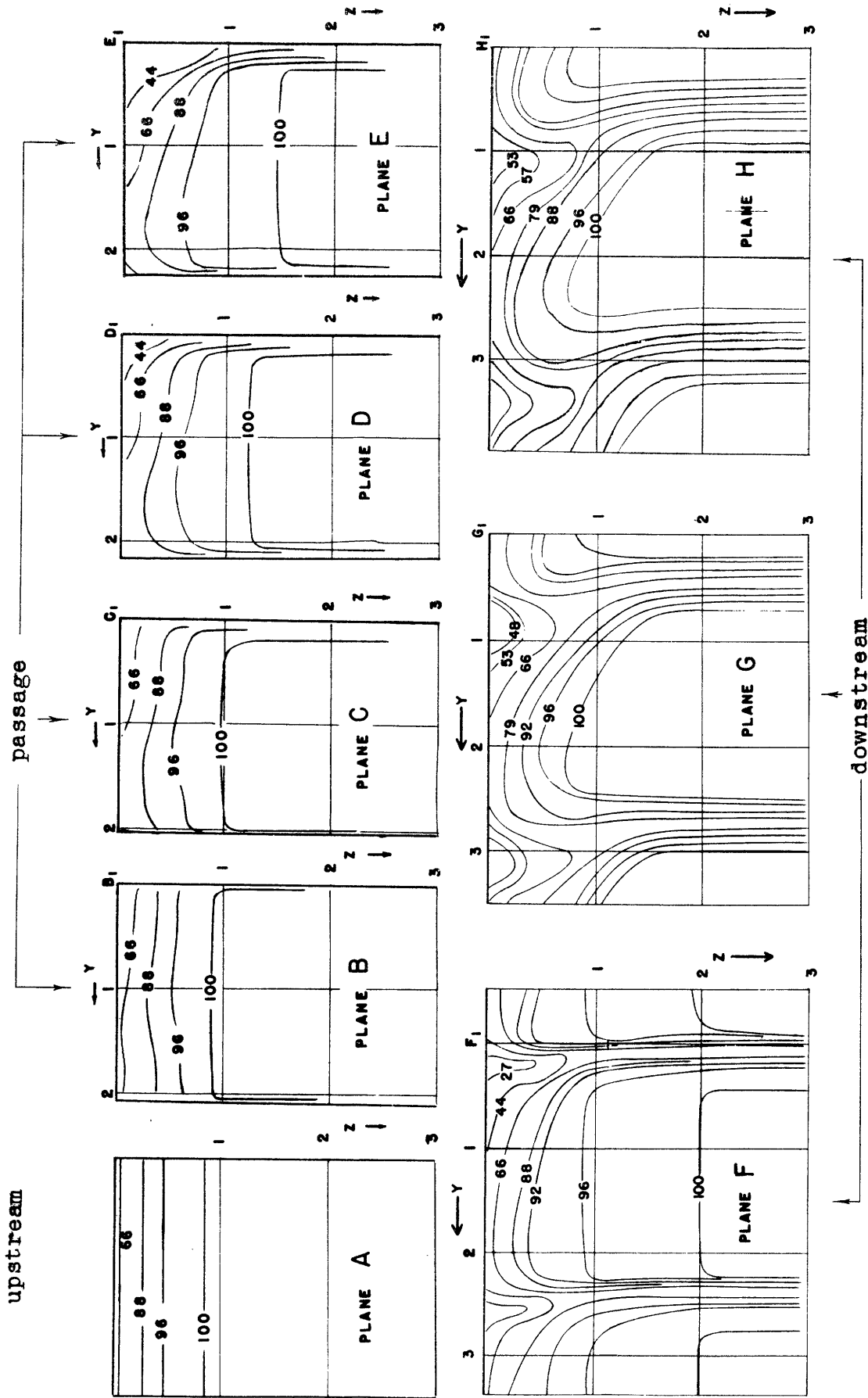
Figure 13 DEVELOPMENT OF SECONDARY CIRCULATION IN A COMPRESSOR CASCADE (Blade pitch 2.3", Chord 3", Length 9", Turning Angle 24°, Inlet Angle 40°)

the displacements are larger for a given turning angle. This ob-
servation is to be expected since the flow in the cascade proceeded
against an adverse pressure gradient which forced low energy fluid
to escape more rapidly down the blade suction surface (i.e., the
inside of the bend.) A residual secondary circulation can be noted
between planes G and H.

Figure 12 presents the measured variation of stream pressure
downstream of the cascade; the data was taken in the x-direction at
blade midspan and the center of the channel. The locations of the
planes of Figure 11 are noted. It should be remembered that the
cascade discharged directly into the atmosphere.

Figure 14 illustrates pressure distributions around the
blades at various distances from the wall. Two facts should be
noted: First, that the pressure distribution on the pressure side
of the blade does not change significantly on approach to the wall,
while the pressure distribution of the suction surface is markedly
altered. This observation can easily be explained by the observed
secondary displacement of high energy fluid toward the wall on the
pressure surface and the counter displacement of considerable low
energy fluid onto the suction surface. Secondly, it is important
to note that the net pressure force on the blade does not diminish
to zero at the wall even though the fluid velocity must be zero at
the wall. This observation is also to be expected since the tip is
bounded by the wall in this case, allowing a pressure difference to
be maintained between the two sides of the blade. The problem of a
turbomachine blade immersed in a boundary layer is dissimilar to
that of a finite wing unless the tip clearance becomes very large.

CURVE 3

Inlet Velocity Profile

U/V_1

z/L

0.15

0.10

0.05

0

0.60   0.80   1.0

* Data Shown for Curve 4.

V_1 = Mid-Span Velocity Ahead of Cascade

p_1 = Stream Pressure Ahead of Cascade

Aspect Ratio = 3

Blade Length, l = 9"

Pitch, S = 2.3"

Distance Along X Axis

$\dfrac{X}{S}$

$\dfrac{p - p_1}{\dfrac{\rho}{2g_o} V_1^2}$

0.2   0   -0.2   -0.4   -0.6

0.2   0.4   0.6   0.8   1.0   1.2

Curve

1
2
3
4

Distance from Splitter Wall
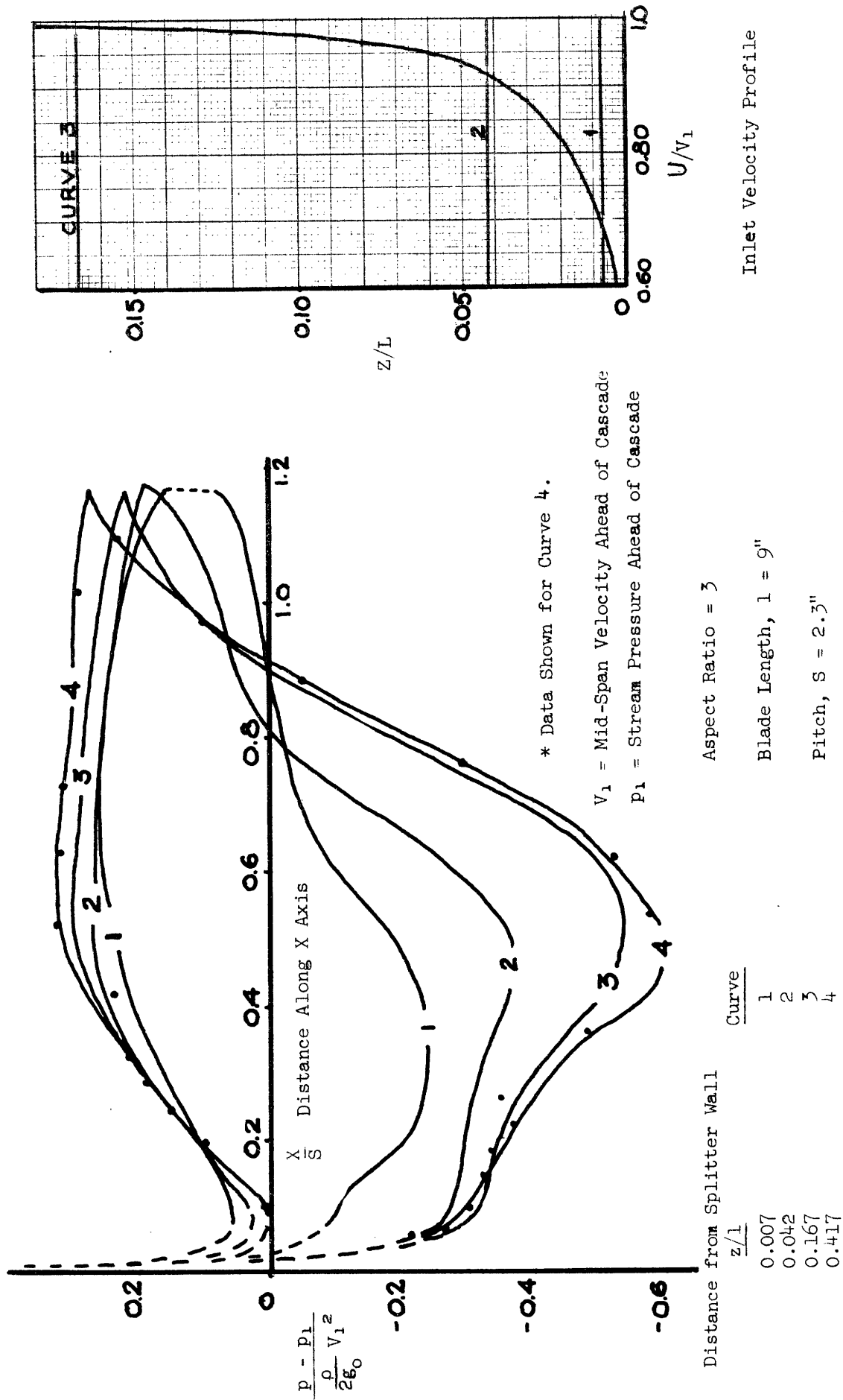
z/l

0.007
0.042
0.167
0.417

FIGURE 14   PROJECTED BLADE PRESSURE DISTRIBUTIONS AT VARIOUS DISTANCES FROM THE WALL.

Theory

Van Le has developed a linearized theory yielding secondary flow velocities downstream of a small turning angle bend conducting an incompressible, inviscid fluid. The theory predicts with considerable accuracy the measured deviation angles, and therefore the secondary flow velocities, in the x-y plane at discharge. However, this theory cannot yield fluid displacement since it assumes that the Bernoulli surfaces remain flat and parallel to the x-y plane. That this assumption is only a rough approximation of the actual flow conditions is obvious from inspection of Figure 13. It can be seen that the Bernoulli surfaces rotate on the order of 30° in the regions of secondary flow when the fluid traverses a 24° turning angle cascade.

By the very nature of an inviscid analysis, the stream-wise pressure gradient (i.e., the cascade pressure rise) must be neglected in a diffusing cascade. Since fluid initially near the wall enters the cascade with very small velocity and the main flow largely controls the cascade pressure rise, the low energy fluid must undergo an increase in its stagnation pressure to pass successfully through the diffusing channel. The essential energizing action normally occurs, in a real fluid, by momentum exchange (viscous and turbulent) with the main flow. In an inviscid, non-turbulent stream such momentum exchange is impossible; thus, some fluid close to the wall must flow backwards in violation of the assumed upstream boundary conditions. Indefinite accumulation of fluid in the blade passage violates the continuity condition. For these reasons, the inviscid

treatment of a diffusing cascade must be indeterminate unless the pressure rise is neglected or a finite velocity is allowed at the wall.

With only tentative knowledge of the importance of viscous forces and turbulent momentum exchange in the secondary flow phenomena, the possibility of a significant analytical attack on this problem is dubious at present.

Extension of the "Simple" Models

Until 1952 only the mechanism of secondary flow in simple passages was under investigation in the Gas Turbine Laboratory. With tentative understanding of that flow, some attention was directed toward other significant effects which may alter or even completely mask secondary flow patterns in a machine. Important additional considerations are:

1) End-leakage between blade end and wall.

2) Passage of a moving wall over the blade end.

3) Distortion of the flow field relative to the succeeding blade row.

4) Behavior of displaced fluid in a centrifugal force field.

5) Relative rotation of the fluid in a rotor passage.

6) Displacement of rotor blade boundary layers toward the blade tip. This action arises because the blade boundary layer fluid travels with a higher whirl velocity than that of the main stream. The boundary layer fluid is not, therefore, in radial equilibrium with the pressure field established by the bulk of the flow.
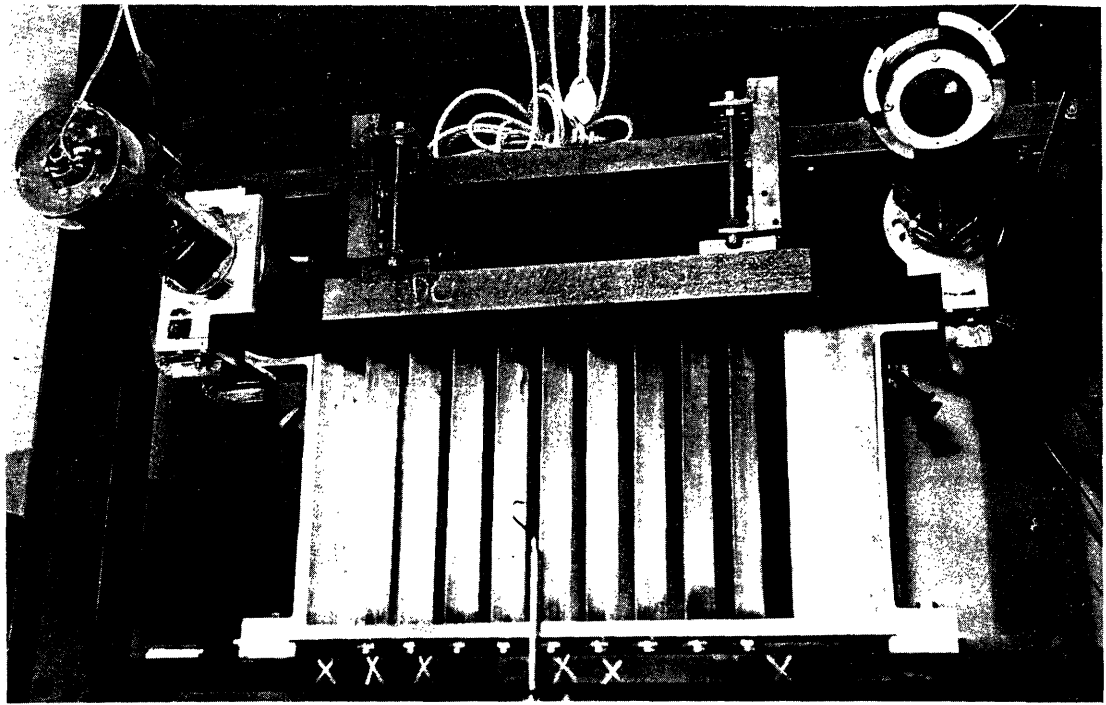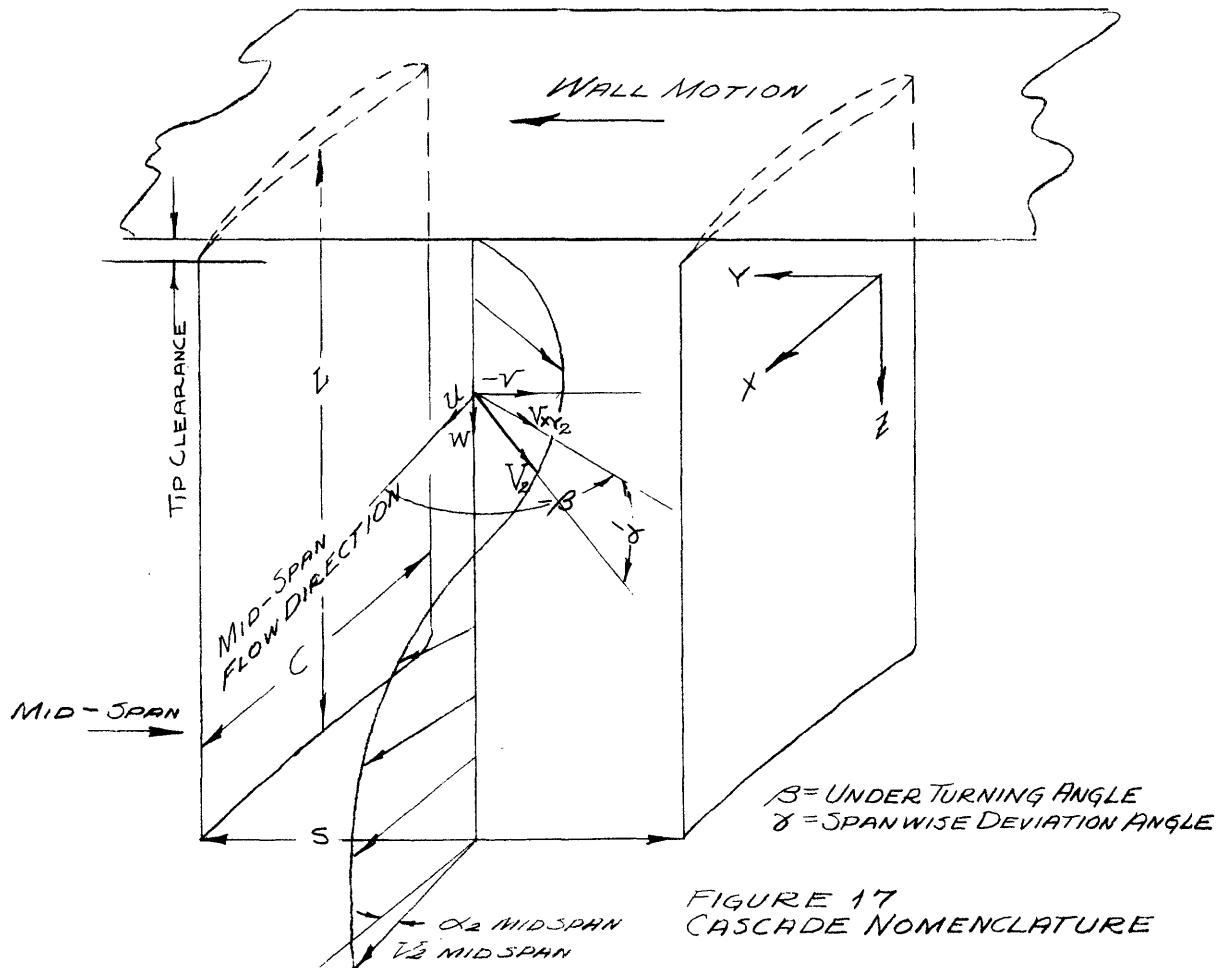
FIGURE 16 VIEW OF CASCADE SHOWING MOVING WALL MECHINISM

β = UNDER TURNING ANGLE
γ = SPANWISE DEVIATION ANGLE

FIGURE 17
CASCADE NOMENCLATURE

7) Influence of blades of non-uniform lift upon a three-
dimensional flow pattern.

Several of these phenomena can be investigated in the recti-
linear cascade; however, no final conclusions can be drawn concern-
ing interaction except by use of a rotating cascade. End clearance
and the influence of a moving wall were investigated by Lt.Cmdr.
Toline and Lt. Watson during 1952-53.

A single-stage, axial compressor has also been constructed and
is now in operation under the sponsorship of the Office of Naval
Research. It serves as a rotating cascade useful for penetration
into the general three-dimensional flow phenomena involving all of
the parameters listed above.

Cascade with Moving Wall and End Clearance

The end-clearance and moving-wall investigations were carried
out in the low-speed cascade wind tunnel with a set of nine blades
of 2.8-inch chord, pitch-chord ratio of 1.0, span of 16", with 40°
air inlet angle and 26° of turning. The profiles were NACA four-
digit series shapes applied to a circular arc camber line. Flow
velocity and Reynolds number were comparable to Van Le's tests.

End clearance was adjusted from 0 to 5/16" (i.e., 0 to 11.4%
of the chord). The boundary layer was generated on the tunnel wall;
it was about 1" thickness of the shape shown in Figure 22.

A sanding belt, driven by two high-speed motors, served ad-
mirably as a moving wall (Fig. 16). The belt develops a suction
between its back surface and a ground steel backing-plate; air
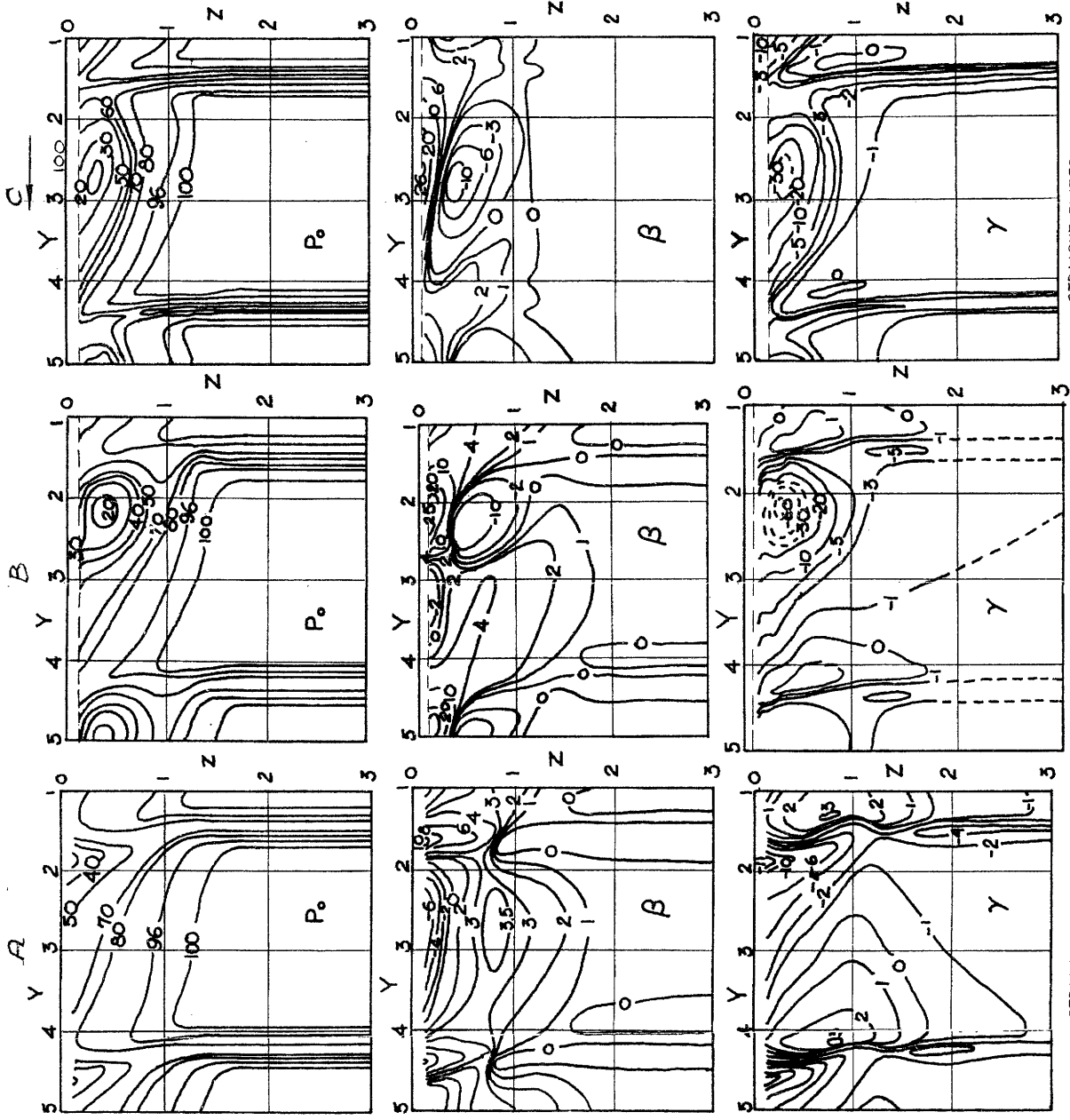lubrication develops above a surface speed of 50 ft/sec which floats

the belt free of the backing-plate. In this manner, a very flat moving surface of adjustable roughness can be driven at high velocity with moderate power consumption.

Toline and Watson's investigation was of a preliminary nature; data particularly lacking are flow conditions with various inlet boundary-layer conditions and various values of the flow parameter c_x/u (where c_x is the air velocity perpendicular to the plane of the cascade and u the blade speed). Tests were conducted with one boundary layer and a c_x/u of 0.87; further tests are reported in References (36) and (38).

Stagnation pressure, underturning angle, and spanwise deviation angle were measured at a (y-z) plane 1/2-chord length behind the trailing edges. Figure 17.

These data were plotted as contours of stagnation pressure, underturning angle and spanwise deviation angle on three plots after the manner of Van Le. Use of these plots requires considerable mental agility; superposition of three parameters at many points in a two-dimensional plane is required to form a mental picture of the flow. The difficulty of this process has led to misinterpretation of the data. In order to aid in comprehension, a vector plotting method was developed. Steel needles are thrust into a balsa (y-z) plane at each measuring point. The inclination of a needle indicates the local flow direction; its length, the magnitude of the local velocity. Circulation, secondary flow, blade wakes--all of the complicated flow pattern becomes visible.

Three comparable sets of data are presented in Figure 18.

BLADE CHORD 2.8" , PITCH 2.8" , LENGTH 16" , TURNING ANGLE 26° INLET ANGLE 40°

STRAIGHT BLADES
NO END CLEARANCE
STATIONARY WALL

STRAIGHT BLADES
4.5% CHORD END CLEARANCE
STATIONARY WALL

STRAIGHT BLADES
4.5% CHORD END CLEARANCE
MOVING WALL $C_x/U = 0.87$

P_o = RELATIVE STAGNATION PRESSURE $\dfrac{p_o - p_{ref.}}{p_{o(midspan)} - p_{ref.}}$

β= UNDERTURNING ANGLE

$\delta^\prime$= SPANWISE DEVIATION ANGLE
(+ TOWARD END OF BLADE)

FIGURE 18 A,B,C.

EXHAUST FLOW FROM A COMPRESSOR CASCADE INFLUENCE OF END CLEARANCE AND A MOVING WALL

Set A illustrates in greater detail than previously the flow pattern with no end clearance and a stationary wall. The complete flow field at a position 1/2-chord length behind the blade trailing edges may be reconstructed from the stagnation pressure, underturning angle and spanwise deviation angle plots. Further discussion of the flow pattern issuing from a "Simple" cascade is in order at this time.

A careful study of Figure 18A yields the following significant observations.

1) Secondary circulation was developed in the cascade and appears as an overturning of the flow close to the wall with a slight underturning at the exterior of the boundary layer. The flow proceeds toward the wall on the blade pressure surface and away from the wall on the suction surface. This pattern is to be expected from the previous consideration of the development of secondary vorticity.

2) Secondary circulation resulted in a displacement of boundary layer fluid toward the suction side of the passage. A marked thickening of the wall suction surface boundary layer results accompanied by a thinning of the wall pressure surface boundary layer. (Figure 22).

3) While not immediately evident in Figure 18A, an average thickening of the entire wall boundary layer results from the cascade pressure rise. This thickening

is evident in Figure 22 plotted from Figure 18A.

4) Blade wakes are readily identified; a slight dis-
placement of the wakes toward the suction side of
the passage near the wall is evident. Underturning
of the fluid discharged close to the wall immediately
off the pressure side of the blade may be observed.

5) Vorticity shed from the blade in the direction of
the flow is evident in the boundary layer, wake
region. The spanwise deviation angle plot shows the
resulting shearing flow in the blade wakes near the
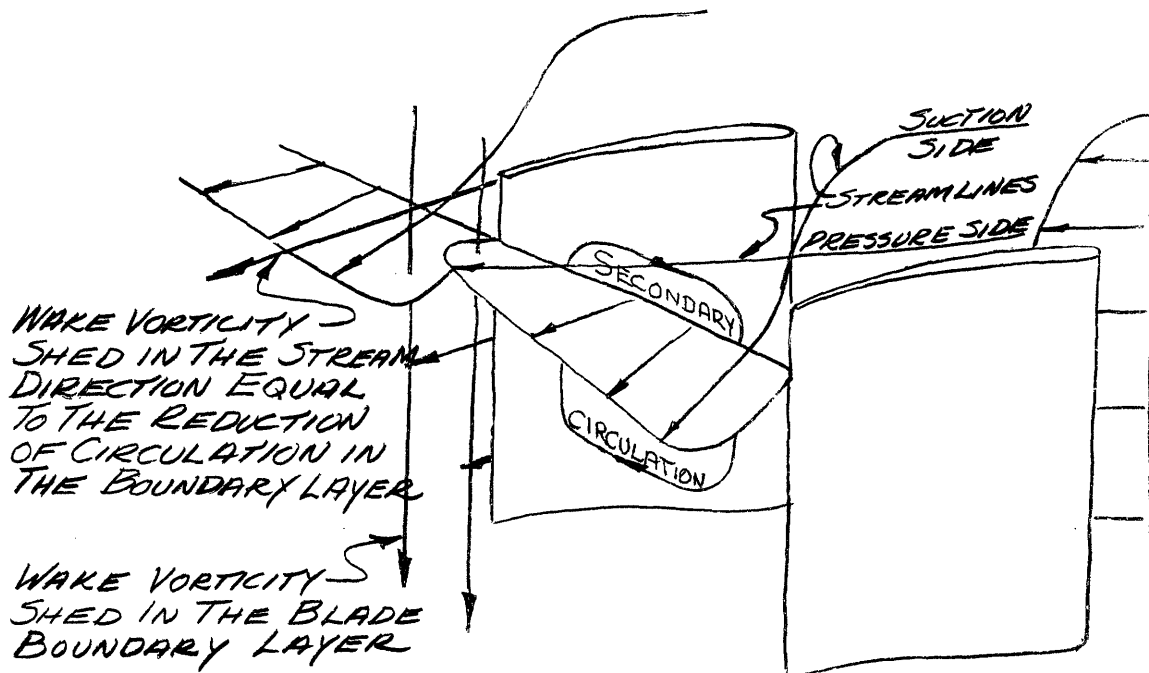wall. The wake pattern may be synthesized, as shown
in Figure 19.

Figure 19

Probably the most serious consequence of secondary flow is
the marked boundary layer thickening in the wall-suction surface

corner. In any real flow, with the stream velocity equal to zero at a bounding wall, some fluid must enter a diffusing cascade with a stagnation pressure lower than the final downstream pressure. Fig. 20.
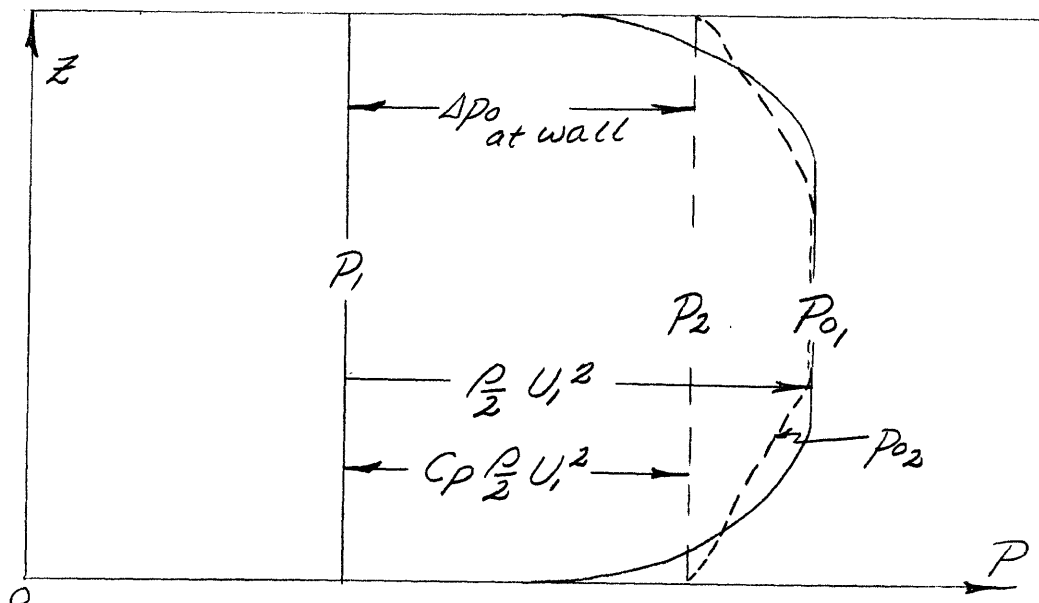
Figure 20

The deficient fluid cannot flow through the diffusion process unless the main stream energizes it by viscous or turbulent momentum exchange. If these energizing forces do not exert sufficient action, the deficient fluid will not successfully negotiate the pressure rise and must flow backwards. Such behavior is commonly termed "stall", in this particular case "wall stall", or "end stall". In case the energizing forces act sufficiently, a rise in stagnation pressure will be noted along interior streamlines with a decrease appearing in the exterior regions of the boundary layer and adjacent fluid of the main stream.

The maximum increase in stagnation pressure is found at the wall. The fluid in this region will rise in stagnation pressure in

an amount equal to the stream pressure rise through the diffusing
passage or,

$$\frac{\Delta P_0}{\rho/2\, U_1^2} = \frac{\Delta P}{\rho/2\, U_1^2} = C_P$$
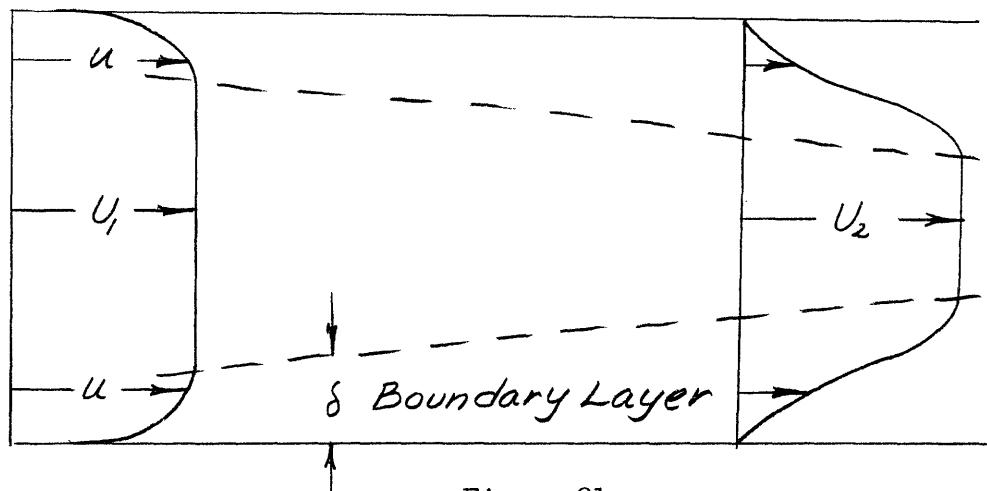
Figure 21

While the energizing action may successfully carry the low-energy
fluid against the pressure rise, this desirable result is not
achieved without a sacrifice.

A part of the main flow initially lying outside the original
boundary layer is de-energized and becomes a part of the final bound-
ary layer. The velocity profile of the thickened boundary layer
degenerates and the flow approaches separation as is indicated by an
increase in the magnitude of the shape factor H. Should this bound-
ary layer now face an additional pressure rise, its depreciated con-
dition will hinder further energizing action by the main stream;
separation will be more likely than before the original pressure
rise.

Returning to the cascade passage, inspection of Figure 22
demonstrates a severe deterioration of the wall suction surface
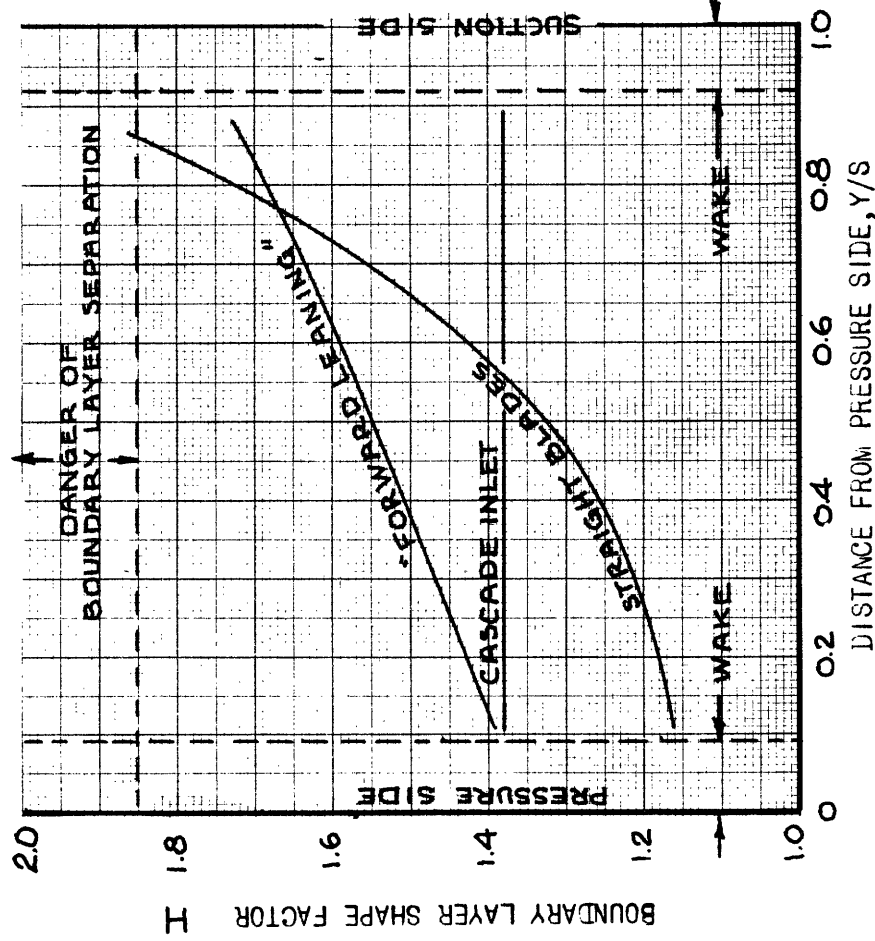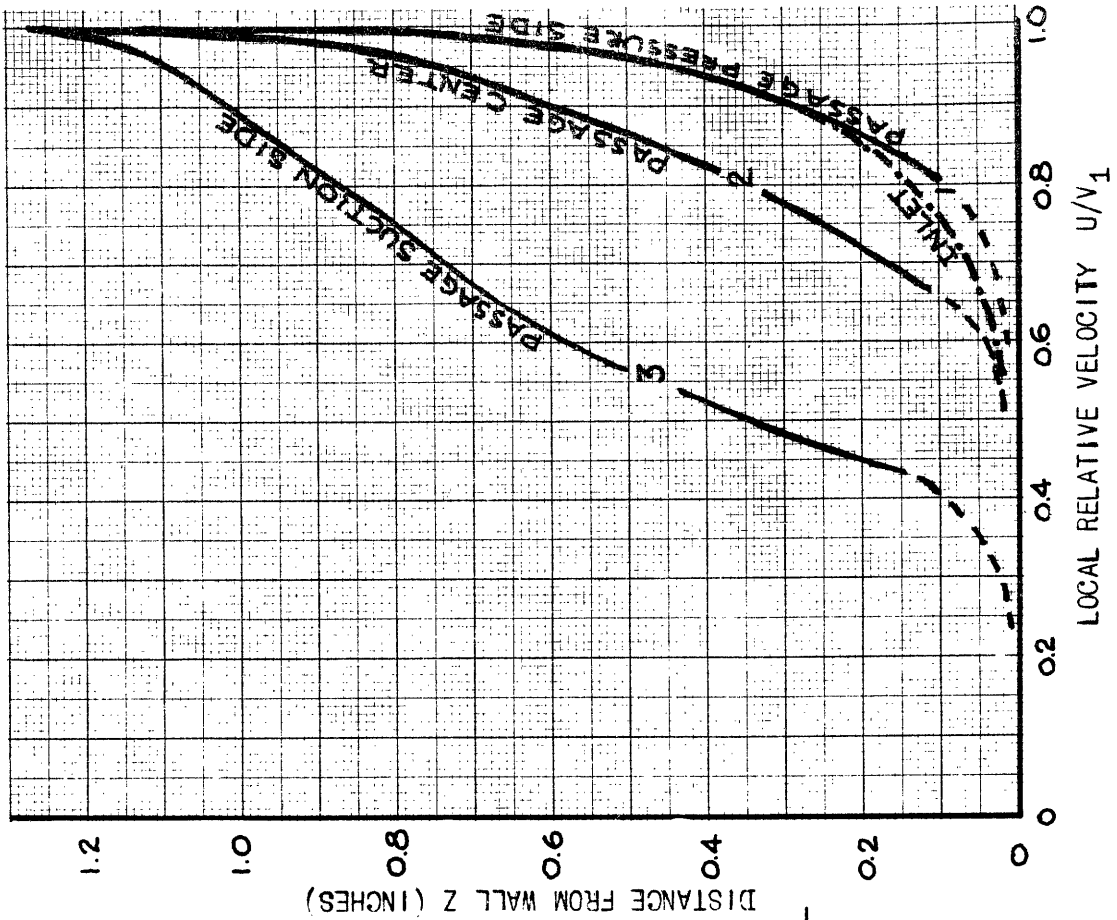
BOUNDARY LAYER VELOCITY PROFILES FOR STRAIGHT BLADES

BOUNDARY LAYER SHAPE FACTOR VS. TANGENTIAL POSITION

FIGURE 22

boundary layer. This deterioration is partially due to the cas-
cade pressure rise but is augmented greatly by the accumulation
of wall boundary layer fluid in this corner. A large tangential
variation of the displacement thickness, momentum thickness and
shape factor of the boundary layer was observed. Now, if this flow
is forced to traverse a still larger pressure rise--say, due to an
increase in incidence angle at cascade inlet--then one would expect
the flow to separate and travel backwards in the wall-suction cor-
ner. Conversely, it can be anticipated that this flow would
successfully negotiate a larger pressure rise before backflow
occurs if the boundary layer were in some way prevented from accu-
mulating in this corner.

In this discussion the words "separation", "stall" and back-
flow" have been freely employed. However, one must use care in
defining such breakdowns. The event we are concerned with in
speaking of separation is a disturbance in the boundary layer of
such a magnitude that it seriously alters the main flow. For
example, boundary layers are often greatly disturbed at local spots
on the wings of aircraft even under normal flight conditions.
These local disturbances are not usually called stall. It is the
point at which the disturbances affect the main flow to such an
extent that the wings can no longer lift the craft that we say
stall has occurred. Similarly, the definition of the onset of
stall or separation in a turbomachine is a subjective matter; the
seriousness of the effect of boundary layer disturbances on the
state of the main flow can only be evaluated in terms of overall
machine performance. The best we can do in a general investigation

is to describe flow geometry as exactly as possible and leave
the evaluation of the quality of the flow to the practitioner.

In all our measurements, we have always observed a region of
reversed flow on the wall as illustrated in Figure 24. Such flow
reversal probably occurs in all diffusing cascades and even in
regions of unfavorable pressure gradient and thick boundary layers
in accelerating cascades. As boundary layer conditions become
more degenerate and as the unfavorable pressure gradients in-
crease, the extent of this region of reversed flow will increase,
penetrating more deeply the main stream and involving a greater
quantity of fluid. Figure 23 presents a stagnation pressure plot
of the discharge from a diffusing cascade. Undoubtedly anyone
would describe this passage as "stalled".

It was noted above that a region of underturned fluid if found
in the proximity of the wake close to the wall. At first, this
observation seems anomalous in comparison to the strong secondary
overturning of the mass of the boundary-layer fluid. As was noted
before in conjunction with Figure 14, little change in pressure-
surface pressure distribution was measured on approach to the wall,
while the suction surface pressures fell off markedly. Although
pressure measurements could not be continued to the trailing edge,
a steep stream pressure gradient apparently existed between suction
and pressure surface at the trailing edge near the wall. Carbon-
black boundary-layer patterns (Figure 24) indicated that flow
separation can account for the lower stream pressure of the suction
surface discharge in comparison to the fluid streaming from the
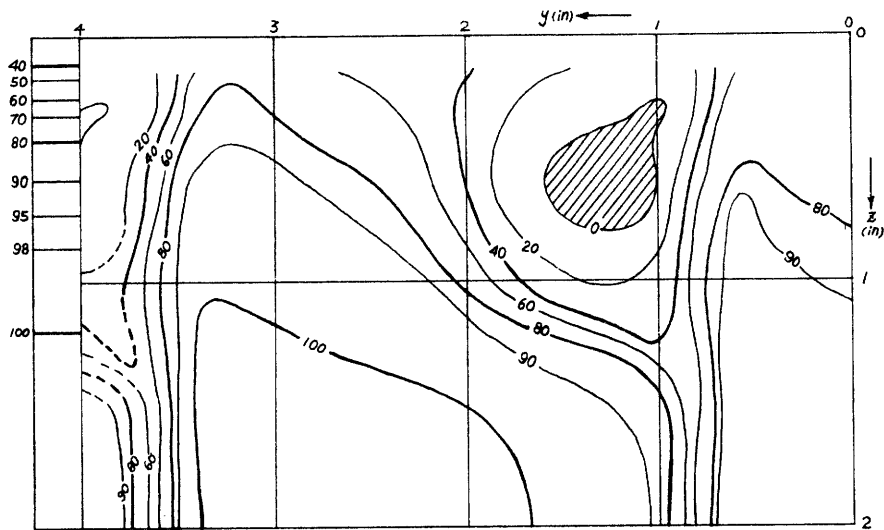
Figure 23 DISCHARGE BERNOULLI SURFACE PATTERN

(Constant lift blade tip)

CARBON-BLACK AND OIL WALL PATTERN

FIGURE 24

other side of the blade. The low pressure in this region can, in turn, account for the expansion and underturning of the pressure surface discharge. This sequence of events is schematically represented below.

The accumulation of wall boundary-layer fluid in the wall-suction corner and consequent flow separation will lead to increased dissipation in the passage as well as higher mixing losses downstream in comparison to a tangentially uniform boundary layer. After discharge from the blade row the distorted pattern from each passage must mix to a tangentially uniform stream in an analogous manner to the dissipation of the blade wakes. Coupled with these losses is an increased passage dissipation arising from the production of new boundary layer in the passage wall-pressure surface corner as the original boundary layer evacuates this region allowing high energy fluid to come in close proximity to the wall.

End-Clearance and a Moving Wall

To study the influence of end-clearance, Figure 18B presents data with 1/8" or 4.5% chord end-clearance and a stationary wall. The data of Set C resulted with 1/8" end-clearance and a wall moving from passage suction to pressure side, as in a compressor, at a velocity equal to the mid-span stream velocity.

Study of Figure 18 reveals that each of the modifications significantly altered the flow pattern at exit from the cascade. Consider the flow phenomena resulting from end-clearance. Two limiting patterns with variable clearance must be, first, the pattern already observed with zero clearance and, second, when the clearance becomes very large, that of a finite wing.

Progressively greater amounts of fluid leak between wall and blade as the clearance, the blade loading or the wall speed (of a compressor) are increased. Extending the behavior of a finite wing to this case would indicate that this leakage flow serves to unload the blade end producing larger adverse spanwise pressure gradients on the blade end surfaces. It would be anticipated from this view that end-leakage augments secondary flow, further deteriorating flow conditions on the suction surface and encouraging flow separation there.

In opposition to this view, it is proposed here that this model may be erroneous and that end-leakage may actually delay the "stall" of compressor passages. The strongest supporting evidence for this statement is found by comparison of Figures 18A, B and C. In Figures 18B and C the action of end-leakage

and a moving wall prevented the accumulating boundary-layer fluid from reaching the suction surface of the blade end. Relatively high energy fluid washes the end suction surface in comparison to the cascade with no end-clearance.

The diversion of accumulated boundary layer fluid from the suction surface may be explained in the following manner. The relatively high energy, end-leakage flow passes over the blade end and is discharged from the slit "nozzle" parallel to the wall at an angle between the cascade inlet and outlet angles. The high energy leakage flow penetrates toward the pressure side of the passage. At the same time, secondary flow is continuously drifting the original boundary layer fluid toward the passage suction side. Somewhere these counter flows must meet and oppose one another with a result that the low-energy secondary flow turns downward into the passage. The original boundary layer is turned back on itself and forms a discrete core or eddy of low-energy fluid removed from the blade suction surface. That the boundary-layer fluid is rapidly driven from the wall is indicated by spanwise deviation angles approaching -60° in Figure 18B. A schematic representation of this process is shown in Figure 25.

The action of the leakage flow may be likened to a scraper moving along the wall pushing the boundary layer ahead of it, diverting the secondary flow of boundary-layer fluid under it and out into the stream. A strong shear band between the leakage flow and the secondary flow can be observed in the underturning angle plots of Figures 18B and C.
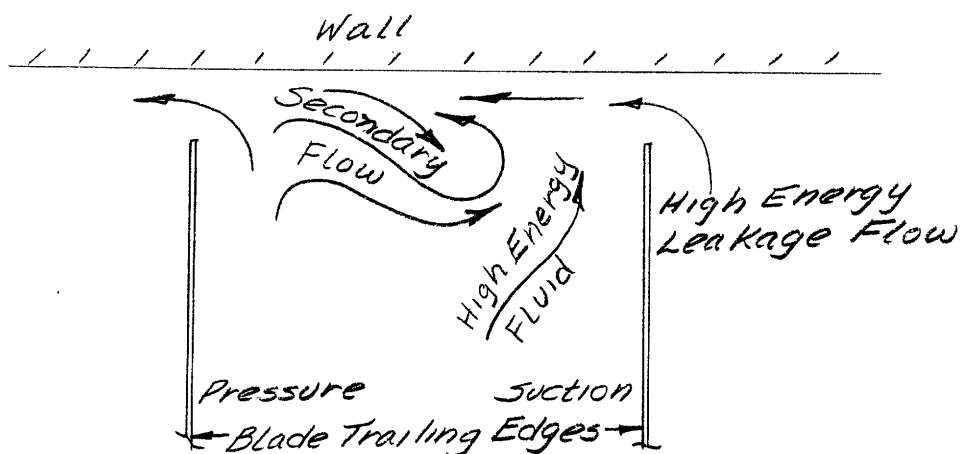
Figure 25

The folded accumulation of boundary layer fluid which, to be sure, contains some residual secondary circulation, has often been described as a discrete vortex.

Figures 18C show the flow pattern with the same end-clearance as before but now with a wall moving at mid-span velocity in the direction of the end-leakage. Note that the wall in this case is a contour of 100% relative stagnation pressure. The pattern is much the same as before except that the energizing action of the wall motion increases the tangential velocity and amount of leakage flow, thus injecting it at an angle closer to the tangential direction. As would be expected, the leakage flow penetrates further across the passage, stripping the accumulating low-energy fluid from the wall closer to the pressure side of the passage. Once again, the strong shear band between the leakage flow and low energy core is clearly apparent. A layer of fluid, moving with the wall, separates the secondary flow from the wall driving it downward into the stream, Figure 26. A still higher wall velocity should force the accumulation of boundary-layer fluid still
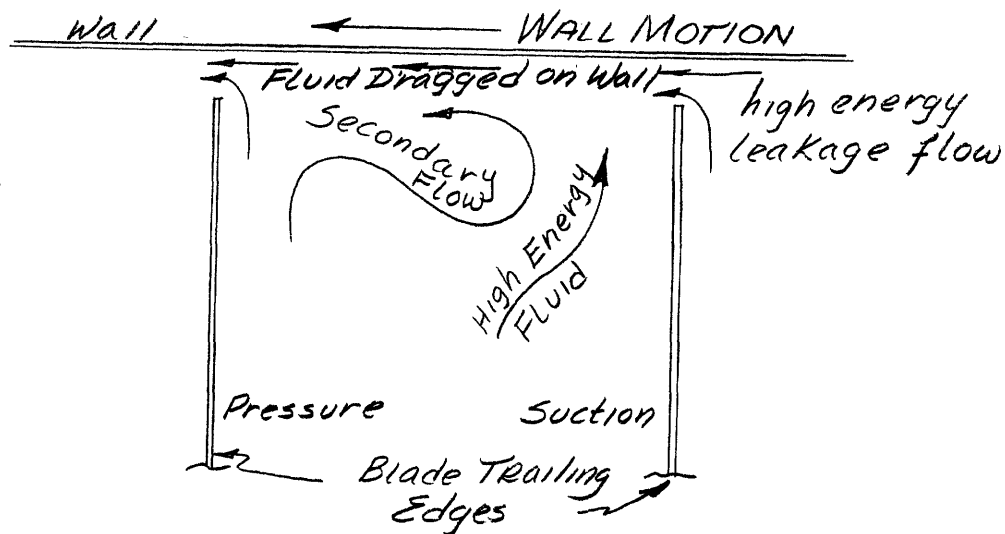
Figure 26

closer to the pressure side of the passage. This action probably

explains the "scraping effect" of wall motion, a term employed by

some investigators to describe similar data. But, it should be

noted, it was the end-leakage and fluid moving with the wall, not

the blade, which scraped the wall of its boundary layer. There

appeared no flow on the pressure surface directed away from the

wall as would be expected if the blades "scraped" the boundary

layer.

Before continuing, it may be of some value to speculate fur-

ther upon the nature of end-leakage and wall motion in compressors

and turbines.

Certainly, if the end-clearance becomes large in a compressor,

the flow pattern will approach that of a finite wing with dele-

terious effect on suction surface conditions. The relation be-

tween suction surface end-stall, end-clearance and velocity of

wall motion can be investigated by experiment. An analytical

attack may also be expected to yield useful information. Experimental removal of the stator shrouds in multi-stage compressors might also shed light on the action of end-leakage.

The discussion above does not include leakage under shroud sealing rings. Such leakage will usually re-enter the main stream normal to the flow thereby seriously harming the boundary layer. When considering leakage results for axial compressors, one must carefully examine the geometry of the leakage paths.

While we as yet have tested no accelerating (i.e., turbine) cascades, some predictions might be made from our previous results concerning the probable flow patterns.

Two important characteristics separate the three-dimensional flow phenomena of compressors and turbines. First, the turning angles of turbine passages are usually much larger than those of compressors. This fact leads to the anticipation of greater secondary vorticity development through turbine passages. However, the overall acceleration of the stream undoubtedly restricts fluid displacement to a smaller magnitude than in the compressor. Secondly, the wall motion in a turbine rotor proceeds from passage pressure to suction side thus augmenting secondary flow.

The exhaust flow from accelerating cascades of 45° turning angle has been observed by smoke tracing in Ref. 24 and by pressure measurements for a 90° accelerating elbow in Ref. 31. The discharge patterns near the wall were similar to the pattern observed by Eichenberger in the constant area bend at 90° turning angle. The accumulated boundary-layer fluid enters the main stream off

the suction surface. This penetration and the residual secondary circulation may be of sufficient extent to form a vortex of the discarded boundary layer fluid. This accumulation has been termed a "passage vortex"; its outstanding characteristic seems to be low energy rather than strong vorticity, but it may produce serious disturbances in the succeeding blade rows.

The action of secondary flow, especially when augmented by wall motion, deteriorates flow conditions on the blade suction surface and apparently leads to very low velocities or back-flow on the rear suction surface of even an accelerating passage. Secondary flow and the presence of adverse pressure gradients in this region can explain dirt marks on the wall and rear blade-end suction surface which usually indicate separation. While strong secondary flows lead to boundary layer separation, higher passage losses, and increased mixing losses downstream of a turbine blade row, they do serve to dump the wall boundary layer into the main stream, vigorously mixing the flow and preserving more uniform, more nearly design conditions, approaching the succeeding rotor. It is dubious, therefore, whether secondary flow is disadvantageous in a turbine or a compressor.

The need for more penetrating measurements of these phenomena is evident. Detailed measurements inside, as well as behind, accelerating and decelerating cascades are underway with varying C_x/u, tip clearance and boundary layer shape and thickness. Methods of determining local losses within the cascade and in the mixing region downstream are under investigation. The influence of secondary flow on boundary layer behavior and separation of

the boundary layer from blade surface and wall is under investigation with varying pressure rises through a passage.

The Influence of Three-Dimensional Flow in Axial Compressors

The ultimate purpose motivating these investigations of three-dimensional flow is the desire for a better understanding of the flow through fluid machinery. Deeper understanding will be decisive for further improvement of turbomachinery.

The present two-dimensional methods of analysis and design cannot offer all the insight necessary for the conception of optimum equipment. As compressors of higher pressure ratio per stage, greater flow velocity and improved efficiency are attempted or when one desires to further improve the efficiency of turbines, the two-dimensional model is inadequate to reveal the true flow pattern and all of the inherent design limits. Further, the simple two-dimensional model offers few avenues toward perfection, while even a qualitative understanding of the actual flow opens many pathways toward improvement.

Let us now examine some of the consequences of three-dimensional flow and possible improvements revealed by the previous qualitative description of the various phenomena. The entire subject may be conveniently split into two parts, passage phenomena and machine phenomena. The two parts, however, are not completely independent.

Passage Phenomena

The influence of an initial boundary layer and the resulting secondary circulation in a turning passage has been discussed.

The action may be summarized as follows. A wall boundary layer and the deleterious influence of secondary flow are responsible for "end-stall" at the extremities of compressor and turbine blading. If the boundary layer can be restricted in growth or removed, end-stall should be delayed or even eliminated entirely. However, if a boundary layer is unavoidable, a control of secondary displacement in the passage should delay end-stall. End-stall increases flow distortion and losses at the blade extremities. Secondary displacement exposes the wall to high velocity fluid increasing annulus drag and decreasing the machine efficiency.

To this point only rectilinear cascades have been under discussion. The presence of a centrifugal acceleration field in the whirling flow of a curvilinear blade row introduces significant, additional forces. Accompanying the centrifugal acceleration field are the centrifugal pressure gradients which are largely produced by the main stream. If low velocity fluid is displaced toward the axis of rotation from the outer casing, the main stream pressure gradient tends to increase the displacement. The boundary layer on the concave casing has but one stable distribution, spread uniformly on the wall. It follows then that a slight radial flow due to secondary circulation or end-leakage may be amplified and seriously alter the stream pattern on the entire blade surface as well as the pattern of the main flow. Evidence of such inward radial flow is found in Refs. 21, 22, and 32.

At the hub casing the situation is reversed; the main stream

pressure gradients tend to return displaced low velocity fluid to a tangentially uniform pattern.

The behavior of a boundary layer in a centrifugal pressure field can explain the observation that a stall at the outer casing of an axial machine often will influence detrimentally the entire flow passage while a stall at the inner casing produces a relatively smaller effect. These considerations also lead to the prediction that any pattern of distortion, such as stall propagation, will show greater stability upon the inner casing than upon the outer.

Especial consideration must be given to the three-dimensional flow through rotors. The flow pattern is influenced by secondary circulation; the centrifugal force field governs boundary-layer stability on the casings and greatly affects the direction of boundary-layer flow on the blade surfaces. In addition, the relative rotation of the fluid in the rotor passages, end leakage, the influence of a moving wall, and the fact that the relative inlet flow varies in time and space all offer the possibility of significant distortion.

The relative flow in a rotor presents a far more difficult problem than that of a stator. This problem has received little attention in the past. It is difficult, at this time, to predict the orders of magnitude of the various phenomena, much more so, to determine how they combine to produce the actual flow through a given rotor.

Stall propagation is suspected to play a decisive role in the failure of compressor blading. The propagation of this disturbance

depends upon the successive stall of blade passages. Since passages appear to stall first in the wall-suction surface corner and since secondary flow partially determines the incidence at which end-stall will occur, it seems reasonable that the stall propagation phenomena and secondary flow may be interrelated. An understanding of secondary flow should aid the investigation of stall propagation.

Machine Phenomena

End-stall in a blade passage has been designated arbitrarily as a passage phenomena although such behavior must produce perturbations along the entire flow path. Considerations, such as this, point to the necessity of evaluating any local stream distortion by examination of its influence along the entire flow path. The behavior of one blade row can deleteriously alter the performance of several succeeding rows. Also, it should be realized that the distortion generated in any blade row is largely a function of the extent of the distortion at inlet to that row. Thus poor behavior of the predecessors figuratively sets a bad example for the successors.

Except in the case of stall, the mere presence of a boundary layer is probably the most serious flow perturbation in turbomachines. The low velocity of the fluid in the proximity of the casings causes the flow field relative to any blade row, after the first, to be distorted in direction. The overturning due to secondary flows produce additional but less significant relative angular distortion. Figure 27 illustrates these effects.
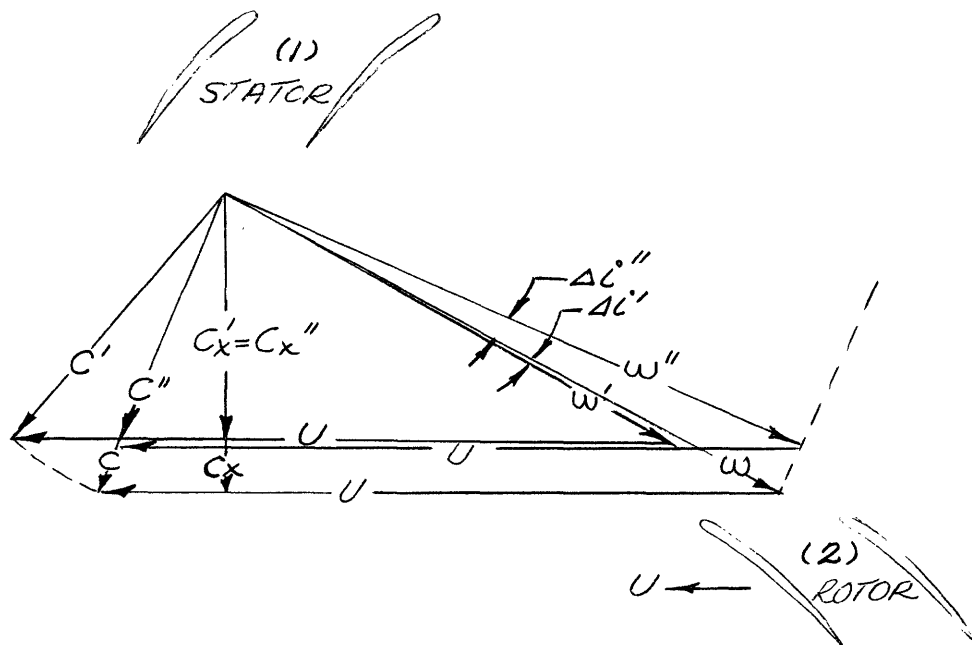
C = Design velocity and outlet angle
C' = Design velocity and underturned discharge
C" = Reduced outlet velocity and design outlet angle
$\Delta i'$ = Change in relative inlet angle to (2) due to variation between
       vector C and C'
$\Delta i"$ = Change in relative inlet angle to (2) due to variation from
       C to C"

Blade row (2) moves relative to (1) at speed U in direction shown.

Influence of Blade Row Discharge Perturbations on the
Flow Relative to the Succeeding Blade Row.

Figure 27

The influence of a boundary layer streaming from a compressor stator passage will increase incidence on the rotor blades due to reduced velocity and secondary overturning. The magnitude of the relative boundary-layer velocity is considerably closer to the free stream value in comparison to the reduction of absolute velocity in the boundary layer.

The increased incidence at rotor tip and root with the usual

velocity diagram will yield an increased change in tangential velocity across the rotor in these regions and consequently more work, and more stagnation enthalpy rise per unit mass of fluid. The consequence of this additional work, at first glance, would be an energizing of the boundary layer, a reduction in its thickness and a flattening of the velocity profile.

Since the stream pressure in the boundary layer is largely controlled by the main flow, an increase in velocity in the boundary layer, a flattening of the velocity profile, must be a result of increased stagnation pressure in the proximity of the casing. Even though a relatively larger rise in stagnation enthalpy must occur at the blade extremities, one cannot per se anticipate a relatively larger increase in stagnation pressure. The stagnation enthalpy rise and the stagnation pressure rise are related by the efficiency (i.e., degree of irreversibility) of the work process. Now, it is well known that the efficiency or dissipation of a blade row is a function of incidence angle, a particularly strong function if incidence angles greater than + or -5° are established. The rapidity of the rate of change of blade row efficiency at larger incidences is due to boundary layer separation and shocks. The severity of the depreciation of efficiency with increasing incidence is accentuated at increasing Mach number. Since the relative inlet angle to the rotor approaches 90° at the wall, large variations of incidence may be expected in the boundary layer.

One must inevitably conclude from these considerations that the self-energizing action of a boundary layer in passage through

the rotor will not be completely realized. The decrease in blade
efficiency will hinder an advantageous stagnation pressure rise
close to the wall; the boundary layer may not be significantly
energized. This conclusion is supported by the peaking tendency
of the axial velocity profile in multi-stage compressors as shown
in Figure 1 and by the "work done" or other experience factors which
must be applied to predict the reduced useful work of an actual
compressor from the two-dimensional calculations.

The mechanism described above can easily account for the rapid
thickening of the boundary layers on compressor casings.

In compressors, advantages might be gained by eliminating or
dumping the casing boundary layers. Nevertheless, the author is
now of the opinion that the boundary layers in compressors cannot
be dumped by secondary circulation without bringing about severe
end-stall and still lower compressor efficiency. There is the pos-
sibility, however, that the presence of end-leakage and a moving
wall in a compressor or some clever blade end modification might
allow dumping without encouraging end-stall. The tendence of any
fluid displaced from the outer casing to quickly seek the inner
casing must be remembered in considering the possibility of strip-
ping the boundary layers from the concave casing. A reduction in
boundary layer on the concave surface might make conditions suf-
ficiently poorer on the convex casing to once again produce an
overall reduction in performance.

To this point, in the present discussion, a uniform boundary
layer has been treated. Further consideration of a tangentially

skewed discharge boundary-layer pattern is in order. It has been demonstrated previously that the boundary-layer thickness may vary by a factor of 4 to 1 in the tangential direction behind a compressor stator. This flow pattern will result in a stream which varies with time both in direction and velocity relative to the rotor. As this unsteady flow passes through the rotor an average amount of work is done. It is problematical how the average work compares to that which would be done if the boundary layer were tangentially uniform. This effect awaits analytical treatment since it probably would be difficult to measure experimentally.

Above has been discussed the detrimental influence of a distorted three-dimensional flow pattern upon axial compressor performance. One more point of interest lies in the anomaly between the large flow distortions measured by Eichenberger in the simple bend and the relatively minor distortion measured in turbomachinery.

One must exercise caution in extrapolating the simple bend or cascade data to multi-stage machines. Other large disturbing phenomena besides secondary flow have been mentioned. In addition, the fluid passes successively through rotors and stators. The relative motion alters the flow pattern; it will chop up and largely disperse any configuration established in a single blade row. The influence of secondary flow through any multi-stage machine is very complicated; it is not understood at all clearly at present. However, we can predict favorable characteristics of multi-stage turbomachines, such as the relative motion, which may be largely responsible for their successful operation in view of all the large distorting forces acting on the fluid.

There is one configuration utilized in axial compressors which, in light of the previous data, should produce large secondary flow effects. This is the tandem stator in which two or three blade rows, all turning in the same direction, are placed together. The secondary distortion produced in one blade row will be directly magnified by the next since no relative motion chops the pattern. The resulting large-scale boundary-layer disturbance probably explains the poor performance delivered by such blading.

Control of Secondary Flow

It seems possible that the extremities of blades could be twisted to accept the relative flow angle of boundary-layer fluid if the flow conditions are predictable in design and if the boundary layer is tangentially uniform. The advantages of such modifications have been realized in the past; the design of end-modifications has been attempted. Seemingly desirable alterations have usually failed to improve, or have even reduced, machine performance. These results may be due to the fact that the boundary-layer conditions were not accurately predicted or that the tangentially skewed boundary layer cannot be treated as a smooth boundary layer of "equivalent" thickness. Also, the simple modification, underturning the stator ends to reduce the relative rotor incidence, actually encourages secondary flow in the stator and, therefore, a more severely distorted stator discharge pattern. The advantage of controlling secondary flow to prevent end-stall in compressors has been mentioned, but in the above considerations lies another advantage of secondary flow control applicable to

both compressors and turbines. If the skewing of the discharge boundary layer can be prevented, attempts to modify the rotor tips to accept the higher incidences in the boundary layer may be more successful. Should this be the case, more stagnation pressure rise possibly could be obtained at compressor rotor extremities thus energizing the boundary layer. While an attempt to repair a badly damaged velocity profile in one stage would surely lead to failure, it is possible that slight increases in work at the walls in each stage might prevent degeneration.

It has been definitely established that control of secondary flow can be achieved through simple blade-end modifications. (Ref.40) Slight control of secondary flow plus increased work in the boundary-layer region may produce a flow through multi-stage compressors free of the detrimental peaking behavior. If this result can be accomplished, the ability of the designer to predict machine performance accurately will be enhanced. In addition, higher efficiencies can be expected by operating the entire length of the blades at optimum conditions. By a delay of end-stall, a higher pressure rise per blade row should be feasible. The surge line of a compressor should move to lower mass flows, under these ideal conditions, thereby widening the operating region of the machine.

II. The Boundary Layer Problem

In Section I of this work, experimental data was presented which has led to a qualitative model of boundary-layer behavior in rectilinear, stationary, diffusing cascades.

Only through exhaustive experimentation could sufficient experimental data be gathered to reveal the important parameters governing three-dimensional boundary-layer behavior in such simple passages. The variables manipulated should include all the cascade geometry in addition to the characteristics of the approaching flow. Because an effort of many years' duration is just now beginning to produce a complete understanding of two-dimensional cascade performance, a generalized three-dimensional investigation can be predicted to require vast expenditures of time, effort and money. It is worthwhile, therefore, to run selected experiments as a guide toward the development of appropriate analytical models, to devise analyses of these models aimed toward revelation of the important parameters and then to test the analysis with as broad a spectrum of experiments as possible.

Such an attack has been followed in this investigation with the exception that conclusive tests of the theory have not been completed yet.

Three analyses are reported herein, based on three approximate models of different degrees of refinement. The purpose of these analyses is common to all--to reveal the physical parameters governing the state of the three-dimensional boundary layer. The

relationship between the state of the boundary layer and the onset

of separation is still more difficult to determine analytically and

is only discussed in general terms.

The General Problem

Given an inlet flow to a blade row of specified geometry,

one desires to determine the flow in the passage and the configu-

ration of the discharged stream. Several analyses are available

in the literature (3, 4, 5, 10, 26, 33) which predict secondary

flow velocities downstream of a blade row and one which predicts

fluid displacements (34). However, all neglect viscosity and

turbulence. Cases with a positive streamwise pressure gradient

may not be treated unless a substantial velocity is assumed at

the wall to allow any sort of solution. The necessary assumption

of finite wall velocity or the neglect of pressure gradients ap-

parently does not invalidate the solution for secondary velocities

in regions removed from the wall. However, all these solutions

break down deep in the boundary layer, that is, in the very regions

where flow geometry determines the onset of separation.

A three-dimensional, momentum analysis presented in Section V

is aimed at prediction of flow conditions deep in the boundary

layer. To include viscous, turbulent and streamwise pressure

stresses, a model must be constructed which compromises the analysis

of secondary flow in the outer regions of the boundary layer. How-

ever, since the purpose is to study conditions leading to separation,

this deficiency is not serious.

A less elaborate analysis of secondary flow is included in

Section IV which neglects viscous and turbulent shear stresses, but which includes all pressure stresses. This analysis is an attempt to produce analytical expressions and, through them, reveal important parameters. The common solutions of secondary flow patterns require relaxation or other numerical methods to arrive at a solution. Unless results are correlated from many calculations, little physical understanding is gained. Thus, even an inexact analytical expression should aid in an understanding of the problem.

To relate macroscopic boundary-layer behavior to passage and flow parameters, an analysis neglecting streamwise pressure gradients follows.

III. Bernoulli Surface Rotation, Boundary-Layer Thickening and Discharged Vorticity

Hawthorne's equation, expressing the rate of change of secondary vorticity along streamlines, is as follows;

$$V \cdot \Delta \left(\frac{\xi}{u} \right) = - \frac{2}{u} \left| \nabla \frac{P_0}{\rho} \right| \frac{\sin \phi}{R} \qquad (1)$$

or integrating along streamlines;

$$\Delta \left(\frac{\xi}{u} \right) = - 2 \int \frac{1}{u^2} \left| \nabla \frac{P_0}{\rho} \right| \frac{\sin \phi}{R} \qquad (2)$$

where terms are defined in Figure 4, Section I. This equation results from an application of Newton's laws to an incompressible, inviscid fluid steadily moving without body forces.

Supposedly, if one can neglect viscous and turbulent stresses and if one knew the path of the streamlines, the secondary vorticity could be calculated at each point. Or still better, one can apply this result in a stepwise manner and determine the streamline trajectories and secondary vorticity simultaneously. This latter attack has been undertaken by Ehrich and Detra and is reported in Reference 34. However, the analysis is still numerical; it does not readily reveal the governing physical parameters. A simpler model is required if one is to obtain analytical results.

The following model is employed here:

1) Streamlines are assumed to flow along sheets of constant stagnation pressure or Bernoulli surfaces.

2) The Bernoulli surfaces approach the turning passage parallel to the plane wall.

3) In transit through the passage, the Bernoulli sur-
faces rotate in such a manner that their inter-
sections with a cross section of the bend remain
straight lines.

4) Each Bernoulli surface rotates at an angular velo-
city calculated from Eqn. 1 which varies along
the passage but which is based on the inlet stag-
nation pressure gradient $\nabla (\frac{p_o}{\rho})$ at the appropriate
distance from the wall.

5) All the streamlines are assumed to follow the cur-
vature of the walls, here taken as concentric arcs.
The fluid is assumed inviscid, non-turbulent, in-
compressible in the absence of body forces and in
steady flow.

6) The streamwise pressure gradient is neglected. The
stream pressure gradient normal to the wall is
taken as zero; in other words, all pressure changes
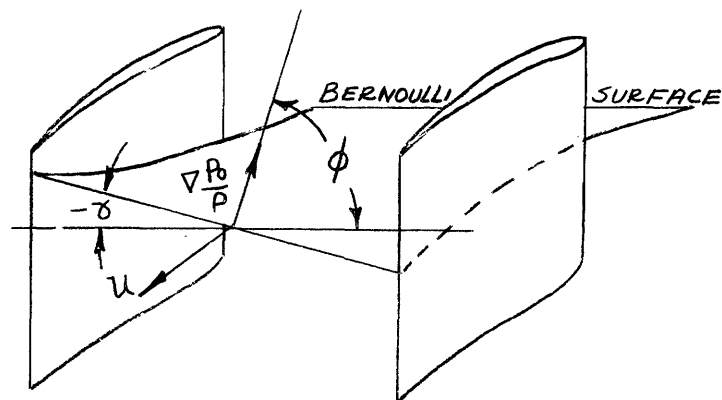are produced by the two-dimensional main flow.

Figure 29

Because it is assumed that the Bernoulli surfaces rotate in a simple manner and that changes in the variables R, $\nabla p_0/\rho$ and u are negligible, it is possible to integrate eqn. 14 for the angle of rotation of any Bernoulli surface. The vorticity component in the direction of the streamline will then be equal approximately to twice the angular velocity, ω, of the intersection line. Equation 1 in this case may be written as:

$$\frac{d}{ds}\left(\frac{\xi}{u}\right) = \frac{d}{ds}\left(\frac{2\omega}{u}\right) = -\frac{2}{u^2}\left|\nabla\left(\frac{p_0}{\rho}\right)\right|\frac{\sin\phi}{R} \tag{2}$$

We have assumed the stream pressure constant along any line normal to the wall and that the stagnation pressure varies only in this direction, accordingly:

$$\left|\nabla\frac{p_0}{\rho}\right| = \frac{d}{dz}\left(\frac{p}{\rho} + \frac{u^2}{2}\right) = u\frac{du}{dz} \tag{3}$$

If θ is the angle through which the streamline has turned, and $ds = rd\theta$, then:

$$\omega = \frac{d\phi}{dt} = \frac{d\phi}{ds}\frac{ds}{dt} = \frac{u}{R}\frac{d\phi}{d\theta} \tag{4}$$

Therefore, eqn. 2 may be expressed as:

$$\frac{d^2\phi}{d\theta^2} = -\left(\frac{R}{u}\frac{du}{dz}\right)\sin\phi \tag{5}$$

This equation is identical, except for the constant, to that of the simple pendulum.

The first integration of eqn. 5 proceeds directly after multiplying both sides by $d\phi/d\theta$:

$$\frac{d}{d\theta}\left(\frac{d\phi}{d\theta}\right)^2 = \left(\frac{2R}{u}\frac{du}{dz}\right)\frac{d}{d\theta}(\cos\phi) \tag{6}$$

Integrating:

$$\left(\frac{d\phi}{d\theta}\right)^2 - \left(\frac{d\phi}{d\theta}\right)_1^2 = \left(\frac{2R}{u}\frac{du}{dz}\right)(\cos\phi - \cos\phi_1)$$

But, in our model $(d\phi/d\theta)_1 = 0$ and $\phi_1 = \pi/2$, so

$$\frac{d\phi}{d\theta} = \pm\sqrt{\frac{2R}{u}\frac{du}{dz}\cos\phi} \tag{7}$$

We can predict that $d\phi/d\theta$ will be negative. Selecting the negative

value and separating, the second integration follows:

$$\int_1^2 d\theta = -\left(\frac{2R}{u}\frac{du}{dz}\right)^{-\frac{1}{2}}\int_1^2 \frac{d\phi}{(\cos\phi)^{\frac{1}{2}}} \qquad (8)$$

The right term is an elliptic integral which cannot be expressed

in terms of simple functions but can be evaluated by series expan-

sion. To facilitate such a solution, the angle γ between the

Bernoulli surface and the plane of the bend is employed instead

of ϕ.
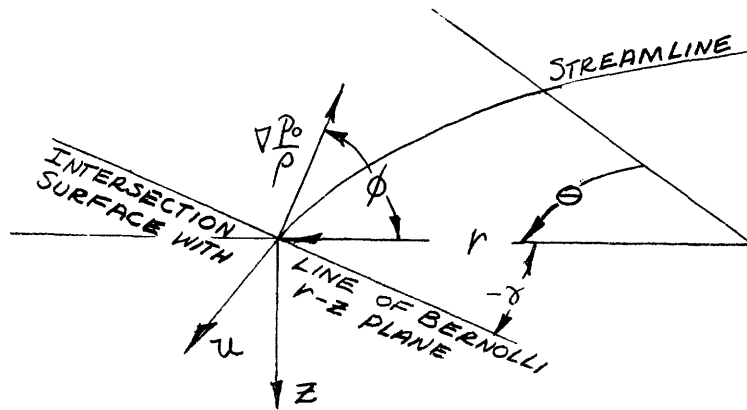
Figure 30

Since $\phi = 90 + \gamma$, $\cos\phi = -\sin\gamma$ and $d\phi = d\gamma$, then:

$$\left(\frac{2R}{u}\frac{du}{dz}\right)^{\frac{1}{2}}(\theta - \theta_1) = \int_1^2 \frac{d(-\gamma)}{\sqrt{\sin(-\gamma)}} \qquad (9)$$

Since γ will always be less than zero and cannot exceed

-90° without invalidating the model, the $\sin(-\gamma)$ always will

be positive and the square root real.

Now let us approximate $\sqrt{\sin(-\gamma)}$ by a double series

expansion.

$$Sin(-\gamma) = (-\gamma) - \frac{(-\gamma)^3}{3!} + \frac{(-\gamma)^5}{5!} - \cdots \tag{10}$$

Since $(-\gamma)$ will usually be less than one radian over most of a compressor passage, we need only employ the first two terms. Accordingly,

$$\left[Sin(-\gamma)\right]^{-\frac{1}{2}} \simeq \left[(-\gamma) - \frac{(-\gamma)^3}{3!}\right]^{-\frac{1}{2}} \tag{11}$$

which can be expanded by the binomial theorem.

$$\left[Sin(-\gamma)\right]^{-\frac{1}{2}} = (-\gamma)^{-\frac{1}{2}} + \frac{1}{12}(-\gamma)^{\frac{3}{2}} + \frac{3}{288}(-\gamma)^{\frac{7}{2}} + \cdots \tag{12}$$

Again, terms may be eliminated and only the first term retained as an approximation. The integral then becomes

$$\left(\frac{2R}{u}\frac{du}{dz}\right)^{\frac{1}{2}}(\theta - \theta_1) = \int_1 (-\gamma)^{-\frac{1}{2}} d(-\gamma) \tag{13}$$

Or

$$\left(\frac{2R}{u}\frac{du}{dz}\right)^{\frac{1}{2}}(\theta - \theta_1) = 2\left[(-\gamma)^{\frac{1}{2}} - (-\gamma_1)^{\frac{1}{2}}\right] \tag{14}$$

But, $\gamma_1 = 0$ and $\theta_1 = 0$, so

$$\gamma = -\frac{1}{2}\left(\frac{R}{u}\frac{du}{dz}\right)\theta^2 \tag{15}$$

which is the same result that would be obtained by substituting γ for ϕ and assuming cos $\gamma = 1$ before the first integration of eqn. 5. The above derivation, on the other hand, allows us to evaluate the error in the various approximations.

For circular arc blades of small turning angle, $R \simeq c/\varepsilon$, where c is the blade chord and ε the total turning angle. If δ is the boundary layer geometrical thickness, then the total angular rotation of the Bernoulli surfaces through the blade passage becomes

$$\gamma_2 = -\frac{\varepsilon}{2}\left(\frac{1}{\delta/c}\right)\left(\frac{1}{u}\frac{du}{dz/\delta}\right) \tag{16}$$

Assuming an exponential velocity profile:

$$\frac{u}{U} = \left(\frac{z}{\delta}\right)^{1/n}$$

equation 16 becomes:

$$\gamma_z = -\frac{\mathcal{E}}{2n}\left(\frac{1}{\delta/c}\right)\left(\frac{1}{z/\delta}\right) \tag{17}$$

It can be seen from eqn. 17, for a given turning angle $\mathcal{E}$, profile shape n and boundary layer thickness δ/C, that the rotation of the Bernoulli surfaces increases on approach to the wall. Likewise, at a given position in the boundary layer z/δ, the rotation increases as the boundary layer becomes thinner. This latter result can explain the violent secondary flows observed in turbine nozzle passages even when the inlet boundary layer is vanishingly thin.

As a test of the validity of eqns. 16 and 17 for small turning angle passages with relatively thin boundary layers, Bernoulli surface rotation is calculated for the compressor cascade investigated by Van Le (Reference 5). Figure 13, Section I, presents measured Bernoulli surface configuration at the cascade discharge. The average slope of each Bernoulli surface was estimated graphically; these estimates are plotted in Figure 31. Approximation of the average slope of the Bernoulli surface becomes increasingly difficult on approach to the wall.

The Bernoulli surface rotation was calculated first from eqns. 16, taking R as $c/\mathcal{E}$ and determining $\frac{1}{u}\frac{du}{dz}$ for each Bernoulli surface from the shape of the inlet velocity profile shown in Figure 14, Section I.

Second, an exponential velocity profile was fitted to the measured inlet boundary layer. While the fit was only approximate,
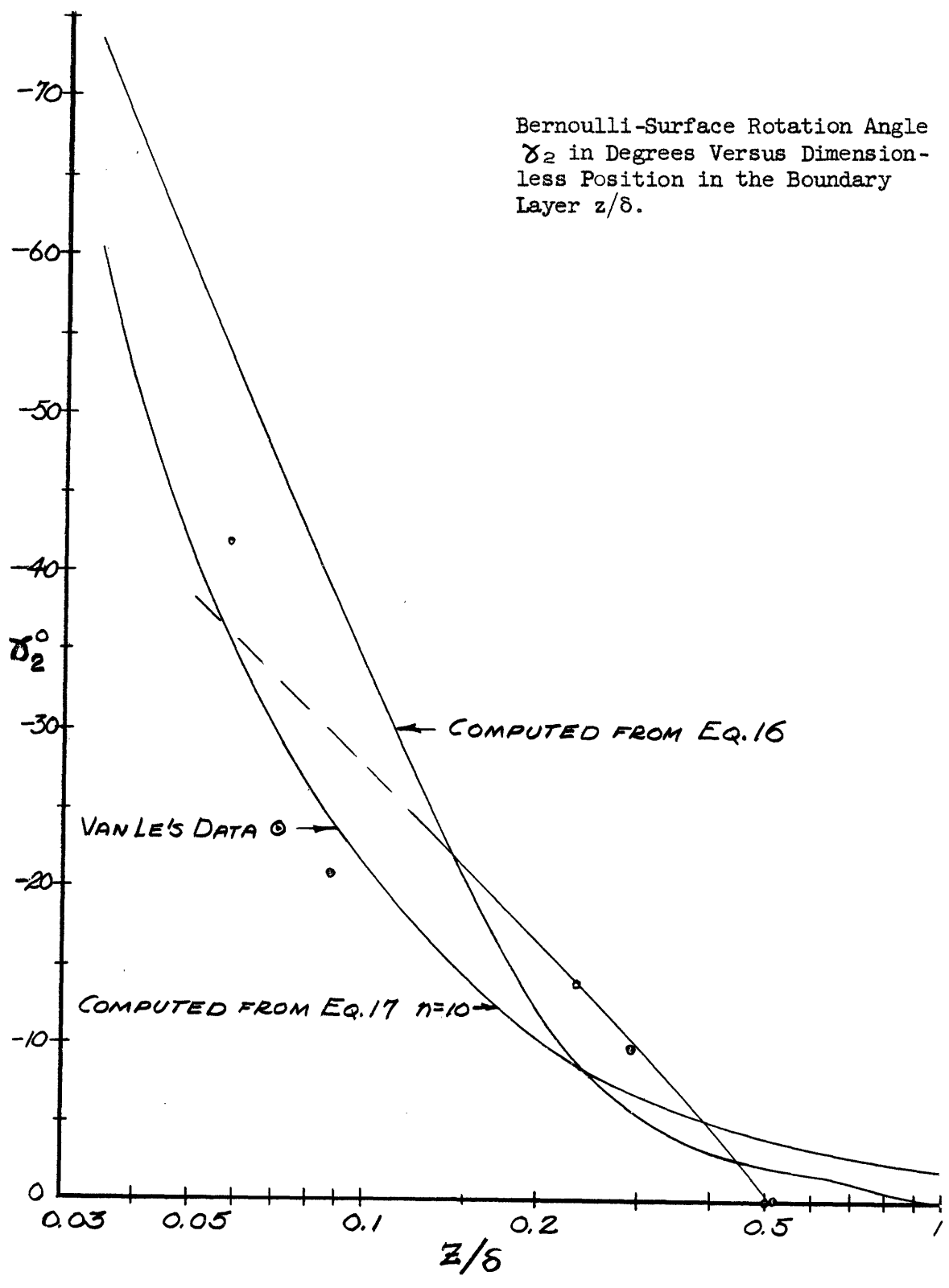
Bernoulli-Surface Rotation Angle γ_2 in Degrees Versus Dimensionless Position in the Boundary Layer z/δ.

Figure 31

a value of n = 10 produced the best representation. For this exponent, δ_2 was calculated as a function of z/δ from eqn. 17 and plotted in Figure 31.

Both equations predict correct orders of magnitude and trends through most of the boundary layer. The discrepancy in the outer region of the boundary layer is due, undoubtedly, to the three-dimensional nature of the boundary constraint. Fluid suffering a large y displacement close to the wall accumulates in the wall-suction corner after evacuating the wall-pressure corner. These large mass transfers deep in the boundary layer force the main stream away from the wall on the suction side and toward the wall on the pressure side of the passage, thus producing a sizable rotation in fluid possessing a small stagnation pressure gradient. The analysis above cannot take this effect into account.

Close to the wall, the boundary constraint hinders rotation of the Bernoulli surfaces and causes them to bend. Fluid friction also retards the development of strong, secondary circulation near the wall.

The experiments of Van Le which produced the data employed in this comparison were not designed to yield accurate boundary layer velocity profiles or even an accurate and detailed pattern of the Bernoulli surfaces. Significant discrepancies can arise between the theory and data from this source. To better test this analysis, more appropriate measurements could be undertaken.

It follows, that the lack of close agreement between theory

and data is not surprising. The agreement is sufficiently close, however, to tentatively accept eqns. 16 and 17 as expressive of the relationship between boundary layer skewing and the parameters describing the turning passage and approaching flow.

The analysis will not predict the pattern of the discharged Bernoulli surfaces, except for their slope, since motion of the secondary flow toward the suction side sweeps the Bernoulli surfaces in that direction at an increasing rate on approach to the wall. The wall constraint also forces Bernoulli surfaces in the vicinity of the wall to assume a bent configuration. This behavior is of course not predicted by eqn. 18. However, at the outer edge of the boundary layer, secondary velocities parallel to the wall are small; the Bernoulli surfaces remain essentially flat, and thus appear to rotate about the center of the passage. This simple behavior allows us to make further use of eqn. 17 to predict overall boundary-layer thickness as a function of the distance across the passage.

From the assumed geometry of rotation, the z-deflection of a streamline is $\Delta z = y\Delta \gamma$, where y is measured from mid-passage. The maximum and minimum z-deflections of the streamlines on any Bernoulli surface are given by:

$$\Delta \left(\frac{z}{\delta}\right)_{\substack{max.\\min.}} = \pm \frac{s/\delta}{2} \Delta \gamma \tag{18}$$

where s is the blade pitch.

A value for $\Delta \gamma$ at the center of the original boundary layer ($z/\delta = 0.5$) is chosen as indicative of the average skewing of the boundary layer. The change in boundary-layer thickness $\Delta \delta$ then

can be expressed by:

$$\frac{\Delta\delta}{\delta} = \pm \frac{\epsilon}{4}\left(\frac{s}{c}\right)\left(\frac{\delta}{c}\right)^{-2}\left(\frac{1}{u/U}\frac{du/U}{dz/\delta}\right)_{\frac{z}{\delta}=0.5} \tag{19}$$

or for an exponential profile:

$$\frac{\Delta\delta}{\delta} = \pm \frac{\epsilon}{2n}\left(\frac{s}{c}\right)\left(\frac{\delta}{c}\right)^{-2} \tag{20}$$

Examination of eqns. 19 and 20 reveals that, for a given velocity profile shape, a reduction in tangential skewing can be obtained by reducing the turning angle and the pitch-chord ratio and increasing the relative boundary-layer thickness. The characteristics of this equation should be remembered whenever one considers the flow through blade rows which receive a thin boundary layer. The nature of the secondary boundary-layer thickening might partially explain poor behavior of inlet guide vanes in axial compressors. It would be interesting to examine wall boundary-layer configurations discharged from such blade rows. An experimental study of boundary-layer behavior in a diffusing passage with varying inlet boundary-layer thickness is planned.

Finally, as an example of the magnitude of secondary boundary-layer thickening, consider a typical compressor blade row with $\epsilon = 25°$, s/c = 1, and a flow approaching with n = 7 and δ/c = 0.25. The percentage thickening of the boundary layer on the suction side of the passage amounts to 50% according to eqn. 20.

Vorticity Distribution at Discharge

In order to arrive at a vorticity distribution at cascade discharge, eqn. 15 is converted to relate the angle ϕ to flow and cascade geometry.

$$\phi = \frac{\pi}{2} - \frac{1}{2}\left(\frac{1}{\delta/c}\right)\left(\frac{1}{u}\frac{du}{dz/\delta}\right)\frac{\Theta^2}{\varepsilon} \qquad (21)$$

This expression may be placed in eqn. 2, giving:

$$\frac{d\xi}{d\Theta} = -2\frac{du}{dz}\sin\left[\frac{\pi}{2} - \frac{1}{2}\left(\frac{1}{\delta/c}\right)\left(\frac{1}{u}\frac{du}{dz/\delta}\right)\frac{\Theta^2}{\varepsilon}\right] \qquad (22)$$

Or

$$\frac{d\xi}{d\Theta} = -2\frac{du}{dz}\cos\left[\frac{1}{2}\left(\frac{1}{\delta/c}\right)\left(\frac{1}{u}\frac{du}{dz/\delta}\right)\frac{\Theta^2}{\varepsilon}\right] \qquad (23)$$

Expanding the cosine in series:

$$\frac{d\xi}{d\Theta} = -2\frac{du}{dz}\left[1 - \frac{1}{4}\left(\frac{1}{\delta/c}\right)^2\left(\frac{1}{u}\frac{du}{dz/\delta}\right)^2\frac{\Theta^4}{\varepsilon^2} + ..\right] \qquad (24)$$

Integrating:

$$\xi_2 - \xi_1 = -2\frac{du}{dz}\Big|\Theta - \frac{1}{20}\left(\frac{1}{\delta/c}\right)^2\left(\frac{1}{u}\frac{du}{dz/\delta}\right)^2\frac{\Theta^5}{\varepsilon^2} + ..\Big|_{\Theta_1}^{\Theta_2} \qquad (25)$$

All series terms beyond the first will be neglected for small

turning angle passages. Since $\xi_1 = 0, \Theta_1 = 0, \Theta_2 = \varepsilon$, we get:

$$\xi_2 = -2\frac{du}{dz}\varepsilon \qquad (26)$$

Further, it may be shown from Ref. 35 that

$$V \times \Omega = \nabla\frac{P_0}{\rho} \qquad (27)$$

for a steady, incompressible, inviscid flow. For the model in

use:

$$|V \times \Omega| = |u\eta_1| = |\nabla\frac{P_0}{\rho}| = u\frac{du}{dz} \qquad (28)$$

a vector perpendicular to the original Bernoulli surface by de-

finition. The variable η_1 is the resultant vorticity vector at

inlet which is parallel to the wall and normal to the streamline.

The discharge vorticity then becomes:

$$\xi_2 = -2\eta_1\varepsilon \qquad (29)$$

which is a special case of the result derived by Squire and

Winter (3). To facilitate appreciation of the relation, eqn.26,

it is put in the terms employed previously:

$$\xi_2 = -\frac{2U}{\delta}\left(\frac{du/U}{dz/\delta}\right)\varepsilon \qquad (30)$$

Or assuming an exponential profile:

$$\zeta_2 = -\frac{2U}{\delta n} \frac{\mathcal{E}}{(z/\delta)^{(n-1)/n}} \tag{31}$$

Thus, for a given profile shape $n(>1)$ and a given position in the boundary layer z/δ, ζ_2 increases directly as $\mathcal{E}$ and inversely as the boundary layer thickness. It follows, that one should expect the strength of a vortex formed in a large turning-angle passage to increase as the inlet boundary layer becomes thinner or as the turning angle increases. Compressor inlet guide vanes probably shed discrete passage vortices, as do turbine nozzles, since the inlet boundary layer usually is very thin.

IV. Boundary-Layer Stream-Line Trajectories

As mentioned previously, all secondary-flow solutions to date have neglected streamwise pressure gradients. No one has claimed that the error so introduced is negligible, only that inclusion of this pressure gradient makes the conventional equations difficult to solve. The analysis that follows takes an approximate model which, with some simplification of the boundary-layer equations, allows a solution including all pressure stresses. Viscous and turbulent stresses are neglected. If this neglect is not serious throughout most of the boundary layer, the results should demonstrate the influence of pressure changes along the stream.

The Model

Assumptions:

1) The flow is incompressible, inviscid, non-turbulent, and steady.

2) The streamlines of the boundary layer and main flow proceed on flat sheets parallel to the lower plane wall of the bend. This assumption implies that the pressure gradient normal to the wall is zero (i.e., the main flow determines all pressures).

3) The main flow travels between concentric walls and all its streamlines rotate about the center of curvature of the passage. At each angular position the radial distribution of velocity in the bulk of the fluid is that of a free vortex. Each level of the boundary layer is assumed to enter the bend with a free-vortex, radial-velocity distribution.

4) The curved walls of the passage are assumed to exert
no constraint on the radial motion of the boundary-
layer fluid. The outer and inner walls can be con-
sidered as a line source and a line sink, respectively,
supplying or withdrawing fluid at a rate sufficient
to eliminate wall interference. In an actual passage,
if the secondary flow does not become too violent,
fluid from the outer wall boundary layer descends
this wall into the outer edge of the plane wall
boundary layer, while fluid displaced to the inner
curved wall apparently escapes without difficulty
into the boundary layer of that wall. (See Eichen-
berger's data, Figure 6 , Section I.) These obser-
vations suggest that this assumption should be fairly
accurate for a real fluid in regions removed from the
curved walls of a passage with less than 40° of turn-
ing.

5) The pressure gradient is imposed on the bulk of the
flow by divergence or convergence of the upper wall
or by mass removal or addition through that wall.
This upper wall is assumed to be far removed from
the lower plane wall under consideration. The imposed
tangential pressure gradient $\frac{\partial p}{\partial \theta}$ is assumed to be only
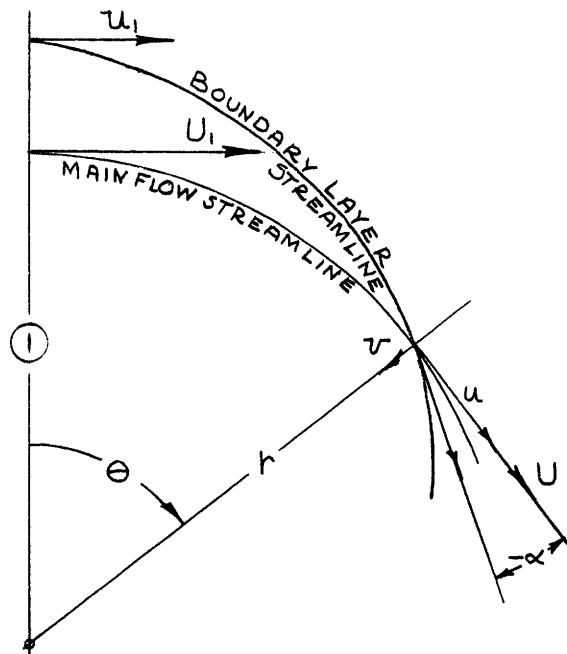a function of radius.

Figure 32

The Main Flow

From assumption 3:

$$Ur = K = f(\theta) \qquad (32)$$

Assumption 1 assures that the stagnation pressure of the main

flow remains constant,

$$P_0 = P + \frac{\rho}{2} U^2 = constant \qquad (33)$$

The tangential equation of motion of the main flow in this case

can be written as:

$$\frac{UV}{r} + \frac{U}{r}\frac{\partial U}{\partial \theta} + V\frac{\partial U}{\partial r} + W\frac{\partial U}{\partial z} = -\frac{1}{\rho r}\frac{\partial P}{\partial \theta} \qquad (34)$$

where U, V, W are the tangential, radial and normal (to wall) velo-

city components, respectively. Since the streamlines proceed on

circular arcs of radius r parallel to the plane wall, V = W = 0.

Then we have,

$$\frac{1}{2}\frac{\partial U^2}{\partial \theta} = -\frac{1}{\rho}\frac{\partial P}{\partial \theta} \qquad (35)$$

The same equation would result from differentiation of eqn.33.

For the radial direction,

$$-\frac{U^2}{r} + \frac{U}{r}\frac{\partial V}{\partial \theta} + V\frac{\partial V}{\partial r} + W\frac{\partial V}{\partial z} = -\frac{1}{\rho}\frac{\partial P}{\partial r} \tag{36}$$

But

$$\frac{\partial V}{\partial \theta} = \frac{\partial V}{\partial r} = \frac{\partial V}{\partial z} = 0$$

so

$$\frac{U^2}{r} = \frac{1}{\rho}\frac{\partial P}{\partial r} \tag{37}$$

Taking the partial derivative of eqn. 37 with respect to θ and

changing the order of integration on the right gives:

$$\frac{1}{r}\frac{\partial^2 U}{\partial \theta^2} = \frac{1}{\rho}\frac{d}{d\theta}\left(\frac{\partial P}{\partial r}\right) = \frac{1}{\rho}\frac{d}{dr}\left(\frac{\partial P}{\partial \theta}\right) \tag{38}$$

Inserting eqn. 35 into eqn. 38:

$$-\frac{2}{r}\frac{\partial P}{\partial \theta} = \frac{d}{dr}\left(\frac{\partial P}{\partial \theta}\right) \tag{39}$$

But, we have assumed $\frac{\partial p}{\partial \theta} = f(r)$, so:

$$\frac{d}{dr}\left(\frac{\partial P}{\partial \theta}\right) = -\frac{2}{r}\left(\frac{\partial P}{\partial \theta}\right) \tag{40}$$

Integrating and letting C_1 be the constant of integration,

$$\frac{\partial P}{\partial \theta} = \frac{C_1}{r^2} \tag{41}$$

To determine the velocity distribution, we can write the partial

differential, eqn. 35, as:

$$\frac{\partial U^2}{\partial \theta} = -\frac{2}{\rho}\frac{C_1}{r^2} \tag{42}$$

Integrating eqn. 42 with respect to θ:

$$U^2 = -\frac{2C_1\theta}{\rho r^2} + f(r) \tag{43}$$

But from eqn. 32, $(Ur)^2 = f(\theta)$, so

$$f(r) = \frac{C_2}{r^2} \tag{44}$$

Inserting eqn. 44 into eqn. 41,

$$(Ur)^2 = C_2 - \frac{2C_1\theta}{\rho} \tag{45}$$

At $\theta = 0$, $U = U_1$ and $U_1 r = K_1$, making $C_2 = (U_1 r)^2 = K_1^2$. Finally,

the main stream velocity distribution results in the form:

$$U^2 = U_1^2 - \frac{2C_1\theta}{\rho r^2} \tag{46}$$

where C_1 is determined by a specified value of $\frac{\partial p}{\partial \Theta}$ at a given radius. It is useful to note that for this model, if $\triangle p$ is the stream pressure change along any streamline of the main flow from the initial conditions to a line at $\Theta = \mathcal{E}$ and, if we define the pressure coefficient C_p as

$$C_p = \frac{\triangle p}{\frac{1}{2}\rho U_1^2} \tag{47}$$

where U_1 is the initial velocity on a given streamline, then C_p is only a function of Θ. This is true since $\frac{\partial p}{\partial \Theta}$ = constant at a given radius and

$$\triangle p = \frac{\partial p}{\partial \Theta} \Theta = \frac{C_1 \Theta}{r^2} \tag{48}$$

From eqn. 47, since $(U_1 r)^2 = K_1$,

$$C_p = \frac{C_1 \Theta}{\frac{1}{2}\rho (U_1 r)^2} = \frac{2 C_1}{\rho K_1^2} \tag{49}$$

The Boundary Layer

Assumptions 1 and 2 assure, for the boundary layer, that the stagnation pressure will be constant along boundary-layer streamlines although the constant will vary with z or,

$$p_o' = p + \frac{\rho}{2}\left(u^2 + v^2 + w^2\right) = p_{o_1}' = f(z) \tag{50}$$

where p_o' is the stagnation pressure, p the stream pressure, and u, v and w the tangential, radial and normal velocity components, all at a given point in the boundary layer. p_{o_1}' is the initial value of the stagnation pressure for the streamline passing through that point.

At this stage, it is worthwhile to note that this model, by ignoring viscous and turbulent stresses, will suffer a collapse of the analysis for fluid close to the wall in a diffusing passage. This difficulty is discussed in Section I; this difficulty also

casts doubt on any boundary-layer analysis which ignores the shear stresses. However, we are seeking the effect of a pressure gradient on streamline trajectories so, later on, we shall neglect the fluid close to the wall and only apply the analysis to fluid which initially possesses enough velocity to negotiate, unaided, the given pressure rise. Inclusion of the shear stresses gives rise to a three-dimensional equation, perhaps insoluble, but in any event undoubtedly requiring numerical solution, thus, losing its value here. A momentum-control surface analysis is more appropriate for this task; such an attack is presented in the next Section.

To proceed, the dynamic, continuity and condition of irrotationality equations are written with the normal velocity w and the normal pressure gradient $\frac{\partial p}{\partial z}$ equal to zero, as follows:

$$\frac{uv}{r} + \frac{u}{r}\frac{\partial u}{\partial \theta} + v\frac{\partial u}{\partial r} = -\frac{1}{\rho r}\frac{\partial p}{\partial \theta} \tag{51}$$

$$-\frac{u^2}{r} + \frac{u}{r}\frac{\partial v}{\partial \theta} + v\frac{\partial v}{\partial r} = -\frac{1}{\rho}\frac{\partial p}{\partial r} \tag{52}$$

$$\frac{1}{r}\frac{\partial u}{\partial \theta} + \frac{\partial v}{\partial r} + \frac{v}{r} = 0 \qquad \text{(continuity)} \tag{53}$$

$$\frac{1}{r}\frac{\partial v}{\partial \theta} - \frac{\partial u}{\partial r} - \frac{u}{r} = 0 \qquad \text{(irrotationality)} \tag{54}$$

The absence of all shear stresses implies the condition of two-dimensional irrotationality in all planes of flow parallel to the wall.

Now, we further assume that

$$\frac{\partial v}{\partial \theta} << \frac{\partial u}{\partial r} \tag{55}$$

a good assumption if the secondary flow does not become too violent.

Then from eqn. 54

$$\frac{\partial u}{\partial r} \simeq -\frac{u}{r} \tag{56}$$

Integrating with respect to r

$$ur = k = f(\theta) \tag{57}$$

Inserting eqn. 56 into eqn. 51, we get

$$\frac{\partial u^2}{\partial \theta} = -\frac{2}{\rho}\frac{\partial p}{\partial \theta} \tag{58}$$

Since $\frac{\partial p}{\partial \theta}$ is the same in all parts of the boundary layer as in the

main stream by assumption 2, insertion of eqn. 41 into eqn. 58 and

integration with respect to θ gives

$$u^2 = f(r) - \frac{2}{\rho}\frac{C_1\theta}{r^2} \tag{59}$$

But, by eqn. 57, $(ur)^2 = f(\theta)$, so

$$r^2 f(r) = C_3 \tag{60}$$

and eqn. 59 becomes:

$$u^2 = \frac{C_3}{r^2} - \frac{2}{\rho}\frac{C_1\theta}{r^2} \tag{61}$$

But at $\theta = 0$, $u = U_1$ and $U_1 r = k_1$ so,

$$(ur)^2 = k_1{}^2 - \frac{2}{\rho}C_1\theta \tag{62}$$

or,

$$u^2 = u_1{}^2 - \frac{2C_1\theta}{\rho r^2} \tag{63}$$

which is a form analogous to the distribution of the main stream

velocity, eqn. 46.

Consideration of eqns. 58 and 41 shows $\frac{\partial u^2}{\partial \theta}$ equal to a con-

stant at a given radius. It follows that

$$\Delta u^2 = -\frac{2}{\rho}\frac{\partial p}{\partial \theta}\Delta\theta \tag{64}$$

But $\frac{\partial p}{\partial \theta}\Delta\theta = C_p \frac{\rho}{2} U_1{}^2$ so eqn. 64 becomes

$$(u_2{}^2 - u_1{}^2) = -U_1{}^2 C_p \tag{65}$$

Now, let us find the value of u_1 for which $u_2 = 0$ at the end of a

given dimensionless pressure rise Cp. Setting $u_2 = 0$, it can be

seen that this analysis is valid only if

$$\left(\frac{u}{U}\right)_1 \gtreqless C_p^{1/2} \tag{66}$$

This limit, in combination with the inlet velocity profile, deter-

mines the depth into the boundary layer which can be treated by

this model. This depth is a constant with radius at $\theta = 0$ since

Cp is independent of radius and

$$\left(\frac{u}{U}\right)_1 = \frac{u_1 r}{U_1 r} = \frac{k_1}{K_1} \tag{67}$$

will be constant at a given z level.

To proceed, eqn. 53 is inserted into eqn. 52 and the result

combined with eqn. 37 by assumption 2, giving:

$$\frac{u}{r}\frac{dv}{d\theta} - \frac{v^2}{r} - \frac{v}{r}\frac{du}{d\theta} = -\frac{1}{r}\left(U^2 - u^2\right) \tag{68}$$

Now, since the flow is steady and $u = \dfrac{r d\theta}{dt}$

$$v = \frac{dr}{dt} = \frac{dr}{d\theta}\frac{d\theta}{dt} = \frac{u}{r}\frac{dr}{d\theta} \tag{69}$$

then,

$$\frac{dv}{d\theta} = \frac{d}{d\theta}\left(\frac{u}{r}\frac{dr}{d\theta}\right) = \frac{u}{r}\frac{d^2r}{d\theta^2} + \frac{1}{r}\frac{du}{d\theta}\frac{dr}{d\theta} - \frac{u}{r^2}\left(\frac{dr}{d\theta}\right)^2 \tag{70}$$

Inserting eqn. 70 into eqn. 68, with $r = f(\theta)$ only, gives

$$\frac{d^2r}{d\theta^2} - \frac{2}{r}\left(\frac{dr}{d\theta}\right)^2 + r\left(\frac{U^2}{u^2} - 1\right) = 0 \tag{71}$$

This equation is non-linear and must be linearized by assuming

$(\frac{dr}{d\theta})^2 = 0$ to be soluble. Since $\frac{dr}{d\theta} = r\,\frac{v}{u}$, this neglect probably

will not introduce significant errors if the secondary flow is not

violent (i.e., if $v \ll u$ or if the boundary layer streamlines do

not diverge by large angles from the direction of the main stream).

Equation 71 then becomes

$$\frac{d^2r}{d\theta^2} = r\left(\frac{U^2 - u^2}{u^2}\right) = 0 \tag{72}$$

which is soluble provided u does not diminish to zero along the

path of integration.

Inserting eqns. 46 and 63 for U and u , we get.

$$\frac{d^2r}{d\Theta^2} + r \left[\frac{(K/k)_1^2 - 1}{1 - 2C_1\Theta/\rho k_1^2} \right] = 0 \tag{73}$$

Letting

$$B \equiv \left(\frac{k}{k}\right)_1^2 - 1 = f(z) \qquad D \equiv \frac{2C_1}{\rho k_1^2} = f(z) \tag{74}$$

equation 73 finally takes the form,

$$\frac{d^2r}{d\Theta^2} + r \left(\frac{B}{1 - D\Theta} \right) = 0 \tag{75}$$

On any plane of flow B and D are constants, so we can integrate eqn. 74 for the trace of a streamline. The equation, in its general form, cannot be integrated directly, but if D = 0 (i.e., $\frac{\partial p}{\partial \Theta}$ = 0), the solution for the constant pressure case is readily obtained.

The Constant Pressure Case

$$\frac{d^2r}{d\Theta^2} = -Br \tag{76}$$

This equation has two solutions depending on the sign of B (i.e., whether $\left(\frac{U}{u}\right)_1$ is greater than or less than 1. The case for $\frac{U}{u}$ less than 1 will be described later and applies when the boundary layer fills the passage).

For B > 0:

$$r = C_1 \sin B^{\frac{1}{2}}\Theta + C_2 \cos B^{\frac{1}{2}}\Theta \tag{77}$$

$$\frac{dr}{d\Theta} = B^{\frac{1}{2}} \left(C_1 \cos B^{\frac{1}{2}}\Theta - C_2 \sin B^{\frac{1}{2}}\Theta \right) \tag{78}$$

The initial conditions for this model are at $\Theta = 0$, $r = r_1$, $\alpha = \alpha_1$. Inserting these in eqns. 77 and 78 determines

$$C_2 = r_1 \qquad C_1 = B^{-\frac{1}{2}} \left(\frac{dr}{d\Theta}\right)_1 = B^{-\frac{1}{2}} r_1 \tan\alpha_1 \tag{79}$$

Therefore:

$$\frac{r}{r_1} = \cos B^{\frac{1}{2}}\Theta + \left(B^{-\frac{1}{2}} \tan\alpha_1 \right) \sin B^{\frac{1}{2}}\Theta \tag{80}$$

$$\tan\alpha = -\frac{r_1}{r} \left(B^{\frac{1}{2}} \sin B^{\frac{1}{2}}\Theta - \tan\alpha_1 \cos B^{\frac{1}{2}}\Theta \right) \tag{81}$$

For $B < 0$:

$$r = C_3 e^{|B|^{\frac{1}{2}}\theta} + C_4 e^{-|B|^{\frac{1}{2}}\theta} \tag{82}$$

$$\frac{dr}{d\theta} = |B|^{\frac{1}{2}} \left(C_3 e^{|B|^{\frac{1}{2}}\theta} - C_4 e^{-|B|^{\frac{1}{2}}\theta} \right) \tag{83}$$

With the same initial conditions as previously,

$$C_3 = \frac{1}{2} r_i \left(1 + |B|^{-\frac{1}{2}} \tan\alpha_i \right) \tag{84}$$

$$C_4 = \frac{1}{2} r_i \left(1 - |B|^{-\frac{1}{2}} \tan\alpha_i \right) \tag{85}$$

Then eqns. 82 and 83 become,

$$\frac{r}{r_i} = \frac{1}{2}\left(e^{|B|^{\frac{1}{2}}\theta} + e^{-|B|^{\frac{1}{2}}\theta} \right) + \frac{|B|^{-\frac{1}{2}}\tan\alpha_i}{2} \left(e^{|B|^{\frac{1}{2}}\theta} - e^{-|B|^{\frac{1}{2}}\theta} \right) \tag{86}$$

$$\tan\alpha = \frac{r_i}{r} \frac{|B|^{\frac{1}{2}}}{2} \left[\left(e^{|B|^{\frac{1}{2}}\theta} - e^{-|B|^{\frac{1}{2}}\theta} \right) + |B|^{-\frac{1}{2}}\tan\alpha_i \left(e^{|B|^{\frac{1}{2}}\theta} + e^{-|B|^{\frac{1}{2}}\theta} \right) \right] \tag{87}$$

Or,

$$\frac{r}{r_i} = \cosh |B|^{\frac{1}{2}}\theta + |B|^{-\frac{1}{2}}\tan\alpha_i \sinh |B|^{\frac{1}{2}}\theta \tag{88}$$

$$\tan\alpha = \frac{r_i}{r} \left(|B|^{\frac{1}{2}} \sinh |B|^{\frac{1}{2}}\theta + \tan\alpha_i \cosh |B|^{\frac{1}{2}}\theta \right) \tag{89}$$

At present, the only data available to test the validity of this constant pressure analysis is that of Eichenberger (Fig. 7, Section 1); however, more appropriate measurements are in progress. Eichenberger's bend flow does not fit this model too well because, in all his experiments, the boundary layer filled the entire channel. The boundary layer, therefore, was by no means thin compared to the dimensions of the apparatus. It is not valid in this case to assume that $\frac{\partial p}{\partial z} = 0$; nevertheless, it is interesting to note that no variation in stream pressure could be measured in the z-direction across the flow (4). A further difficulty arises from assuming that the flow outside the boundary layer establishes the pressures

throughout the fluid. In Eichenberger's case, there is no "outside" to the boundary layer. To circumvent this difficulty in a test of this analysis, it will be assumed that the pressures of the entire flow are a function of the bulk mean velocity $\overline{U}$.

The flow investigated by Eichenberger to test his theory (4) will be employed here. A triangular velocity profile was fed into the bend. Both comparisons were effected at 30° bend angle along a z-line at the mean radius of the bend.

From the measured inlet stagnation pressure map, shown in Figure 33, $\frac{\overline{U}}{u}$ was calculated and tabulated as a function of z .* At a number of arbitrary z values, eqns. 81 and 89 (depending on the sign of $B = (\frac{\overline{U}}{u})_1{}^2 - 1)$ were utilized to calculate α at 30° bend angle. Then, determining the magnitude of the resultant velocity vector from Eichenberger's measurements of stagnation pressure over the 30° cross section, Figure 34, the radial secondary component v of the velocity vector was calculated at each of the chosen z-positions. The results are plotted in Figure 35 which shows, in addition to the measured data, the results of Eichenberger's theoretical calculations.

Figure 35 demonstrates that this analysis predicts orders of magnitudes and trends of the secondary flow quite well. The three-dimensional nature of the flow, resulting primarily from the very

----

*For this case, Eichenberger does not state in his report (4) the value of the reference pressure against which he measured stagnation pressures or the value of the stream pressure at each cross section. However, these values were stated for a different inlet velocity profile. It was assumed, here, that the measurements were made against the same reference pressure and that the stream pressure variation along the bend was identical in each case. This assumption can lead to error in converting Figures 33 and 34 to the velocity profiles necessary for this analysis. Such error may be responsible, in part, for the lack of close agreement between the results of eqn. 80 and eqn. 88 and the experimental data.
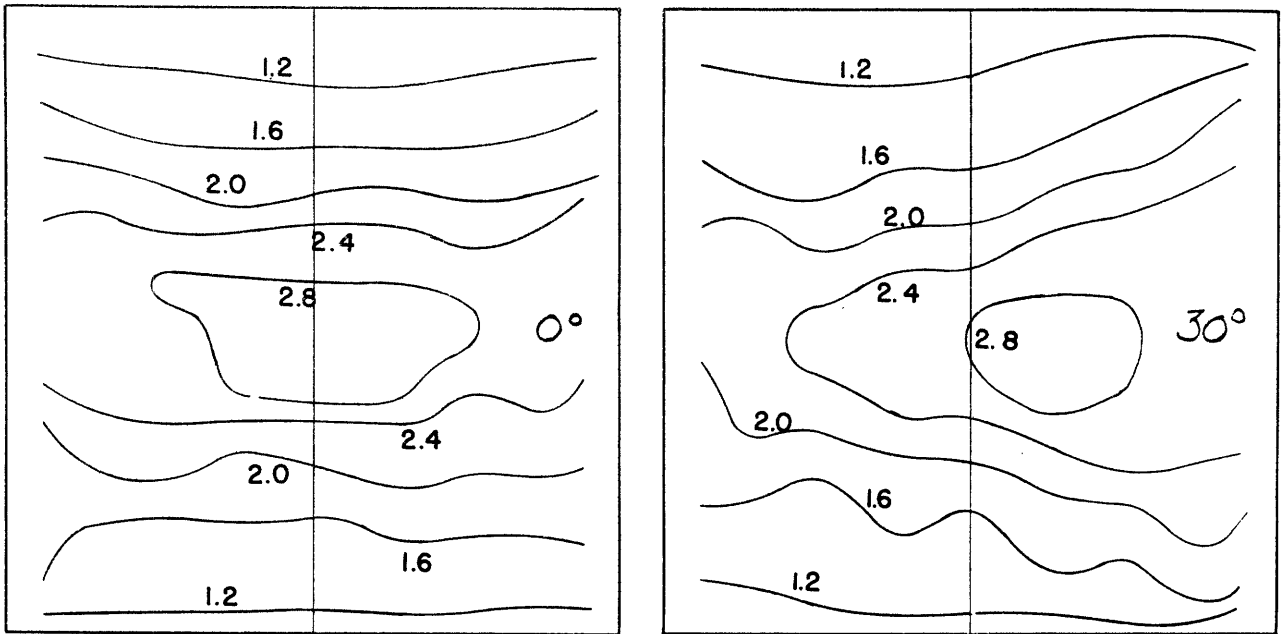
Figures 33 and 34:   STAGNATION PRESSURE CONTOURS from reference 4

at 0° and 30° bend angle. Stagnation pressures
in inches of water above reference pressure.
Bend 8" x 8" square; inside of bend at left.

SECONDARY FLOW VELOCITY

Radial Component v vs. Distance
from Wall z - for Eichenberger's
Bend with a Linear Inlet Velocity
Profile. Velocities shown are at
30° bend angle and mean radius.
Values computed from eq. 81 and
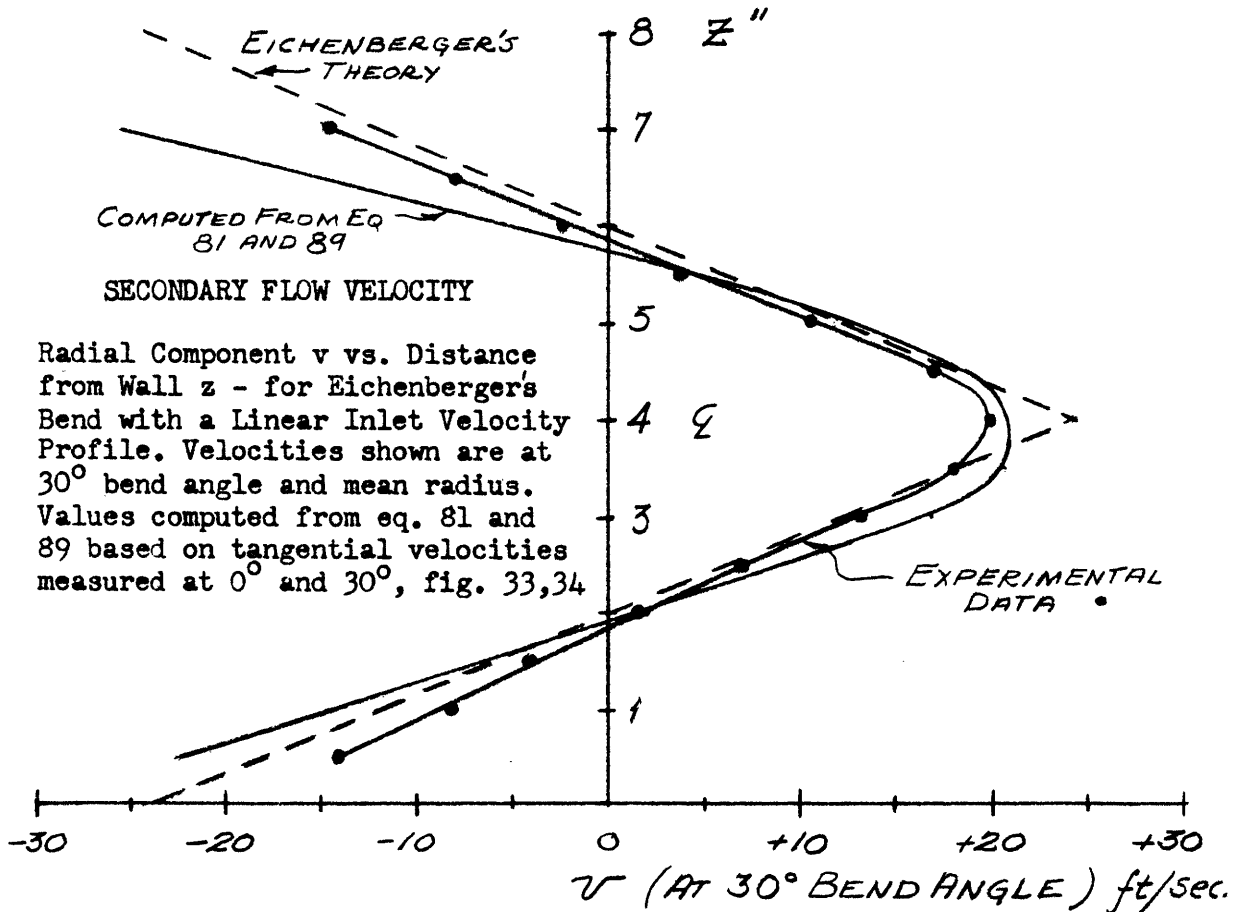89 based on tangential velocities
measured at 0° and 30°, fig. 33,34

Figure 35

thick boundary layer, probably is responsible for most of the discrepancy in regions removed from the wall. One might account for the discrepancies, particularly in the regions close to the wall, by the neglect of shear stresses in the analysis. However, Eichenberger's inviscid theory fits the data better than the present analysis indicating the falsity of this explanation.

Another potential source of discrepancy is due to the fact that the calculations were based on flow conditions at 0° bend angle. The secondary flow was assumed to commence at this point. But, inspection of Figure 7a, Section I, reveals an established secondary flow at 0° bend angle. This observation is not surprising since any subsonic flow will commence its adjustment from a linear pattern to a curvilinear pattern ahead of the turning passage. For this reason the calculations should be based on flow conditions several channel widths upstream of the 0° section. Neither this data nor flow angles at 0° were available, preventing the use of the proper inlet conditions.

Finally, it is interesting to note that the angular deviation α predicted by eqns. 81 and 89 is not a function of radius. The measured data in Eichenberger's bend (Figures 7a, b, c Section I) agrees with this result, even at 90° turning angle, in regions of the plane wall removed from the curved walls.

The General Case

If D is not zero, eqn. 75 must be solved by series approximation. The method of Frobenius (39) is employed here. The general form of a second-order differential equation can be taken as:

$$R(\theta)\frac{d^2 r}{d\theta^2} + \frac{1}{\theta} P(\theta)\frac{dr}{d\theta} + \frac{1}{\theta^2} Q(\theta) r = 0 \qquad (90)$$

Then R, P and Q are expressed in series,

$$R(\Theta) = R_0 + R_1\Theta + R_2\Theta^2 + \cdots$$
$$P(\Theta) = P_0 + P_1\Theta + P_2\Theta^2 + \cdots$$
$$Q(\Theta) = Q_0 + Q_1\Theta + Q_2\Theta^2 + \cdots$$

Comparing eqn. 89 with eqn. 74 shows:

$$R(\Theta) = 1 \qquad P(\Theta) = 0 \qquad Q(\Theta) = \Theta^2\frac{B}{1-D\Theta}$$

$$R_0 = 1 \qquad P_0 = P_1 = \cdots = P_n = 0 \qquad Q(\Theta) = B(\Theta^2 + D\Theta^3 + D^2\Theta^4 \cdots)$$

$$R_1 = R_2 = \cdots R_n = 0 \qquad\qquad Q_0 = 0$$

$$Q_1 = 0$$

$$Q_n = BD^{n-2}$$

The series expansion for $Q(\Theta)$ only converges if $D\Theta < 1$, but this is the same restriction as that on the original equation 75.

Next, we assume that r can be represented as

$$r = \Theta^s \sum_{n=0}^{\infty} A_n \Theta^n \tag{91}$$

Substituting eqn. 91 into eqn. 90 yields two possible values for s (0,1) both of which lead to unique solutions.

For s = 1, a recurrence formula is obtained determining $A_n = N_n$ as functions of a constant N_0. Since $Q_1 = 0$, N_1 is zero. We then get as one particular solution:

$$r = \Theta\left[N_0 + \sum_{n=2}^{\infty}\left(-\frac{B}{n(n+1)}\sum_{j=2}^{n}D^{j-2}N_{n-j}\right)\Theta^n\right] \tag{92}$$

For s = 0, another recurrence formula is obtained relating $A_n = M_n$ as functions of a constant M_0. M_1 is arbitrary and taken equal to zero. We then get another particular solution.

$$r = M_0 + \sum_{n=2}^{\infty}\left(-\frac{B}{n(n-1)}\sum_{j=2}^{n}D^{j-2}M_{n-j}\right)\Theta^n \tag{93}$$

These two particular solutions are added together to give the general solution as:

$$\frac{r}{r_1} = M_0 + \sum_{n=2}^{\infty} \left(-\frac{B}{n(n-1)} \sum_{j=2}^{n} D^{j-2} M_{n-j}\right)\theta^n +$$

$$N_0\theta + \sum_{n=2}^{\infty}\left(-\frac{B}{n(n+1)}\sum_{j=2}^{n} D^{j-2} N_{n-j}\right)\theta^{n+1} \tag{94}$$

The initial conditions are: at $\theta = 0$, $r = r_1$ and $(\frac{dr}{d\theta})_1 = r_1 \tan \alpha_1$.

Then $M_0 = r_1$ and $N_0 = r_1 \tan\alpha_1$. So finally we discover that,

$$\frac{r}{r_1} = 1 + \sum_{n=2}^{\infty}\left(-\frac{B}{r_1 n(n-1)}\sum_{j=2}^{n} D^{j-2} M_{n-j}\right)\theta^n +$$

$$(\tan\alpha_1)\theta + \sum_{n=2}^{\infty}\left(-\frac{B}{r_1 n(n+1)}\sum_{j=2}^{n} D^{j-2} N_{n-j}\right)\theta^{n+1} \tag{95}$$

In case $D = 0$, eqn. 95 reduces to 81 or 89 depending on the
sign of B.

If terms through θ^4 are retained when $\tan \alpha_1 = 0$ ($N_0 = 0$,
therefore all $N_n = 0$) and $B > 0$, eqn. 95 becomes:

$$\frac{r}{r_1} = \cos B^{\frac{1}{2}}\theta - \frac{BD\theta^3}{6}\left[1 + \frac{D\theta}{2}\right] \tag{96}$$

$$\tan\alpha = -\frac{r_1}{r}\left[B^{\frac{1}{2}}\sin B^{\frac{1}{2}}\theta + \frac{BD\theta^2}{6}(3 + 2D\theta)\right] \tag{97}$$

The first term in the bracket is that of the constant pressure

case   . It can be seen that a positive pressure gradient ($D > 0$)

increases the angular deviation α between boundary layer streamlines

and those of the main stream. Conversely, if the pressure gradient

is negative, the angular deviation is reduced. The magnitude of the

change in $\tan \alpha$ depends on the relative magnitude of $B^{1/2}\sin B^{1/2}\theta$

and $\frac{1}{6} B D\theta^2 (3 + 2 D\theta)$. For a given $\theta = \mathcal{E}$, and a given pressure

gradient, the effect of the streamwise pressure stresses increases

on approach to the wall. The following example demonstrates this

behavior in a diffusing cascade. The validity of the theory is

tested also by comparison against experimental data.

The underturning angle ($-\alpha$) is plotted in Figure 36 as measured along a z-line at mid-passage discharge of the cascade investigated by Toline and Watson (11), Figure 18A, Section I. The blade row had 40° inlet- and 14° outlet-angle; the pitch-chord ratio was 1; the chord 2.8" and the aspect ratio equal to 5.7. The inlet bound--ary-layer thickness was about δ/c = 0.36 with the measured velocity profile shown in Figure 22, Section I. The pressure coefficient, calculated from the flow geometry, is C_p = 0.3. The pressure rise was assumed to be linear.

At selected z-positions, B was calculated from the inlet velo-city profile; D was computed likewise from C_p and the velocity pro-file. These values were entered into 97 and α_2 calculated at dis-charge. The results are plotted in Figure 36. The calculations break down when D$\mathcal{E}$>1. Also shown are the angles computed for an imaginary cascade with the same turning angle but no pressure rise. This curve, in comparison with that for C_p = 0.3, illustrates the influence of the streamwise pressure stresses.

Comparison of the curves of Figure 36 shows that the analysis did not predict orders of magnitude well for this case. The trends of the calculated curve are correct except that they do not show underturning as measured in the outer regions of the boundary layer. The presence of underturned fluid can be anticipated from eqn. 1, Section I and indicates that the pressure varies normal to the wall. The discrepancies also are due in part to the thickness of the boundary layer which is by no means small at inlet compared to the passage width and thickens as it moves against the pressure rise.
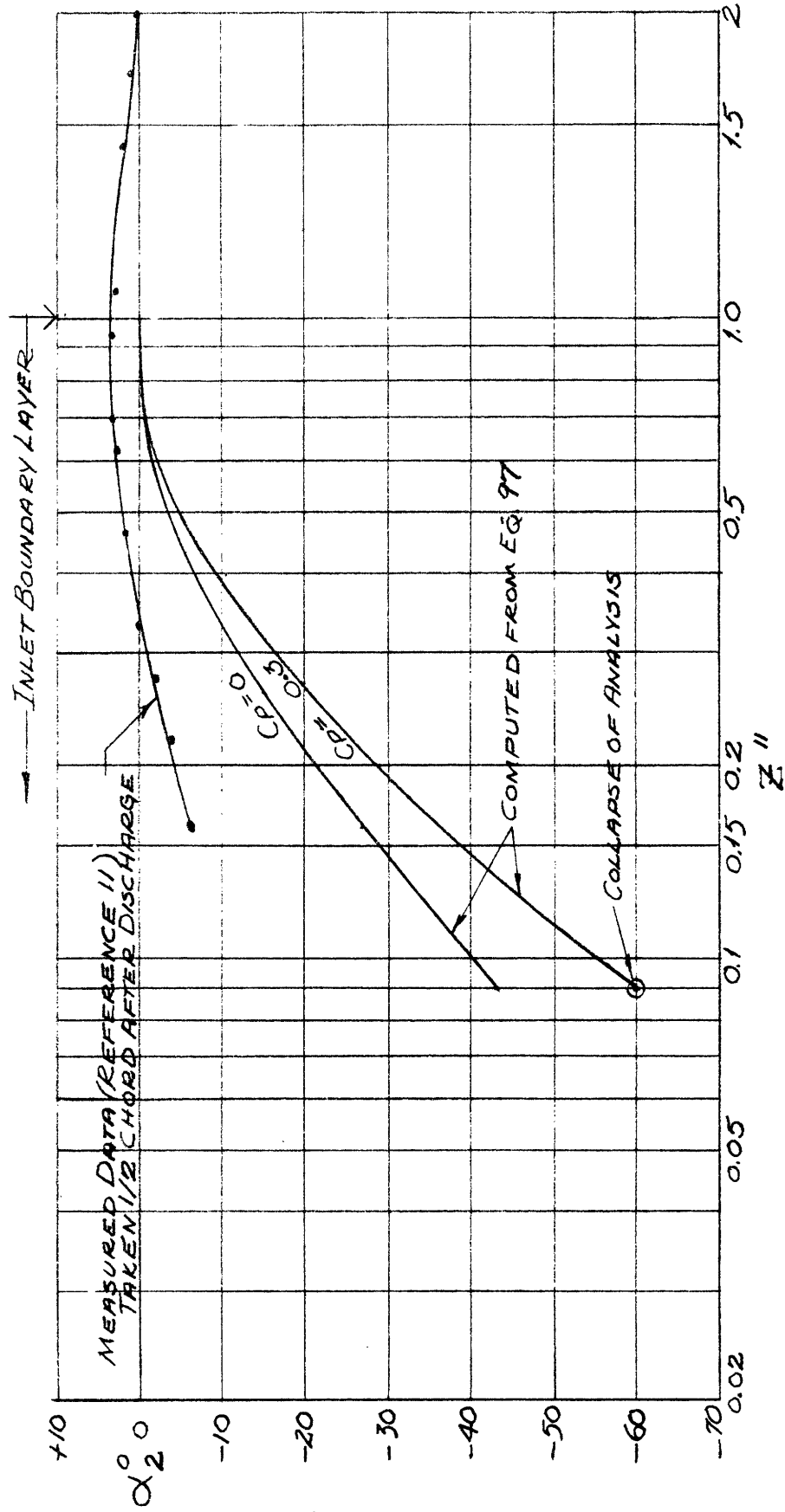
Figure 36   UNDERTURNING ANGLE VS. DISTANCE FROM WALL

Calculated values from eqn. 97 compared with measured data
from reference 11.

The measured angles, plotted in Figure 36, were taken 1/2-chord behind the passage discharge. They may not be representative of conditions in the discharge plane, however, this is the only data available. In addition, it only can be concluded that absence of shear stresses must lead to considerable error for reasons previously discussed. Finally, the two-dimensional model of the main flow is only a rough approximation of the actual pressure field.

Conclusion

None of the data available is strictly suitable to test this theory because the boundary layers in each case were relatively thick. In contrast, turbomachine boundary layers are usually relatively thin. More appropriate measurements are now in progress in the Gas Turbine Laboratory. The agreement in the cases cited is sufficient, nevertheless, to tentatively accept this theory as an indication of the influence of streamwise pressure stresses. All the stresses of a non-turbulent stream are included in analysis of the next Section but, unfortunately, analytical results can not be obtained.

V.   Secondary Flow in a Laminar Boundary Layer

As yet, a model capable of yielding analytical results and in-cluding both pressure and shear stresses has not been devised. The necessities of evaluating the relative importance of wall shear stresses upon a secondary flow pattern and, more important, of understanding the manner in which secondary flow affects the tendency of the boundary layer to separate, have encouraged the following momentum analysis of a laminar boundary layer on the plane wall of a turning passage. It is anticipated that as this research continues, the analysis can be extended to include turbulent flow, at least in an approximate manner. The manual computation of the present simplified case is laborious, but one such effort is justifiable to study the analysis and evaluate the potential of a similar machine computation of more exact analogs of actual flows. An extended machine computation with correlation of the results might eventually reveal the physical parameters governing actual flow patterns.

In this Section, a derivation of the momentum equations for a laminar flow is undertaken first. Then a series approximation after Polhausen is made for the velocity profiles. Finally, the equations are simplified by the adoption of a model similar to that of Section IV. It is on this model, fitted to a cascade we have ex-perimentally investigated, that the stepwise calculations are effected.

The Momentum Analysis of Plane Laminar Flow

At the onset several assumptions are made to simplify this

treatment.

1) The boundary layer flow is assumed to proceed on a plane wall and to be thin relative to the dimensions of the passage.

2) Interference effects of the curved walls of the passage on the boundary layer are assumed negligible (see Section IV).

3) The pressure gradient normal to the plane wall $\frac{\partial p}{\partial z}$ is assumed zero. In other words, the behavior of the main flow outside the thin boundary layer governs all pressures.

4) The main flow is assumed to be two-dimensional (i.e., to proceed on plane sheets parallel to the plane wall). However, a small velocity component in the main flow normal to the wall is allowable to accommodate boundary layer growth or diminution. Radial velocity components, V, in the main flow are assumed to be absent or negligible.

5) The only shear force included is that on the plane wall itself. The shear stress on the top of the control surface is made zero; the shear stresses on the two curved and two plane surfaces normal to the wall are assumed to nullify each other.

6) The fluid is in incompressible, non-turbulent, steady flow. The main flow is assumed potential, but not so the boundary layer.

The implications of these six assumptions demonstrate this so-called "general" analysis not to be completely general after all.

An arbitrary control surface is described in cylindrical coordinates (r, Θ, z) which is formed by two radial plane surfaces and two concentric cylindrical surfaces normal to the plane wall. The cover of the control surface is the warped interface between the boundary layer and the main flow lying at a variable distance δ from the plane wall.
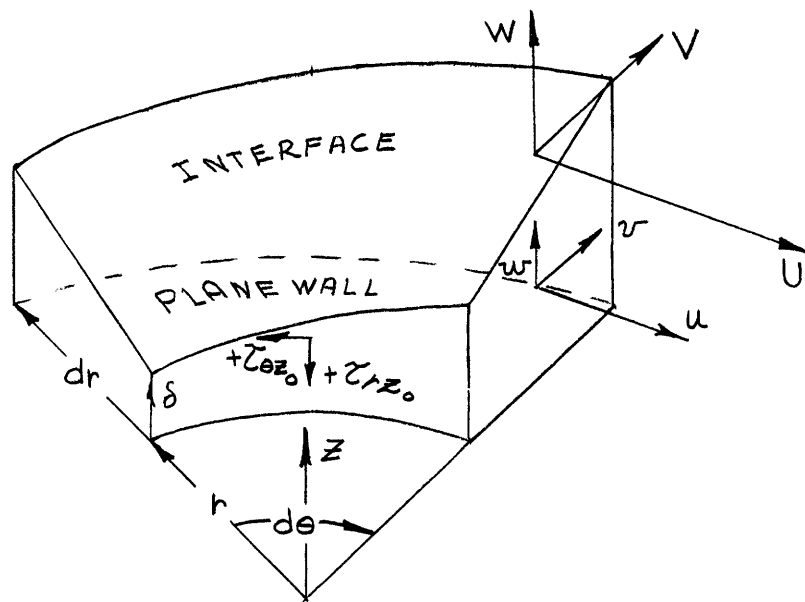
THE CONTROL SURFACE

(The tangential and radial shear stresses are taken in the conventional manner, positive in the negative Θ and r direction, respectively).

Figure 37

Fluid may enter all the surfaces of the control volume except the plane bottom wall. The velocity of the main flow is U in the tangential direction; a function of r and Θ but not of z. The velocity components of the boundary layer are u, v and w, functions

of r, Θ and z. The boundary layer thickness δ and pressure p are functions of r and Θ. The shear stress on the plane wall is broken into two components $\tau_{\Theta z_o}$ and τ_{rz_o} in the -Θ and -r directions, respectively.

The continuity and two momentum equations, one in the Θ- and the other in the r-direction, are derived by considering mass and momentum flux, pressure and shear stresses acting on each surface. The three resulting equations could equally well be derived by integrating the Navier-Stokes and continuity equations simplified, in this case, by the usual boundary-layer assumptions (41). The momentum analysis is rather laborious; fortunately, there is no reason to repeat it here since anyone who can understand this discussion could derive the equations given as much time as it took the author. Also, the results may be checked readily by integration of the familiar boundary-layer equations.

The tangential momentum equation, after combination with the continuity equation to eliminate the normal velocity component at the top of the control volume, appears as:

$$\frac{1}{r}\frac{\partial \frac{\Theta^*}{\delta}}{\partial \Theta} + \frac{\Theta^*}{\delta}\left(\frac{H+2}{2}\right)\frac{1}{rU^2}\frac{\partial U^2}{\partial \Theta} - \frac{\tau_{\Theta z_o}}{\delta \rho U^2} + \frac{1}{\delta r}\frac{\partial \delta}{\partial \Theta}\left(\frac{\Theta^*}{\delta}\right) + \frac{r}{\delta}\frac{\partial[(\frac{\beta^*}{\delta})\delta]}{\partial r}$$
$$+ \left(1 + \frac{r}{2U^2}\frac{\partial U^2}{\partial r}\right)\left(\frac{\beta^*}{\delta} - \int_0^1 u'v'd\eta\right) = 0 \tag{98}$$

where:

δ = boundary layer thickness

Θ* = boundary layer momentum thickness

$$\Theta^* = \delta \int_0^1 u'(1-u')d\eta$$

H = Θ*/δ* = boundary layer shape factor

δ* = boundary layer displacement thickness

$$\delta^* = \delta \int_0^1 (1-u') \, d\eta$$

$$\beta^* = \delta \int_0^1 v' (1-u') \, d\eta$$

$$\eta = z/\delta$$

$$u' = u/U$$

$$v' = v/U$$

The radial momentum equation appears as:

$$\frac{r}{2U^2} \frac{\partial U^2}{\partial r} - \frac{r \tau_{rz_0}}{\delta U^2 \rho} - \left(\frac{r}{U^2} \frac{\partial U^2}{\partial r} + \frac{r}{\delta} \frac{\partial \delta}{\partial r} + 1 \right) \int_0^1 v'^2 \, d\eta$$

$$- r \frac{d}{dr} \int_0^1 v'^2 \, d\eta - \left(\frac{1}{U^2} \frac{\partial U^2}{\partial \Theta} + \frac{1}{\delta} \frac{\partial \delta}{\partial \Theta} \right) \int_0^1 u' v' \, d\eta$$

$$- \frac{d}{d\Theta} \int_0^1 u' v' \, d\eta + \int_0^1 u'^2 \, d\eta = 0 \tag{99}$$

The Velocity Profile Assumption

To evaluate the control surface variables in eqns. 98 and 99 which are functions of the shape of the velocity profile, four-term series approximations are adopted to represent the tangential and radial velocity profiles. The constants of the series are evaluated by the boundary conditions among which lie the two wall shear stresses, thus relating wall shear to profile shape. This relation is supportable for laminar flow, but is untenable for turbulent flows. This analysis also implies that behavior of the fluid at a point in the flow is only a function of conditions at that point and not of the previous history of the fluid. That this implication can be disasterous is obvious if one does not know whether transition has occurred or not. The entire behavior of the fluid is strongly affected if, in its past history, the flow became turbulent.

Proceeding with the laminar case, the two series for the velocity profiles are:

$$u' = a\eta + b\eta^2 + c\eta^3 + d\eta^4 \tag{100}$$

$$v' = e\eta + f\eta^2 + g\eta^3 + h\eta^4 \tag{101}$$

No constant terms appear in either since both u' and v' must be zero at y = 0.

Eight boundary conditions are required. Six of them are:

$$\eta = 0 \quad u' = 0 \qquad\qquad v' = 0$$

$$\eta = 1 \quad u' = 1, \frac{\partial u'}{\partial \eta} = 0, \frac{\partial^2 u'}{\partial \eta^2} = 0 \quad v' = 0, \frac{\partial v'}{\partial \eta} = 0, \frac{\partial^2 v'}{\partial \eta^2} = 0 \tag{102}$$

The remaining two boundary conditions come from the three, point boundary-layer equations which can be written after eliminating terms of small order of magnitude:

$$\frac{uv}{r} + \frac{u}{r}\frac{\partial u}{\partial \theta} + v\frac{\partial u}{\partial r} + w\frac{\partial u}{\partial z} = -\frac{1}{\rho r}\frac{\partial p}{\partial \theta} + \upsilon\frac{\partial^2 u}{\partial z^2} \tag{103}$$

$$-\frac{u^2}{r} + \frac{u}{r}\frac{\partial v}{\partial \theta} + v\frac{\partial v}{\partial r} + w\frac{\partial v}{\partial z} = -\frac{1}{\rho}\frac{\partial p}{\partial r} + \upsilon\frac{\partial^2 v}{\partial z^2} \tag{104}$$

$$\frac{\partial p}{\partial z} = 0 \tag{105}$$

At z = 0, u = v = w = 0, so

$$\frac{\partial^2 u'}{\partial \eta^2} = \frac{\delta^2}{\mu U r}\frac{\partial p}{\partial \theta} \tag{106}$$

$$\frac{\partial^2 v'}{\partial \eta^2} = \frac{\delta^2}{\mu U}\frac{\partial p}{\partial r} \tag{107}$$

Now, combining these eight boundary conditions with this series profiles gives:

$$u' = F(\eta) + \lambda\, G(\eta) \tag{108}$$

$$v' = \gamma\, G(\eta) \tag{109}$$

where

$$F(\eta) = \eta(2 - 2\eta^2 + \eta^3) \tag{110}$$

$$G(\eta) = -\frac{\eta}{6} (\eta - 1)^3 \tag{111}$$

$$\lambda = \frac{\delta^2}{\nu r} \frac{\partial U}{\partial \Theta} \tag{112}$$

$$\gamma = \frac{\delta^2}{\nu} \frac{\partial U}{\partial r} \tag{113}$$

These profile shape approximations yield single parameter profiles for both u' and v'. For u', the magnitude of λ governs size and shape of the velocity profile by varying the proportion of the G function added to the F. However, for v', the parameter γ changes only the magnitude of the profile. The maximum value of v' always occurs at $\eta = 0.3$, an unfortunate restriction that will be discussed further at the end of this Section.

The functions F and G are tabulated in Ref. (42). Figure 38 from this reference illustrates F and G as well as u' profiles for different values of λ.

Inspection of eqns. 112 and 113 reveals that the radial profile parameter γ can be related through the main stream behavior to the tangential profile parameter λ. We can express, therefore, the momentum equations as functions of λ and main stream behavior only. This simplification saves a sizable amount of computation effort.
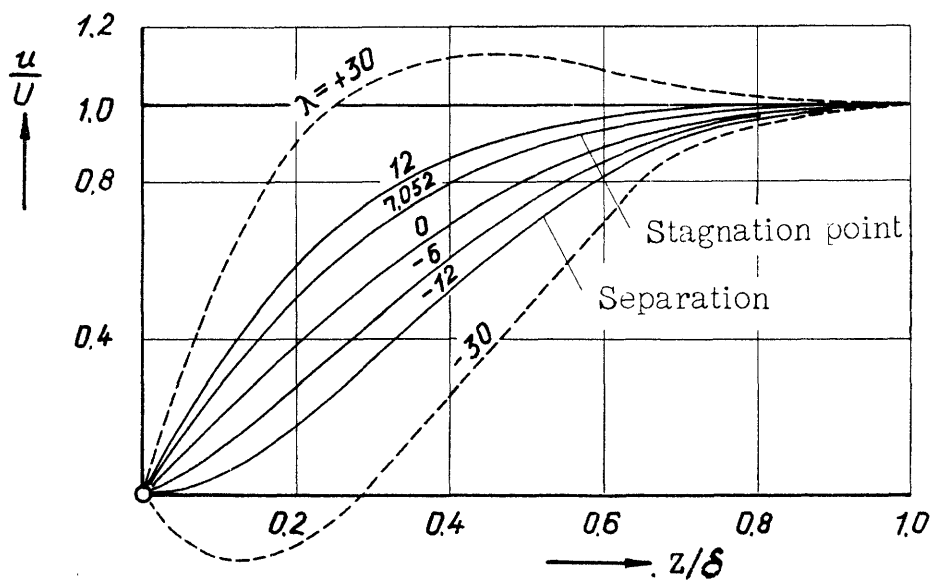
Combining eqns. 112 and 113,

$$\gamma = \lambda r \left(\frac{\partial U}{\partial r}\right)\left(\frac{\partial U}{\partial \Theta}\right)^{-1} \tag{114}$$

Next, all the variables in eqns. 98 and 99 must be evaluated in terms of λ and γ. A tabulation follows:

$$\frac{\tau_{\Theta z_0} \delta}{\mu U} = \frac{12 + \lambda}{6}, \quad \left(\tau_{\Theta z_0} = \mu \left(\frac{\partial u}{\partial z}\right)_0 \right) \tag{115}$$
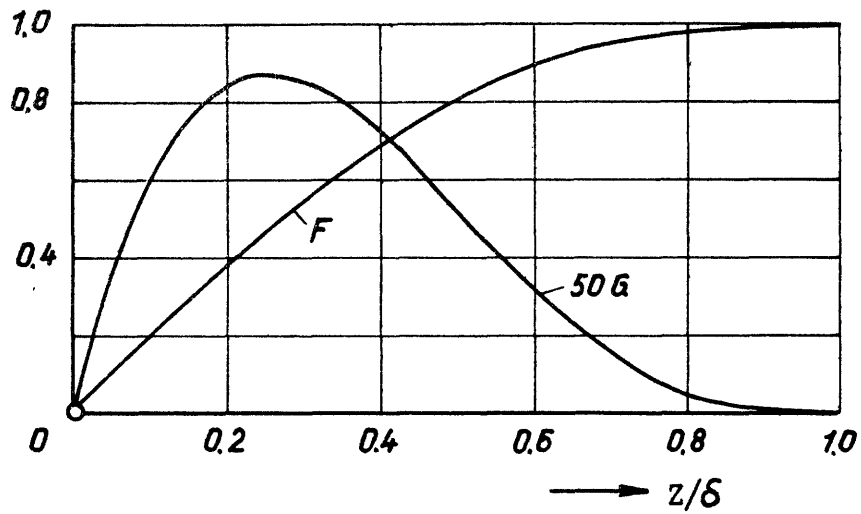
The universal functions $F(z/\delta)$ and $G(z/\delta)$ for the velocity distribution in the boundary layer according to Pohlhausen.

The one-parameter family of velocity profiles according to Pohlhausen.

FIGURE 38

$$\frac{\mathcal{T}_{hz_0}\delta}{\mu U} = \frac{\gamma}{6}, \quad \left(\mathcal{T}_{hz_0} = \mu \left(\frac{\partial v}{\partial z}\right)_0\right) \tag{116}$$

$$\frac{\delta^*}{\delta} = \frac{3}{10} - \frac{\lambda}{120} \tag{117}$$

$$\frac{\Theta^*}{\delta} = \frac{37}{315} - \frac{\lambda}{945} - \frac{\lambda^2}{9072} \tag{118}$$

$$\frac{\partial \Theta^*/\delta}{\partial \Theta} = -\left(\frac{1}{945} + \frac{2\lambda}{9072}\right)\frac{\partial \lambda}{\partial \Theta} \tag{119}$$

$$\int_0^1 u' d\eta = \frac{1}{10}\left(7 + \frac{\lambda}{12}\right) \tag{120}$$

$$\int_0^1 u'^2 d\eta = \frac{1}{9072}\left(\frac{26,424}{5} + \frac{426}{5}\lambda + \lambda^2\right) \tag{121}$$

$$\int_0^1 v' d\eta = \frac{\gamma}{120} \tag{122}$$

$$\int_0^1 v'^2 d\eta = \frac{\gamma^2}{9072} \tag{123}$$

$$\frac{d}{dr}\int_0^1 v' d\eta = \frac{1}{120}\frac{\partial \gamma}{\partial r} \tag{124}$$

$$\frac{d}{dr}\int_0^1 v'^2 d\eta = \frac{2\gamma}{9072}\frac{\partial \gamma}{\partial r} \tag{125}$$

$$\int_0^1 u'v' d\eta = \frac{\gamma}{9072}\left(\frac{213}{5} + \lambda\right) \tag{126}$$

$$\frac{d}{\partial \Theta}\int_0^1 u'v' d\eta = \frac{1}{9072}\left[\left(\frac{213}{5} + \lambda\right)\frac{\partial \gamma}{\partial \Theta} + \gamma\frac{\partial \lambda}{\partial \Theta}\right] \tag{127}$$

$$\frac{d}{\partial r}\int_0^1 u'v' d\eta = \frac{1}{9072}\left[\left(\frac{213}{5} + \lambda\right)\frac{\partial \gamma}{\partial r} + \gamma\frac{\partial \lambda}{\partial r}\right] \tag{128}$$

Inspection of eqn. 115 shows that $\mathcal{T}_{\Theta z_0} = 0$ when $\lambda = -12$. Normally one would specify $\lambda = -12$ as "separation" but, in a three-dimensional flow, this specification may be trivial. (See the discussion of Section I on this point). If $\lambda > +12$, u' will be greater than 1.0 somewhere in the boundary layer in violation of the second law of thermodynamics. For this case, then, λ must not

exceed +12, but no reasonable restriction can be placed as a lower limit except that u' must not be less than -1 for the same reason. To avoid values of $|v'|$ greater than 1, the absolute magnitude of γ must not exceed 58.4. The term "separation" can hardly describe the radial flow when $\tau_{rz_0} = 0$ (i.e., $\gamma = 0$) since this is the normal condition in a linear flow.

Proceeding, eqns. 115 through 128 are substituted into eqns. 98 and 99. Then 114 is employed to eliminate γ. After a great deal of algebraic reduction, the following forms of the two momentum equations appear.

Tangential:

$$A\left(\frac{2664}{5} - \frac{72}{5}\lambda - \frac{5}{2}\lambda^2\right)\frac{\partial\lambda}{\partial\theta} + \frac{\lambda r^2 B}{2}(99 - 5\lambda)\frac{\partial\lambda}{\partial r}$$

$$-\left(9072 - \frac{9684}{5}\lambda + \frac{249}{5}\lambda^2 + \frac{5}{4}\lambda^3\right)A^2 + \frac{\lambda^2 r B}{2}\left(\frac{399}{5} - 7\lambda\right)$$

$$-\frac{(\lambda r B)^2}{2}\left(\frac{48}{5} + 2\lambda\right) - \frac{3(r\lambda)^2 BC}{2}(33-\lambda) + 2(r\lambda)^2 E(33-\lambda) = 0 \quad (129)$$

Radial:

$$\frac{A}{rB}\left(\frac{639}{25} + \lambda\right)\frac{\partial\lambda}{\partial\theta} + \lambda r\frac{\partial\lambda}{\partial r} - \frac{A^2}{rB}\left(1512 - \frac{213}{10}\lambda - \frac{\lambda^2}{2}\right)$$

$$+ \frac{\lambda^2}{5}(7 + 2rB) - \lambda^2 rC + \frac{2}{5}\lambda\left(\frac{213}{5} + \lambda\right)\left[\frac{C}{r}\left(\frac{A}{B}\right)^2 - \frac{2D}{rB}\right]$$

$$+ \frac{8}{5}\lambda^2\left(\frac{rE}{B}\right) - \left(\frac{A}{rB}\right)^2\left(\frac{52,848}{25} + \frac{852}{25}\lambda + \frac{2}{5}\lambda^2\right) = 0 \quad (130)$$

where

$$A \equiv \frac{1}{U^2}\frac{\partial U^2}{\partial\theta} \quad (131)$$

$$B \equiv \frac{1}{U^2}\frac{\partial U^2}{\partial r} \quad (132)$$

$$C \equiv \frac{1}{\partial U/\partial\theta}\frac{\partial^2 U}{\partial\theta\partial r} \quad (133)$$

$$D \equiv \frac{1}{U}\frac{\partial^2 U}{\partial\theta^2} \quad (134)$$

$$E \equiv \frac{1}{U} \frac{\partial^2 U}{\partial r^2} \tag{135}$$

and

$$\gamma = \lambda r \frac{B}{A} \tag{136}$$

Equations 129 and 130 can be solved simultaneously.

$$\frac{4069}{50} A \frac{\partial \lambda}{\partial \theta} = F_3 A^2 - \frac{\lambda^2 rB}{45} (147 + 123 rB) - \frac{r^2 BC}{9} \lambda^3$$

$$+ F_4 r^2 E + F_5 \left(\frac{A^2 C}{B} - 2D\right) + \frac{A^2}{rB} F_6 \tag{137}$$

where

$$F_3 = \frac{1}{10} \left(73{,}080 - \frac{6439}{2} \lambda - \frac{71}{3} \lambda^2\right) \tag{138}$$

$$F_4 = -\frac{2}{9} \lambda^2 \left(\frac{33}{5} - \lambda\right) \tag{139}$$

$$F_5 = -\frac{\lambda}{45} \left(\frac{213}{5} + \lambda\right)(99 - 5\lambda) \tag{140}$$

$$F_6 = \frac{1}{18} (99 - 5\lambda) \left(\frac{52{,}848}{25} + \frac{852}{25} \lambda + \frac{2}{5} \lambda^2\right) \tag{141}$$

Equation 137 allows a simpler solution for $\frac{\partial \lambda}{\partial r}$, if $\frac{\partial \lambda}{\partial \theta}$ has been calculated, than solving explicitly for $\frac{\partial \lambda}{\partial r}$. Equation 137 is put in the skeleton form,

$$\lambda r \frac{\partial \lambda}{\partial r} = -\frac{A}{rB} G_1 \frac{\partial \lambda}{\partial \theta} + \frac{A^2}{rB} G_3 - \frac{\lambda^2}{5} (7 + 2rB) + \lambda^2 rC$$

$$- G_4 \left(\frac{CA^2}{rB^2} - \frac{2D}{rB}\right) - \frac{8}{5} \lambda^2 \frac{rE}{B} + \left(\frac{A}{rB}\right)^2 G_5 \tag{142}$$

where

$$G_3 = \left(1512 - \frac{213}{10} \lambda - \frac{\lambda^2}{2}\right) \tag{143}$$

$$G_4 = \frac{2}{5} \lambda \left(\frac{213}{5} + \lambda \right) \tag{144}$$

$$G_5 = \left(\frac{52,848}{25} + \frac{852}{25} \lambda + \frac{2}{5} \lambda^2 \right) \tag{145}$$

In computing the conversion of a rectilinear flow to a curvilinear flow, rectangular coordinates facilitate the calculation. Equations (137) and (142) may be transformed to:

$$\frac{4069}{50} A' \frac{\partial \lambda}{\partial x} = (A')^2 F_3 - \frac{123}{45} \lambda^2 (B')^2 - \frac{\lambda^3}{9} B'C'$$

$$+ F_4 E' + F_5 \left[\frac{(A')^2 C'}{B'} - 2D' \right] \tag{146}$$

$$\lambda B' \frac{\partial \lambda}{\partial y} = -A G_1 \frac{\partial \lambda}{\partial x} + (A')^2 G_3 - \frac{2}{5} \lambda^2 (B')^2 + \lambda^2 B'C'$$

$$- G_4 \left[\frac{(A')^2 C'}{B'} - 2D' \right] - \frac{8}{5} \lambda^2 E' \tag{147}$$

where

$$A' = \frac{1}{U^2} \frac{\partial U^2}{\partial x} \qquad D' = \frac{1}{U} \frac{\partial^2 U}{\partial x^2}$$

$$B' = \frac{1}{U^2} \frac{\partial U^2}{\partial y} \qquad E' = \frac{1}{U} \frac{\partial^2 U}{\partial y^2} \tag{148}$$

$$C' = \frac{1}{\partial U / \partial x} \frac{\partial^2 U}{\partial x \partial y} \qquad \lambda = \frac{\delta^2}{\nu} \frac{\partial U}{\partial x}$$

Considerable effort was required to bring the original equations down to eqns. 137 and 142. Many algebraic errors were found in the one-hundred and three pages of the original hand written derivation, but the author believes these equations are correct since they reduce to the special case that follows. The special case was derived independently from eqns. 98 and 99. In the reduction of the general case to the special case, all the functions of λ and the functions A through E of the general solution remain

finite eliminating the possibility of errors hidden in terms which might have been multiplied by zero and thus disappear in the reduction.

Conclusion of General Case

The "general" equations 137 and 142 could be applied to any flow where the original assumptions are valid. The analysis could be made still more universal if restrictions on the main flow were relaxed. In the pending turbulent analysis, only the restriction that the main flow must be quasi- two-dimensional will be imposed.

Practical consideration of the numerical computation utilizing these equations will be discussed below.

The Special Case

To study qualitatively the characteristics of this momentum analysis, further restrictions were placed upon the main flow. The model is as follows:

1) The main flow enters a passage with concentric curved walls in a free-vortex radial velocity distribution. The main flow streamlines are concentric, at all times, with the center of curvature of the passage.

2) The streamwise pressure gradient $\frac{\partial p}{\partial \theta}$ is constant at any radius and is imposed by convergence or divergence of, or mass transfer through, a wall far removed from the plane wall under study.

Under these assumptions and those at the beginning of this Section, the main flow will behave exactly as described in Section IV. The distribution of the main flow velocity, eqn. 46, Section IV, is repeated.

$$U^2 = \frac{1}{r^2}\left(K_1{}^2 - \frac{2C_1\theta}{\rho}\right)$$

(149)

where $K_1 = U_1 r$ and C_1 is $\frac{\partial p}{\partial \theta} r^2$.

Equations 137 and 142 may now be simplified if the functions A through E are evaluated from eqn. 149.

$$A = -2Q \,,\; B = -\frac{2}{r} \,,\; C = -\frac{1}{r} \,,\; D = -Q^2 \,,\; E = \frac{2}{r^2} \tag{150}$$

where:

$$Q = \frac{1}{\rho U^2} \frac{\partial p}{\partial \theta} \tag{151}$$

We then get as a result for this case

$$\frac{4069}{80} Q \frac{\partial \lambda}{\partial \theta} = Q^2\left(\frac{-9342}{5} + \frac{21,579}{80}\lambda - \frac{19}{4}\lambda^2 - \frac{5}{24}\lambda^3\right)$$
$$+ \frac{10\lambda^2}{144}(33-\lambda) \tag{152}$$

and

$$\lambda r \frac{\partial \lambda}{\partial r} = -Q\left(\frac{639}{25} + \lambda\right)\frac{\partial \lambda}{\partial \theta} - Q^2\left(\frac{22,752}{25} - \frac{2769}{25}\lambda - \frac{11}{5}\lambda^2\right) \tag{153}$$

Or in skeleton form:

$$\frac{4069}{80} Q \frac{\partial \lambda}{\partial \theta} = F_1 Q^2 + F_2 \tag{154}$$

where

$$F_1 = \left(-\frac{9342}{5} + \frac{21,579}{80}\lambda - \frac{19}{4}\lambda^2 - \frac{5}{24}\lambda^3\right) \tag{155}$$

$$F_2 = \frac{10\lambda^2}{144}(33-\lambda) \tag{156}$$

And,

$$\lambda r \frac{\partial \lambda}{\partial r} = -Q\left(G_1 \frac{\partial \lambda}{\partial \theta} + Q G_2\right) \tag{157}$$

where

$$G_1 = \frac{639}{25} + \lambda \tag{158}$$

$$G_2 = \left(\frac{22,752}{25} - \frac{2769}{25}\lambda - \frac{11}{5}\lambda^2\right) \tag{159}$$

The function Q can be related to the pressure coefficient Cp and passage geometry. It was shown in Section IV, for this same main flow pattern, eqn. 49, that:

$$C_p = \frac{2C_1 E}{\rho K_1^2} \tag{160}$$

where $C_1 = \frac{\partial p}{\partial \Theta} r^2$, $K_1 = U_1 r$ and $\mathcal{E}$ is the turning angle at which the main stream has achieved a dimensionless pressure rise Cp. Combining the definition of Q, eqn. 151, with the definition of C_1, we get

$$Q = \frac{C_1}{\rho (Ur)^2} \tag{161}$$

Substituting for U^2 in eqn. 161 the relation 149 gives:

$$Q = \frac{1}{\rho K_1^2 / C_1 - 2\Theta} \tag{162}$$

Substituting eqn. 160 into eqn. 162 produces,

$$Q = \frac{1}{2} \left(\frac{1}{\mathcal{E}/Cp - \Theta} \right) \tag{163}$$

Q is a function of Θ, the cascade turning angle and pressure rise only.

The pertinent eqns. 154 and 157 are functions of λ, r and Θ only. The profile parameter λ may be evaluated by stepwise calculation through the bend, thus determining the u' velocity profile as a function of r and Θ.

The v' profile is determined from the relation between λ and γ, eqn. 136, in combination with definitions 150 and eqn. 163. From these steps we get,

$$\gamma = \frac{\lambda}{Q} = 2\lambda \left(\mathcal{E}/Cp - \Theta \right) \tag{164}$$

Finally, the boundary layer thickness δ can be determined from the definition of λ or γ. Taking λ, eqn. 112, and $\frac{\partial U}{\partial \Theta}$ from eqn. 149 gives δ as,

$$\delta^2 = \frac{-\lambda \mu U r^3}{C_1} \tag{165}$$

Substituting eqn. 161,

$$\left(\frac{\delta}{r} \right)^2 = -\frac{\lambda}{Q} \left(\frac{v}{Ur} \right) \tag{166}$$

Then eliminating Q by eqn. 163,

$$\left(\frac{\delta}{r}\right)^2 = -2\lambda\left(\mathcal{E}/c_p - \Theta\right)\left(\frac{\nu}{Ur}\right) \tag{167}$$

or

$$\left(\frac{\delta}{r\Theta}\right)^2 = -2\lambda\left(\frac{1}{c_p}\frac{\mathcal{E}}{\Theta} - 1\right)\left(\frac{\nu}{Ur\Theta}\right) \tag{168}$$

Finally,

$$\frac{\delta}{r\Theta} = \sqrt{-2\lambda\left(\frac{1}{c_p}\frac{\mathcal{E}}{\Theta} - 1\right)}\,\left(Re_{r\Theta}\right)^{-\frac{1}{2}} \tag{169}$$

Thus, the relative boundary-layer thickness, compared to the distance the main flow has traveled from the inlet cross section, is a function of λ, the channel geometry and pressure rise, and the length Reynolds number based on the arc length to inlet. The thickness δ will never be imaginary because the signs of λ and Cp are always opposite and Cp can never be greater than +1.

The solution is defined by the above considerations except that inlet conditions must be specified.

Inlet Specifications

A free vortex flow configuration for the main stream has been assumed in this special case. Any inlet conditions must conform to this pattern or eqns. 154 and 157 will not fit the flow.

Within this restriction, we are free to chose $\lambda = f(r)$ at $\Theta = 0$, with one exception that we cannot make $\lambda = 0$ along the $\Theta = 0$ line.

If $\lambda = 0$, the equations for $\frac{\partial\lambda}{\partial\Theta}$ and $\frac{\partial\lambda}{\partial r}$, or $\frac{\partial\lambda}{\partial x}$ and $\frac{\partial\lambda}{\partial y}$, are inconsistent in the general and special case unless $\frac{\partial U}{\partial\Theta}$ or $\frac{\partial U}{\partial x}$ equal zero. The rate of change of λ in the direction normal to the main flow goes to infinity when λ approaches zero. If there are no errors in this derivation, the cause of such inconsistency is

probably that power series velocity profiles cannot be assumed when the boundary layer approaches zero thickness. Equation 112 demonstrates that δ will be zero if λ is zero unless $\frac{\partial U}{\partial \Theta} = 0$.

In choosing a λ distribution at inlet, one must keep in mind that the sign of λ must always agree with the sign of $\frac{\partial U}{\partial \Theta}$ according to eqn. 112. This condition assures that the sign of the curvature of the velocity profile at the wall will agree with the sign of the pressure gradient as demanded by the boundary layer equations 103 and 106. If λ is negative the velocity profile will have an inflection point, if λ is positive it will not. For this model, $\frac{\partial U}{\partial \Theta}$ is negative everywhere whence comes the condition that λ must be negative everywheere in the bend. The initial conditions actually introduced, in the computations that follow, are arbitrary. Three values of λ were assumed at $\Theta = 0$, $r = r_i$. They are $\lambda = -0.5$, $\lambda = -6$, $\lambda = -12$ and were selected to cover the range of permissible inlet boundary layer conditions.

When λ at $\Theta = 0$, $r = r_i$ is greater than about -1.1, $\frac{\partial \lambda}{\partial r}$ is negative decreasing λ across the passage to $r = r_o$. When λ is less than about -1.1, $\frac{\partial \lambda}{\partial r}$ is positive and λ increases across the passage to $r = r_o$, but does not reach zero before the outside radius is attained even when λ at $\Theta = 0$, $r = r_i$ is equal to -12.

It would be desirable in the study of this simplified model to introduce a more realistic flow into the bend than the arbitrary pattern chosen above. Any subsonic flow approaching a turning passage will commence a redistribution of its pattern well upstream of the passage inlet. Such redistribution undoubtedly will

initiate secondary, boundary layer flows. Local variations in the
main stream velocity and streamline pattern will cause alterations
in the boundary-layer thickness and velocity profile. The boundary
layer will arrive at the turning passage, therefore, with signi-
ficant alterations in character. For this reason, it is dangerous
to neglect the actions preceding the turning passage, particularly
since the behavior of the boundary fluid in the passage depends
strongly on its character at the inlet plane.

An attempt was made to devise a simple model of the approach
flow which would condition the boundary layer in a somewhat real-
istic manner. The first model assumed that the flow converted
from a uniform, parallel pattern to the free-vortex pattern at
bend entrance in a distance of one bend width $(r_o - r_i)$ upstream.
Changes in velocity were assumed to be linear. It results from
this assumption, that the flow which approaches close to the inner
wall of the bend is subject to an acceleration while flow approach-
ing close to the outer wall is decelerated. At the inlet plane of
the bend, the model flow, defined previously, commences with the
assumption of decelerating flow everywhere. The welding of the
two models together thus introduces a discontinuity in tangential
velocity gradient. Equation 112 shows that there will result a
discontinuity in the profile parameter λ ; the rate of change of
λ becomes infinite at $\theta = 0$ and no solution is possible. An
attempt was made to circumvent the discontinuity by matching the
boundary layer thickness calculated for each model from eqns. 112
and 148, but meaningless values for λ were produced.

A better model of the approach flow, which allows matching

of the velocity gradients of the bend model and the approach flow
model, can be devised by assuming a power series for the velocity
distribution in the conversion region ahead of the turning passage.

The conversion from a uniform pattern is assumed again to
occur in a distance of one bend width ahead of the inlet plane.
The free-vortex flow at the inlet of the bend model is tied to the
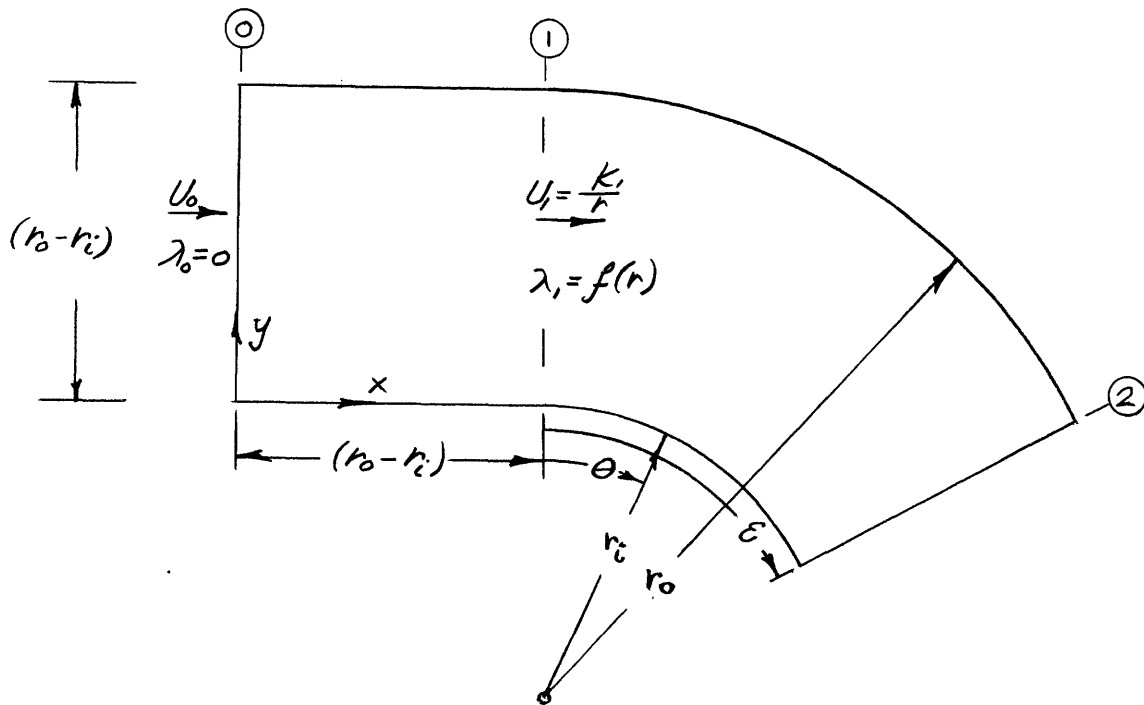linear flow through continuity.

Figure 39

whence,

$$(170)$$

A power series is assumed for U between positions 0 and 1.

$$U' = a + bx' + Cx'^2 + dx'^3 + f(y) \qquad (171)$$

where $U' = \dfrac{U}{U}$ and $x' = \dfrac{x}{r_i}$. The boundary conditions on 171 are:

At $x' = 0$ $\qquad U' = 1$ and $\dfrac{\partial U'}{\partial x'} = 0$ $\qquad\qquad (172)$

At $x' = (\frac{r_o}{r_i} - 1)$ $U' = U_1'$ (eqn. 170) and

$$\frac{\partial U'}{\partial x'} = \frac{r_i}{U_o}\left(\frac{\partial U}{r\partial\Theta}\right)_{\Theta=0} \tag{173}$$

From eqn. 160, eqn. 173 becomes:

$$\frac{\partial U'}{\partial x} = -\frac{r_i}{2r} U_1' \frac{C_p}{\mathcal{E}} \tag{174}$$

Substituting eqn. 170 into 174 and setting r equal to $(y + r_i)$

at $\Theta = 0$, we get

$$\frac{\partial U'}{\partial x'} = -\frac{1}{2(y'+1)^2} \frac{(\frac{r_o}{r_i} - 1)}{\ln r_o/r_i} \tag{175}$$

Since U' is constant with y' at position zero, $f(y)$ in eqn. 171

must be a constant.

If these boundary conditions are combined with eqn. 171, the

velocity distribution for the main flow in the conversion section

appears as:

$$U' = 1 + \frac{3x'^2}{R^2}\left(1 - \frac{2x'}{3R}\right)\left\{\frac{R}{(y'+1)\ln(R+1)}\left[1 + \frac{R}{6(y'+1)}\right]\right\}$$
$$- \frac{x'^3}{6(y'+1)^2 R\ln(R+1)} \tag{176}$$

where $R = (\frac{r_o}{r_i} - 1)$.

Equation 176 can be partially differentiated with respect to

x' and y' and the necessary derivatives obtained to evaluate the

functions A' through d' of definition 148. These functions then

allow stepwise integration of eqns. 146 and 147 yielding λ as a

function of y' at $x' = (\frac{r_o}{r_i} - 1)$ (i.e., $\Theta = 0$). The calculations

are laborious and have not been carried out as yet.

With an untested analysis there is always the possibility

that λ may exceed +12 invalidating the entire analysis. Should

this be the case, another approach model would have to be devised.

A still better approach and one worth the most serious consid-

eration in this laminar analysis would employ a potential solution

for the flow through a cascade or in a bend to determine behavior
of the main flow not only ahead of the passage, but inside as well.
The general equation 137 and 142 would be employed over the entire
field.

Whether this extensive calculation will be effected or not
depends primarily upon the success of a forthcoming attack on the
turbulent boundary layer.

The Bend Model

To allow some test of this analysis, a bend model was selected
which approximately fits a cascade for which boundary-layer data
is available. Of course, the fit is not exact since the cascade
passages are formed by airfoils; the width of the passage changes
along its length, and the walls are not concentric. The most
questionable factor in the fit is that the model does not satis-
fy the Kutta condition at discharge. Therefore, the pressure
fields of the model and cascade are essentially different. Ex-
perimental measurements of boundary-layer behavior in a variable
area bend would be better approximated by this model, but such
data is not available as yet.

In spite of these serious discrepancies, a bend model was
selected which had the same turning angle and a constant width
equal to the mean passage width of the cascade. The cascade
blades had circular arc camber lines, thus the mean lines of the
cascade passage and the model passage correspond. The fit and
pertinent dimensions are shown in Figure 40.

Calculations for the Bend Flow Model

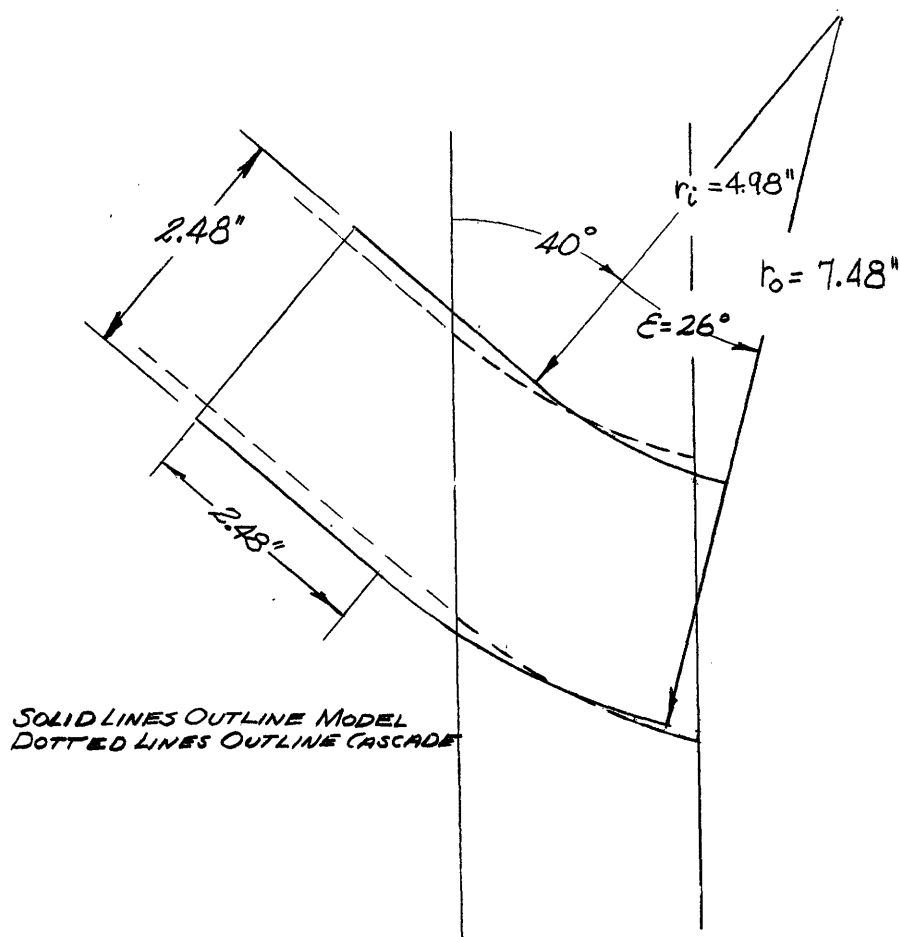Starting from one of the arbitrary assumptions of λ at

2.48"

2.48"

$r_i = 4.98"$

$40°$

$\xi = 26°$

$r_o = 7.48"$

SOLID LINES OUTLINE MODEL
DOTTED LINES OUTLINE CASCADE

Figure 40

$\Theta = 0$, $r = r_i$, eqns. 154 through 159 and 163 were employed to stepwise compute λ as a function of r and Θ. The variation of was computed along arcs at r_o, r_m and r_i.

At angular positions of $\Theta = 0$, $13°$ and $26°$, the variation of λ was determined as a function of radius. The values so obtained are plotted in Figure 41 and 42. The lines of incipient backflow are shown in Figure 43.

The local values of λ and of γ, from eqn. 164, were utilized to determine the local velocity profiles from eqns. 108
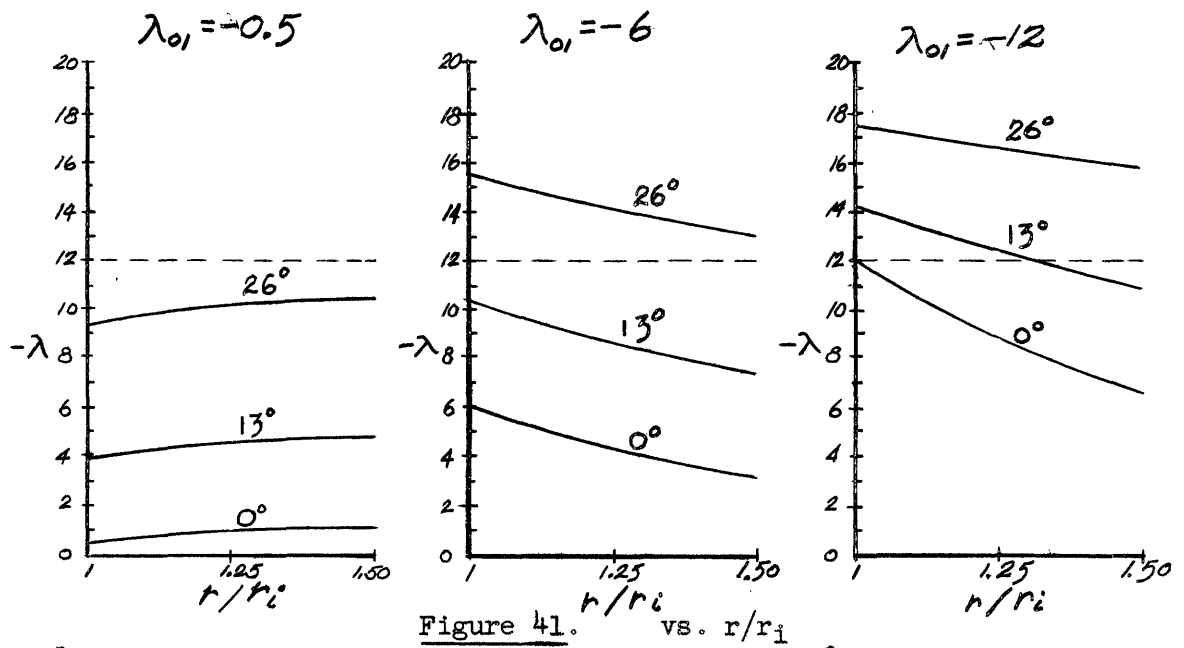
Figure 41. $-\lambda$ vs. r/r_i
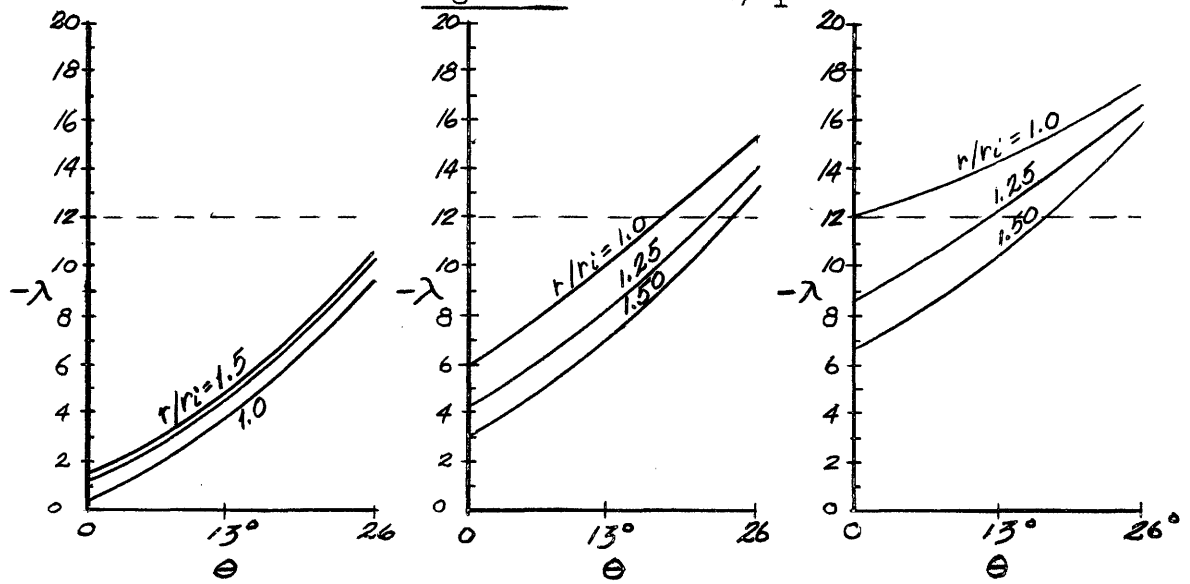
Figure 42. $-\lambda$ vs. θ
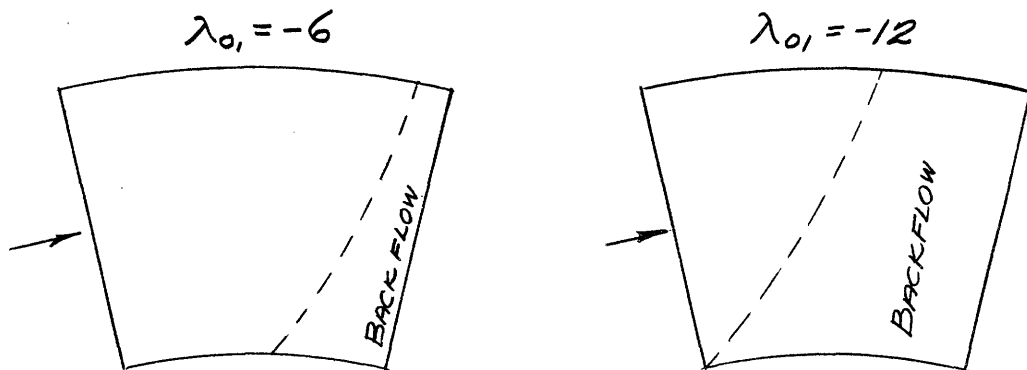
Figure 43.
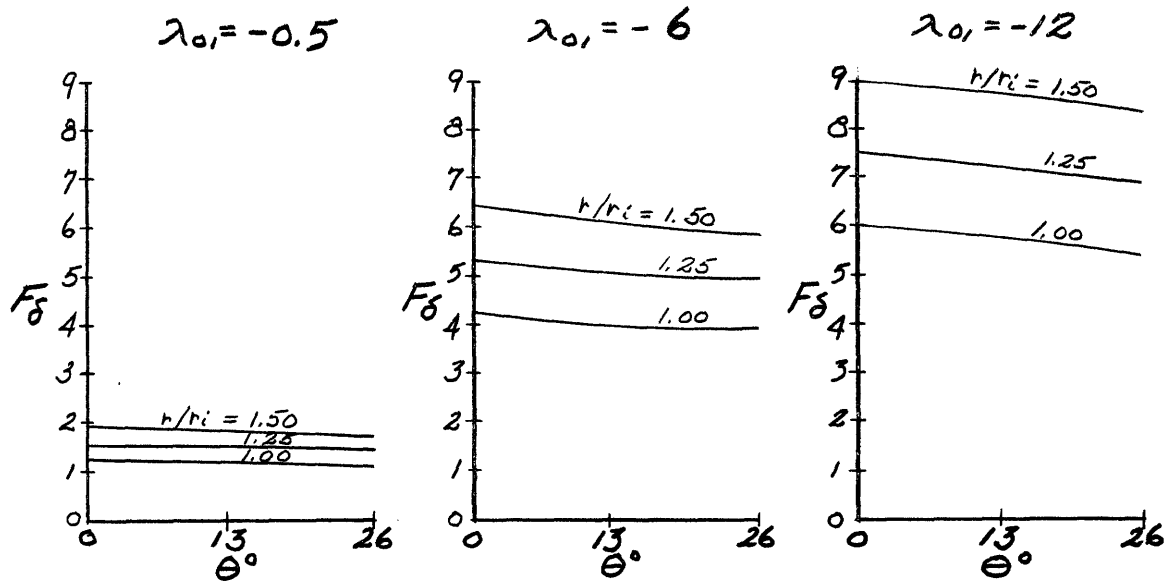Showing Lines of Incipient Backflow

Figure 44 $F_\delta = \left(\dfrac{\delta}{r_i}\right)\left(\dfrac{U_1 r}{\nu}\right)^{\frac{1}{2}}$ vs. Θ
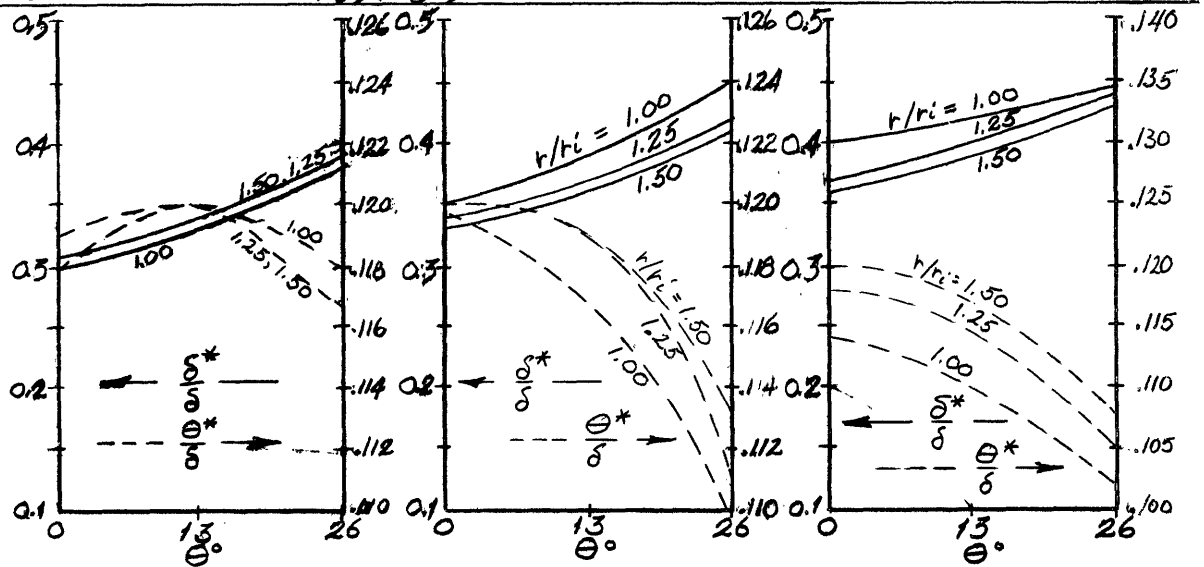

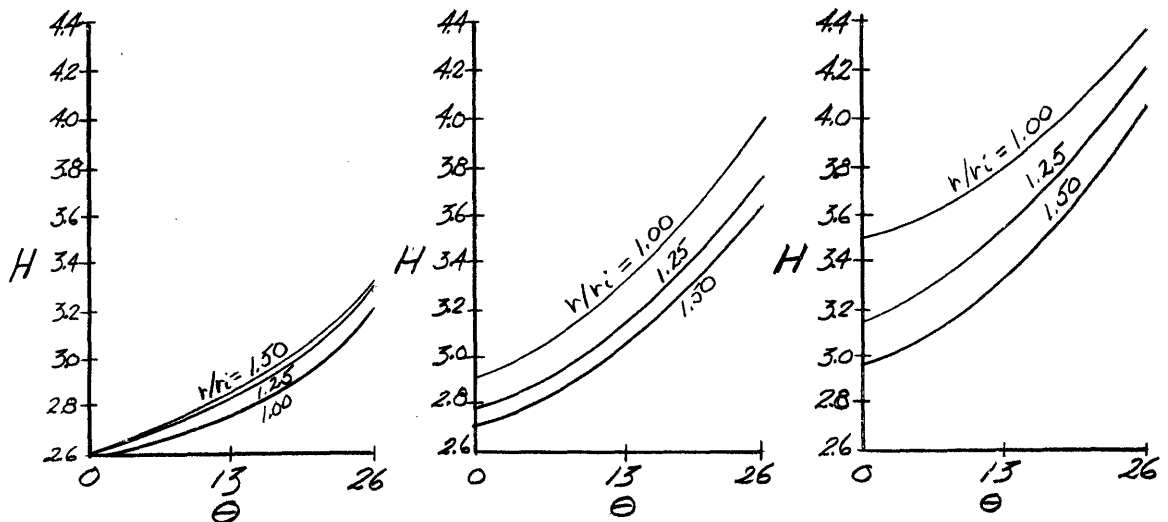Figure 45   Displacement and Momentum Thickness vs. Θ
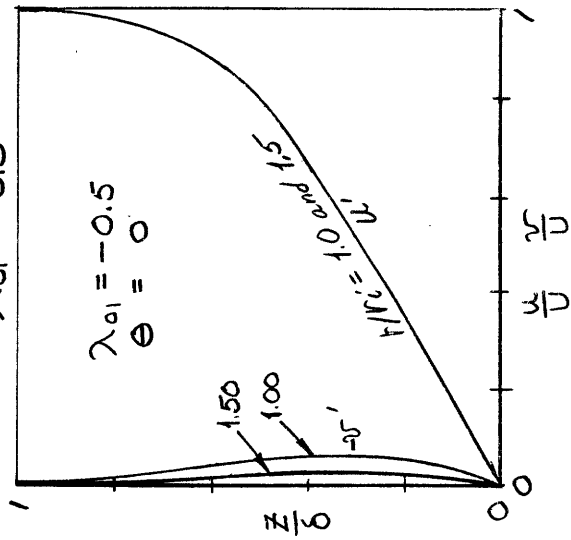

Figure 46   Shape Factor vs. Θ

Figure 47 $\lambda_{o1} = -0.5$
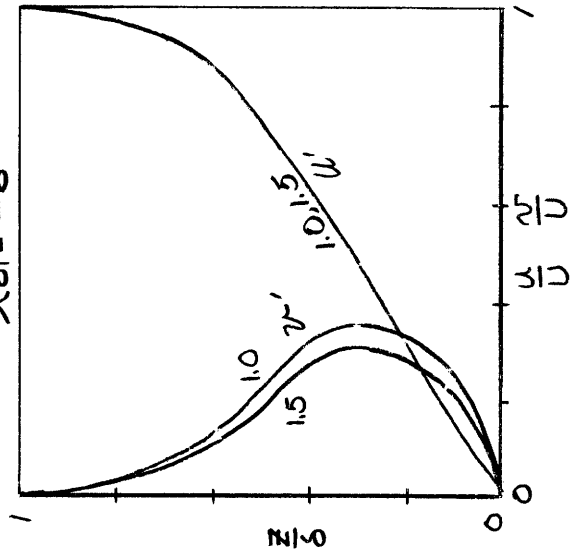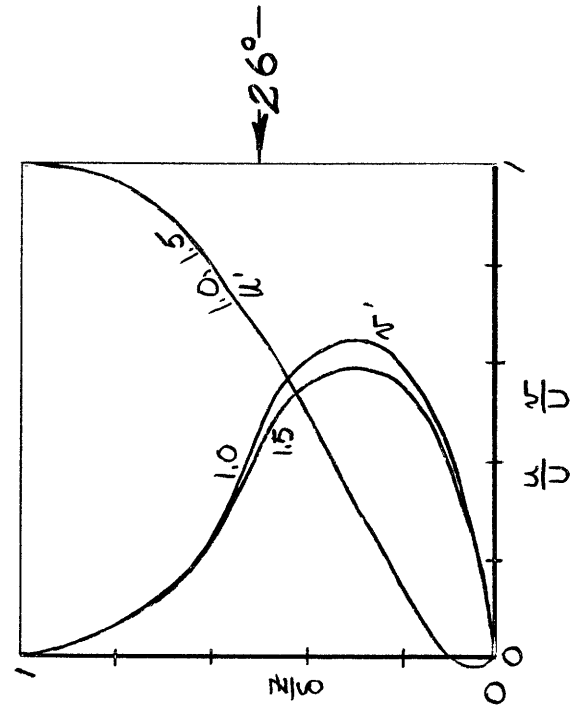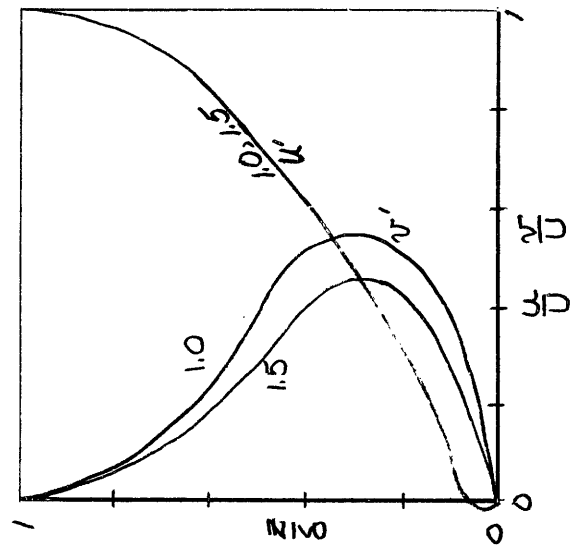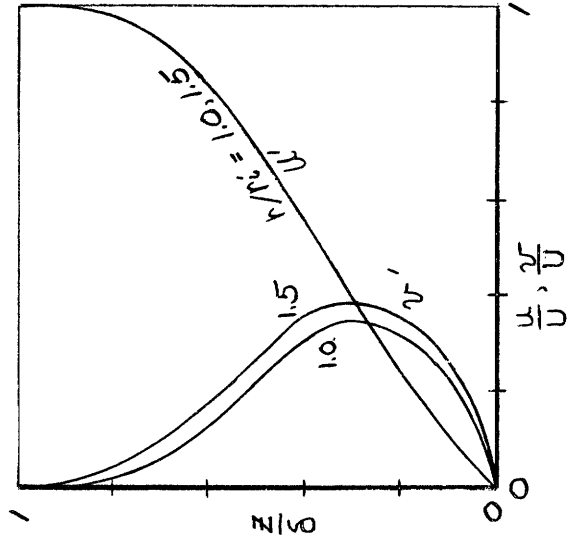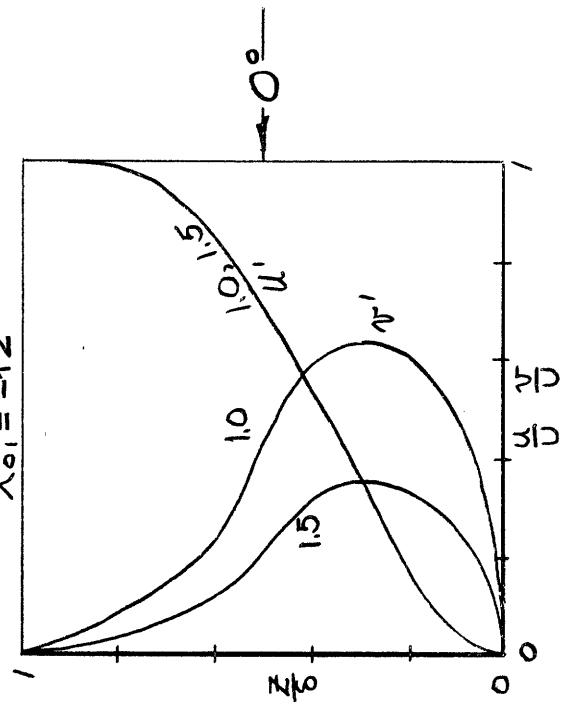
Figure 48 $\lambda_{o1} = -6$

Figure 49 $\lambda_{o1} = -12$

Sketches of the Tangential And Radial Velocity Profiles at $0°$ and $26°$ (for the three different inlet conditions)

through 111. The local boundary-layer thickness δ was determined as a function of r and Θ from eqn. 169. In addition, the local values of the tangential momentum thickness $\Theta*$, the tangential displacement thickness $\delta*$ and the tangential shape factor H were computed respectively from eqns. 118, 117 and the definition of $H = \frac{\delta*}{\Theta*}$. The values of δ, $\delta*$, $\Theta*$ and H are plotted in Figures 44, 45 and 46.

The velocity profiles are plotted as functions of Θ in Figure 47, as functions of r in Figure 48 and isometrically as functions of r and Θ in Figure 49.

Computation

A brief discussion of the computation procedure is in order. At first glance, it would seem that poor accuracy or no solution at all would be obtained from the boundary layer momentum equations. They contain subtractive constants as large as 73,000; the resulting values of λ must be determined to the first decimal place for reasonable accuracy. Normally, this would be an impossible situation except for the fact that all the numbers in the equations are exact values. No terms were rounded off in the derivations. Therefore, the required accuracy may be achieved by carrying six places in computation.

Aside from the fact that manipulation of the general equations is extremely tedious--the values of the functions F_3 through F_6 and G_3 through G_5 must be calculated for each new λ --the computations proceed without difficulty. At each point $\frac{\partial \lambda}{\partial \Theta}$ and $\frac{\partial \lambda}{\partial r}$ (or $\frac{\partial \lambda}{\partial x'}$ and $\frac{\partial \lambda}{\partial y'}$) are determined from the local value of λ. Then

a small step in Θ, r, x' or y' is taken and a new value of λ computed by multiplying the slope of λ by the step.

These equations are of a "propagation" type where all values depend on the initial conditions and the behavior of the main stream velocity U. Boundary conditions cannot be placed on the boundary layer flow except at the inlet and through the indirect effects of boundary conditions imposed on the main flow. This fact is the underlying reason for assumption 2, at the beginning of this Section, which allows us to ignore wall interference and eliminates the necessity of specifying boundary conditions at the curved walls of the passage.

Conclusion of the Momentum Analysis

At this point it is appropriate to discuss the inherent re-
strictions placed upon this analysis by the velocity-profile assump-
tions of eqns. 100 and 101. It has been demonstrated in linear
laminar flow that the Polhausen profile approximation employed
herein does lead to significant results in the prediction of bound-
ary-layer behavior. In this analysis, the tangential velocity
profile approximation is probably still in order. However, the
radial velocity profile approximation undoubtedly compromises the
results.

Consider boundary-layer separation. In a linear decelerating
flow, the accumulation of low energy fluid close to the wall in-
creases until backflow commences and the boundary layer is said to
be "separated". On the other hand, in a curvilinear flow the low
energy fluid close to the wall is subject to radial forces roughly
proportional to the square of the fluid velocity. The radial force
field tends to sweep low energy fluid toward the center of rotation
of the flow pattern. Fluid with the lowest velocity will be sub-
ject to the highest radial accelerations. This action tends to re-
move low energy fluid from one region of the flow and transport it
to another. The action is analogous to an imaginary internal
boundary-layer suction or injection.

Now, it is very important to the flow, as it approaches separa-
tion, just which part of the boundary layer is removed or, in the
opposite case, just what energy level is possessed by the fluid
radially injected into the local boundary layer.

The radial velocity profiles, determined by eqn. 109, have a fixed shape and vary only in magnitude. The peak of the profile always occurs at a position $z/\delta = 0.3$. The profile shape was determined by boundary conditions at the wall and outer edge of the boundary layer; the shape between these limits is rather arbitrary. If the peak of the radial profile occurred closer to the wall, backflow should be further delayed in some localities and encouraged in others, since the low-energy fluid close to the wall would undergo more vigorous radial transport.

It can be seen from these considerations that the radial velocity profile should be specified more strictly in any three-dimensional boundary-layer analysis that attempts to predict the flow in greater detail than merely the determination of the average properties (i.e., displacement thickness, momentum thickness and shape factor). To determine the radial pattern more exactly, we must impose another condition somewhere inside the boundary layer. A realistic choice of this condition demands a prediction of the dynamics of the internal boundary-layer flow. But this detailed prior knowledge is exactly that which we wish to avoid in a momentum analysis. To predict the radial flow, one must know the solution to the problem, while a significant solution requires some prior knowledge of the radial flow pattern. Thus, we have a hen and egg problem. Two attacks seem possible to evaluate the significance of this effect.

An arbitrary specification can be introduced for the z-position of the radial velocity peak. For a given flow, discrete solutions

can be effected for several peak positions. The results of these
calculations should demonstrate the sensitivity of the flow to this
variable.

Another possible attack involves a very difficult iteration pro-
cess which might lead to an exact solution within the original assump-
tions. The boundary layer would be treated first by the momentum
integral relations developed herein. Then, the resulting configura-
tion may be sliced into thin layers by cuts parallel to the wall.
Utilizing the shear stress distribution from the velocity profile
of the integral solution, the flow in each slice of the boundary
layer may be recomputed. Now the slices may be pasted back together
giving new velocity profiles throughout the boundary layer. These
profiles could then be approximated by more extensive series than
employed here and injected back into the integral momentum relations.
The process may be repeated until not only the entire boundary layer,
but also arbitrarily thin slices thereof, obey the equations of
motion.

While the process imagined above might lead to excellent results,
laminar flow is so rare in turbomachinery that such a major effort
is not warranted.

The assumption of various arbitrary radial peak positions
appears to be the most satisfactory method of studying this im-
portant restriction.

Inspection of Figures 43 through 49 reveals that the boundary
layer of the free-vortex model behaves in a manner similar to the
measured behavior of the cascade of Figure 22 in Section I. The

shape factor of the boundary layer increases most rapidly near the convex wall of the passage. The variation of shape factor with radius is, on the other hand, much more gradual than that of the cascade discharge. Essential differences between the pressure field and boundary-layer thickness of model and actual passage are important factors. The fact that the cascade flow was turbulent is a serious inconsistency. Wall interference effects are unobtainable due to the lack of compatibility between model and cascade. Results from a flow better suited to this model are forthcoming. In spite of all these anomalies, it is significant that the model does predict behavior at least qualitatively similar to an actual flow. The line indicating the onset of back flow in Figure 43 compares favorably with the actual carbon-black traces of Figure 24, in Section I.

As a last comparison, the underturning angle was computed for the model from the tangential and radial velocity profiles of Figures 47, 48 and 49 at mid-passage discharges. These flow angles are plotted in Figure 50 which also shows the results of the analysis of Section IV.presented in Figure 36 of that Section. Figure 50 illustrates graphically the effect of viscous stresses deep in the boundary layer. Where the inviscid analysis predicts large negative underturning angles at the wall, the momentum analysis predicts an underturning angle of zero*.

It should be remembered that the viscous curve of Figure 50 is

----

*The carbon-black diagram, Figure 24, Section I, indicates finite underturning angles at the wall. Nevertheless, since some fluid motion is required to distribute the carbon black and since the velocity at the wall is zero, the carbon-black pattern must be representative of flow deep in the boundary layer but not actually on the wall.
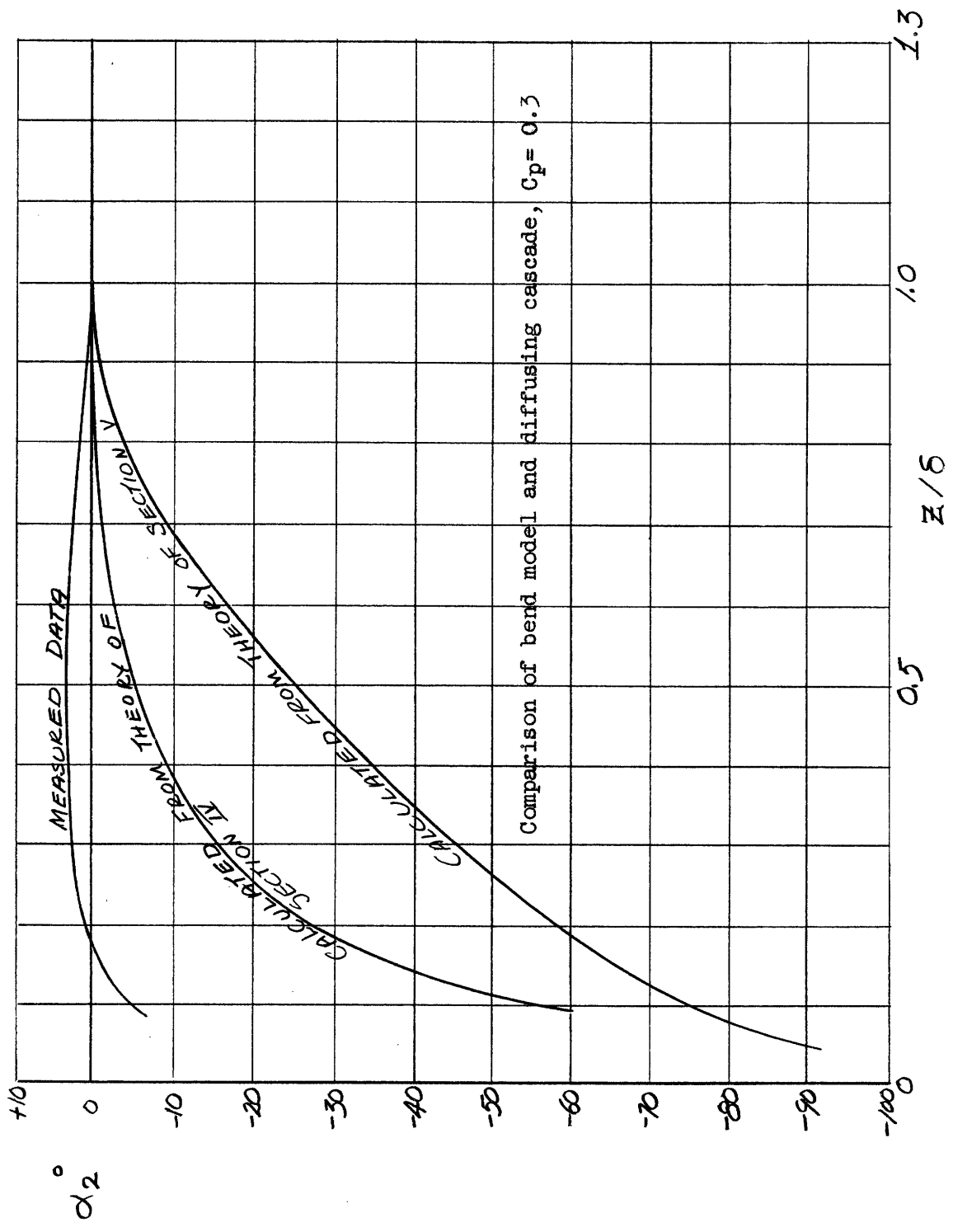
UNDERTURNING ANGLE VS POSITION IN THE BOUNDARY LAYER
Showing results from fig. 36, section IV

Figure 50

subject to the same criticisms leveled against the radial velocity profile approximation. The shape of the underturning angle curve is no better than the profile assumption.

In conclusion, it may be stated that while this analysis is only approximate, it does demonstrate, as intended, the importance of viscous stresses and, by implication, of turbulent stresses in governing the streamline pattern and condition of the flow deep in a boundary layer suffering secondary flow effects.

VI. Closure and Suggestions for Further Research

As stated at the commencement of these three analyses, an initial exploration of the influence of pressure and shear stresses upon the behavior of a secondary-flow pattern has been effected. Many more restrictions and failures of the analysis result than clear answers to any problem. It is anticipated, however, that the experience obtained in this work will be a valuable guide in further treatment of the general boundary-layer problem. Whether solutions capable of predicting boundary-layer behavior in turbomachine passages ever will be effected or not is questionable. Treatment of turbulent flow presents more pitfalls today than those encountered herein. Also, the actual three-dimensional nature of turbomachine flow with strong radial currents and the effect of such patterns on the boundary layer may require treatments of such complexity that the problem will be ignored until empirical results show obvious avenues toward perfection.

Suggestions for Continued Investigation

As a result of this work, the following suggestions for continued investigation are in order:

1. Data should be obtained on a simple secondary-flow pattern within thin shear flows to test the validity of this quasi-two-dimensional attack. Wall interference effects should be investigated to determine if the neglect of such are critical to an analysis.

2. The momentum integral treatment should be extended, in as enlightened manner as possible, to turbulent flow. If turbulent analysis appears promising, calculations are suggested employing

the measured or potential pressure distributions through actual blade rows. Correlation of calculated results should demonstrate the influence of passage geometry.

3. Employing the approximate relations obtained herein, the entire specialized subject of secondary flow in thin boundary layers should be related to turbomachine behavior and the other significant disturbing effects.

4. If analysis is possible and the influences of the flows treated herein are significant, improved blade-row configurations should be tested in cascade and in rotating machines. Only a significant improvement in machine performance can justify any concern with these matters.

Bibliography

1. Hawthorne, W. R., "Secondary Circulation in Fluid Flow", Gas Turbine Laboratory Report, MIT, 1951; Proc. Royal Soc. A, Vol. 206, 1951.

2. Hawthorne, W. R., "A Theory of Struts in Boundary Layers", Gas Turbine Laboratory Report, MIT, 1951.

3. Squire, H. B. and Winter, K. G., "The Secondary Flow in a Cascade of Airofoils in a Non-Uniform Stream", RAE Report, Aero. 2317, March 1949, and Jour. Aero. Scis., Vol. 18, No. 4, April 1951.

4. Eichenberger, Hans P., "Shear Flow in Bends", Sc.D. Thesis, MIT, 1952; Gas Turbine Laboratory Report, MIT, 1952.

5. Van Le, Nguyen, "Three-Dimensional Flow in a Cascade--Effect of the Boundary Layer", Sc.D. Thesis, 1952; Gas Turbine Laboratory Report 2006-8, MIT, 1952.

6. Hawthorne, W. R. and Horlock, J. H., "Actuator Disc Theory Applied to Wall Boundary Layers in Cascades", Gas Turbine Laboratory Memorandum.

7. Bragg, S. L. and Hawthorne, W. R., "Some Exact Solutions of the Flow through Annular Cascade Actuator Discs", Jour. Aer. Sci., Vol. 17, No. 7, April 1950.

8. Pinsley, E. A., "An Investigation of Secondary Cascade Flows", MIT Thesis, June 1950.

9. Von Doenhoff, A. E. and Tetervin, N., "Determination of General Relations for the Behavior of Turbulent Boundary Layers", NACA Report 772, 1943.

10. Detra, R. W., "Secondary Flow in Curved Pipes", Mitterlungen aus dem Institut fur Aerodynamik an der E.T.H., Zurick, Nr. 20.

11. Toline, F. R. and Watson, R. H., "The Effects of a Moving Wall on Secondary Flow in a Cascade", S.M. Thesis, MIT, 1953.

12. Elliott, C.E. and Glass, R. W., Progress Report, Low-Speed Cascade, Gas Turbine Laboratory Report No. 2006-2, MIT, 1949.

13. Elliott, C. E. and Glass, R. W., Progress Report, Low-Speed Cascade, Gas Turbine Laboratory Report No. 2006-3, MIT, 1950.

14. Graff, Truls W., Progress Report, Low-Speed Cascade, Gas Turbine Laboratory Report No. 2006-4, MIT, 1950.

15. Sorensen, H. A., "Gas Turbines", Ronald Press Company, New York 1951.

16. Howell, A. R., "The Present Basis of Axial-Flow Compressor Design", ARC, R and M 2095; Proc. Inst. Mech. Engrg., Published in U.S. by ASME.

17. Carter, A. D. S., Cohen E. M., "Preliminary Investigation into Three-Dimensional Flow through a Cascade of Airfoils", ARC R and M No. 2339.

18. Carter, A. D. S.,"Three-Dimensional Flow Theories for Axial Compressors and Turbines", Internal Combustion Turbines, Inst. of Mech. Engrs., Published in U.S. by ASME, 1949.

19. Herzig, H., Hansen, A. E., and Costello, G. R., "Visualization of Secondary Flow Phenomena in a Blade Row", NACA RM E52F19, 1952.

20. Hansen, A. G., Costello, G. R. and Herzig, H. Z., "Effect of Geometry on Secondary Flow in Blade Rows", NACA RM E52H26, Oct. 1952.

21. Allen, H. W., Kofskey, M. G. and Chamness, R. E., "Experimental Investigation of Loss in an Annular Cascade of Turbine Nozzle Blades of Free-Vortex Design", NACA TN 2871, Jan. 1953.

22. Rohlik, H. E., Allen, H. W. and Herzig, H. Z., "Study of Secondary Flow Patterns in an Annular Cascade of Turbine Nozzle Blades with Vortex Design", NACA TN 2909, Feb. 1953.

23. Hansen, A. G., Herzig, H. Z. and Costello, G. R., "Smoke Studies of Secondary Flows in Bends, Tandem Cascades, and High-Turning Configurations", NACA RM E52I24a, March 1953.

24. Hansen, A. G., Herzig, H. Z. and Costello, G. R., "A Visualization Study of Secondary Flows in Cascades", NACA TN 2947, May 1953.

25. Ainley, D. G., Jeffs, R. A., "Analysis of the Air Flow through Four Stages of Half Vortex Blading in Axial Compressors", ARC RM No. 2383.

26. Kronauer, R., "Secondary Flow in Fluid Dynamics", Ph.D. Thesis, Harvard University, 1951.

27. Gazarin, Adel., "Graphische Behandlung der Kompressiblen und Incompressiblen Stromung Durch Turbomaschinenstufen", Verlag Leemann, Zurick, Switzerland, 1951.

28. Straub, L. G. and Anderson, A. G., "Fluid Flow Division, A Summary and Bibliography of Literature", St. Anthony Falls Hydraulic Laboratory, University of Minnesota Project Report No. 1, Aug. 1947.

29. University of Minnesota, St. Anthony Falls Hydraulic Laboratory, Project Report S--Nature of Flow in an Elbow.

30. Alsworth, C. G., Iura, T., Rannie, W. D., "Theoretical and Experimental Investigations of Axial Flow Compressors". Research conducted under ONR Contract N6-ori.102 Task Order IV, Part III. Progress Report on Loss Measurements in Vortex Blading, Mech. Engrg. Lab., Cal. Inst. of Tech., Pasadena, July 1951.

31. Stanitz, John D., Osborn, W. M. and Mizisin, S., "An Experimental Investigation of Secondary Flow in an Accelerating Rectangular Elbow with 90° of Turning", NACA TN 3015.

32. Herzig, H. Z. and Hansen, A. G., "Visualization Studies of Secondary Flows with Application to Turbomachines", ASME Paper, 53-A-101, Dec. 1953.

33. Smith, L. H., Jr., "Three-Dimensional Flow in Axial Flow Turbomachinery. Part 1.", Johns Hopkins University, Mech. Engrg. Dept. Rept., Nov. 1953.

34. Ehrich, F. F. and Detra, R. W., "Transport of the Boundary Layer in Secondary Flow", Jour. Aero. Scis., Feb. 1954.

35. Lamb, Sir Horace, "Hydrodynamics", Cambridge University Press, Sixth Edition, 1932, p.244.

36. Rex, Edward, "Effects of Tip Clearance and Wall Motion on Secondary Flow", S.M. Thesis, Mech. Engrg. Dept., MIT, 1954.

37. Roache, Robert, and Thomas, Lee, "Effect of Slotted Blade Tips on the Secondary Flow in a Compressor Cascade", S.M. Thesis, Mech. Engrg. Dept., MIT, 1954.

38. Cunavelis, P. J. and Christie, K. V., "The Effect of Tip Clearance and Moving Wall Velocity on the Lift Characteristics of Stationary Blades", S.B. Thesis, Mech. Engrg. Dept., MIT, 1954.

39. Hildebrand, F. B., "Advanced Calculus for Engineers", Prentice-Hall, 1950.

40. Zika, Vaclav Jan., "Control of Secondary Flow in Decelerating Cascade", S.M. Thesis, Mech. Engrg. Dept., MIT 1954.

41. Goldstein, S., "Modern Developments in Fluid Dynamics", Vol. 1, Chap. IV, Clarendon, Oxford, 1938.

42. Schlichting, H., Lecture Series, "Boundary Layer Theory. Part I. Laminar Flows", NACA TM No. 1217, 1949.

Biography

The author was born on April 13, 1928, in Atlanta, Georgia, of parents Robert C. Dean, Architect, and Ruth Andrews Dean. He attended Phillips Academy, Andover, Massachusetts, and graduated in 1945. He received an S.B. and an S.M. Degree in Mechanical Engineering from the Massachusetts Institute of Technology in 1949.

From 1949 until 1951, he was employed by the Ultrasonic Corporation of Cambridge, Massachusetts, as an engineer concerned with the application of high-intensity sound to industrial processes. In September 1951 he received an appointment at MIT as assistant professor of Mechanical Engineering. Since that time he has instructed in courses of the Mechanical Engineering Department and has been attached to the Gas Turbine Laboratory Staff. His research efforts have been largely concerned with three-dimensional flow in turbomachines.

During the summers of 1952 and 1953, he supervised the presentation of a Special Summer Course entitled "Aerodynamic Measurements" and edited the book by that same title published by the Gas Turbine Laboratory in 1953.